MECHANISTIC MODEL VALIDATION OF DECLINE CURVE ANALYSIS FOR UNCONVENTIONAL RESERVOIRS

A Thesis

by

ERIC WAYNE BRYAN

Submitted to the Office of Graduate and Professional Studies of
Texas A&M University
in partial fulfillment of the requirements for the degree of

MASTER OF SCIENCE

Chair of Committee,	Thomas A. Blasingame
Committee Members,	George J. Moridis
	Zenon Medina-Cetina
Head of Department,	Jeff Spath

May 2020

Major Subject: Petroleum Engineering

ABSTRACT

The primary objective of this work is to provide the validation and ranking of numerous decline curve analysis models. From the validation cases analyzed in this research best practice guidelines for each of the decline curve analysis models are presented. In addition to the decline curve specific guidelines, general best practices are outlined to be implemented when performing decline curve analysis.

A built-for-purpose mechanistic model was developed and used successfully as a validation tool for the decline curve analysis models. The primary validation cases are analyzed using typical properties and parameters from the Haynesville, Eagle Ford, and the Wolfcamp formations. The effect of non-constant pressure production on time-rate data is also analyzed. Investigation into the effect of available time-rate data on the estimation of ultimate recovery at the end of a wells producing life is presented for each of the investigated decline curve analysis models.

A methodology is proposed in order to assist with poor time-rate data quality from unconventional reservoirs. The respective necessary equations for the power-law exponential, stretched exponential, and modified hyperbolic decline curve models are derived and presented, as well as the associated modified "*qDb*" plot (referred to as the rate-integral "*modified qDb*" plot).

It was concluded from this research that the power-law exponential decline curve model is the most valid for the representation of time-rate data from unconventional reservoirs.

DEDICATION

To my family: *Scott, Theresa, and Wyatt Bryan*

ACKNOWLEDGEMENTS

The author expresses his gratitude towards the following individuals for their assistance in the development of this thesis:

Dr. Thomas A. Blasingame for his constant encouragement to produce the highest quality research and results.

Dr. George J. Moridis for his continued support in the development of the mechanistic model.

Dr. Zenon Medina-Cetina for his service as a member of the advisory committee.

Dr. Andreas Kronenberg for his participation in my thesis defense.

My parents for their constant support throughout my educational career.

CONTRIBUTORS AND FUNDING SOURCES

Contributors

This work was supervised by a thesis committee consisting of Dr. Thomas Blasingame and Dr. George Moridis of the Department of Petroleum Engineering and Dr. Zenon Medina-Cetina of the Department of Civil Engineering.

Funding Sources

Graduate study was supported by the Crisman Institute for Petroleum Research from Texas A&M University. The contents of this thesis are solely the responsibility of the authors and do not necessarily represent the official views of the Texas A&M Department of Petroleum Engineering or the Crisman Institute for Petroleum Research from Texas A&M University.

NOMENCLATURE

Field Variables

a_{LF} = Constant linear flow parameter, [bbl] or [Mscf]

a_{BLF} = Constant bilinear flow parameter, [bbl] or [Mscf]

a_{MFF} = Constant multi-fracture flow parameter, [bbl] or [Mscf]

B_o = Oil formation volume factor, [RB/STB]

B_{ob} = Oil formation volume factor at bubble point pressure, [RB/STB]

b = Klinkenberg parameter, [Pa] or [psi]

c_f = Formation compressibility, [psi^{-1}]

c_o = Oil compressibility, [psi^{-1}]

c_t = Total compressibility, [psi^{-1}]

C = Heat capacity, [J kg^{-1} K^{-1}]

C_D = Wellbore storage coefficient, [dimensionless]

EUR = Estimated ultimate recovery, [Mbbl] or [BSCF]

F = Mass or heat flux, [kg m^{-1} s^{-1}] or [J m^{-2} s^{-1}]

F_{CD} = Dimensionless fracture conductivity, [dimensionless]

g = Gravitational acceleration vector, [m s^{-2}] or [ft s^{-2}]

GOR = Gas-oil-ratio, [dimensionless]

h = Specific enthalpy of component in phase, [J kg^{-1}]

h = Net formation thickness, [ft]

H = Phase specific enthalpy, [J kg^{-1}]

k = Formation permeability, [md] or [nd]

k_f = Fracture permeability, [md]

k_r = Relative permeability, [dimensionless]

L = Smoothing parameter for Bourdet numerical pressure derivative, [dimensionless]

L_w = Horizontal Well length, [ft]

m = Time exponent for the Duong time-rate model, [dimensionless]

M = Mass or heat accumulation, [kg m^{-3}] or [J m^{-3}]

MW = Molecular weight [kg $kmol^{-1}$]

n_f = Number of hydraulic fractures, [dimensionless]

p = pressure, [Pa] or [psia]

p_b = Bubble point pressure, [Pa] or [psia]

p_c = Critical pressure, [Pa] or [psia]

p_i = Initial reservoir pressure, [Pa] or [psia]

p_{tbg} = Surface flowing pressure, [Pa] or [psia]

p_{wf} = Bottomhole flowing pressure drop, [Pa] or [psia]

q = Production rate, [bbl/D] or [Mscf/D]

q_g = Gas production rate, [Mscf/D]

q_o = Oil production rate, [bbl/D]

q_w = Water production rate, [bbl/D]

Q = Cumulative production rate, [bbl] or [Mscf]

r_w = Wellbore radius, [ft]

R = Gas constant, [J kg^{-1} mol^{-1}]

R_s = Solution gas-oil ratio, [scf/STB]

R_{sb} = Solution gas-oil ratio, [scf/STB]

s = Skin factor, dimensionless

s_f = Fracture spacing, [ft]

S = Phase saturation, [fraction]

S_{irr} = Irreducible phase saturation, [fraction]

t = Production time, [days]

T = Temperature, [°C] or [°F]

T_c = Critical temperature, [°C] or [°F]

T_r = Reservoir temperature, [°C] or [°F]

u = Specific internal energy of a component in phase, [J kg^{-1}]

U = Phase specific internal energy, [J kg^{-1}]

V = Volume, [m^3] or [ft^3]

V_c = Critical volume, [m^3] or [ft^3]

V_M = Molar volume, [m^3 mol^{-1}]

X = Mass fraction, [kg/kg]

X_f = Effective fracture half length, [ft]

Y = Mole fraction, [mol/mol]

Z = Gas Z-factor, [dimensionless]

Decline Curve Analysis Variables

a = Model coefficient for the Duong time-rate model, [D^{-1}]

a = Model coefficient for the Logistic Growth time-rate model, [D^{-1}]

b = Arps' hyperbolic decline exponent, [dimensionless]

b = Derivative of the loss-ratio, [dimensionless]

b_{int} = Derivative of the loss-ratio for the rate-integral, [dimensionless]

D = Reciprocal of the loss-ratio, [D^{-1}]

$1/D$ = loss-ratio, [D]

D_1 = Decline coefficient at 1 day for the Power-Law Exponeitial relation, [D^{-1}]

D_{min} = Terminal decline constant for the exponential time-rate relation, [D^{-1}]

D_i = Initial decline constant for the exponential and hyperbolic time-rate relations, [D^{-1}]

D_{int} = Reciprocal of the loss-ratio for the rate-integral, [D^{-1}]

$\hat{D}_i$ = Decline coefficient for the Power-Law Exponential time-rate model, [D^{-1}]

D_∞ = Terminal decline coefficient for the Power- Law Exponential time-rate model, [D^{-1}]

K = Carrying Capacity for the Logistic Growth time-rate model, [bbl] or [scf]

n = Time exponent for the Power-Law time-rate model, [dimensionless]

n = Time exponent for the Stretched Exponential time-rate model, [dimensionless]

n = Time exponent for the Logistic Growth time-rate model, [dimensionless]

q_1 = Initial rate coefficient for the Duong time-rate model, bbl/D or Mscf/D

q_i = Initial rate for the exponential and hyperbolic time-rate models, bbl/D or Mscf/D

q_i^* = Initial rate for the exponential decline in the Modified Hyperbolic time-rate model, bbl/D or Mscf/D

$\hat{q}_i$ = Initial rate coefficient for the Power-Law time-rate model, bbl/D or Mscf/D

q_{int} = rate integral, bbl/D or Mscf/D

q_o = Initial rate coefficient for the Stretched Exponential time-rate model, bbl/D or Mscf/D

rp = Recovery potential for Stretched Exponential time-rate model, dimensionless

t_{lim} = Time to exponential decline for Modified Hyperbolic time-rate model [days]

τ = Time coefficient for the Stretched Exponential time-rate model, D^{-1}

Greek Variables

γ_{API} = Oil API Gravity, [ºAPI]

γ_g = Gas specific gravity, [dimensionless] (air =1)

γ_o = Oil specific gravity, [dimensionless] (water =1)

γ_w = Water specific gravity, [dimensionless] (water =1)

λ = Thermal conductivity, [W m^{-1} K^{-1}]

μ = Viscosity, [Pa s] or [cP]

ρ = Density, [kg m^{-3}] or [lbm ft^{-3}]

ϕ = Porosity, [fraction]

ω = Acentric factor, [dimensionless]

Mechanistic Model Subscripts

A = Aqeuous phase

G = Gaseous phase

O = Organic phase

Mechanistic Model Superscripts

o = Oil component

g = Gas component

w = Water component

Mathematical Functions

Γ = Incomplete and complete Gamma function

TABLE OF CONTENTS

Page

Page

Page

LIST OF FIGURES

FIGURE Page

FIGURE Page

FIGURE Page

LIST OF TABLES

TABLE Page

CHAPTER I

INTRODUCTION

In this chapter, the general overview of the thesis is presented. This chapter has been divided into three sections. In the first section, the motivation of this research problem is presented. Next, the main objectives of this research are outlined. Finally, the basic and recurrent concepts used throughout this research are defined.

1.1. Statement of the Problem

The purpose of this thesis is to establish an extensive validation, comparison, and analysis of decline curve analysis (or DCA) models. These DCA modes are used for the analysis and interpretation of time-rate data. DCA models can be applied to time-rate data from both conventional and unconventional reservoirs, however this research will focus on primarily on their application in unconventional reservoirs. A broad compilation of current and evolving models used for decline curve analysis were investigated in this study. This range includes traditional "Arps" relations (*i.e.,* exponential and hyperbolic time-rate models), to more recently developed models. Many of these new "modern models" attempt to capture particular features of the time-rate decline profile in order to "estimate" reservoir properties or ultimate recovery. The validity of these claims was investigated in this study.

Decline curve analysis in unconventional reservoirs has been problematic due to the nature of the decline exhibited in the time-rate data. Before our pursuit into these low permeability reservoirs the Arps' (1945) equations were the standard for evaluating estimated ultimate recovery (EUR) in petroleum systems. The traditional Arps' equations have difficulty representing long-term

transient flow, which leads to an over estimation of reserves, particularly if the *b*-parameter in the hyperbolic equation is greater than 1 [Maley 1985]. This causes the hyperbolic equation to become unconstrained and will likely lead to an over estimation of reserves. The standard today for unconventional reservoir production forecasting is to use the modified hyperbolic decline curve model due to its ability to allow for an initial unconstrained hyperbolic relation, followed by an exponential terminal decline [Robertson 1988]. However, this is a non-unique approach and quite often yields a wide range of estimated reserves.

The primary decline curve analysis methods that were investigated in this study are as follows:

- Modified Hyperbolic Decline [Robertson 1988]
- Power Law Exponential Decline [Ilk 2008, 2009]
- Stretched Exponential Decline [Valkó 2009]
- Duong's Method [Duong 2010]
- Logistic Growth Model [Clark *et al.* 2011]

Each of the DCA models was be tested against numerous "typical" well and reservoir conditions to provide an exhaustive set of validation cases for each of the DCA models. In addition to mechanistic behavior models, this work also investigated the following non-mechanistic behavior production periods:

- Early-time performance, where the production is dominated by high water cut from the fractures.
- Transient performance, where linear or bi-linear flow regimes can be clearly identified.
- Transitional performance, where linear or bi-linear flow regimes cannot be clearly identified.

- Late-time performance, where pressure-dependent fractures and/or liquid-loading hinder well performance.

Due to the erratic and variable nature of unconventional reservoirs, DCA models often cannot accurately represent reservoir conditions. Some of these variable conditions include:

- Various fracture conditions.
- Pressure-dependent reservoir and fracture properties.
- Multiphase behavior of black oil, compositional, and dry gas reservoirs.
- Flowback conditions.

The built-for-purpose reservoir model constructed for this study is able to accurately represent all the variable conditions mentioned above.

With the recent increase in the exploitation of unconventional reservoirs, the oil and gas industry has adapted a magnitude of different hydraulic fracturing techniques. Various fracture conditions can be due to both the properties of the reservoir, as well as the hydraulic fracture design. Hydraulic fracturing design parameters that can affect fracture conditions include, but aren't limited to:

- Stage length.
- Cluster Spacing.
- Amount of fracturing fluid.
- Type of fracturing fluid.
- Amount of proppant.
- Type of proppant.

Unconventional reservoirs tend to experience pressure-dependent reservoir and fracture properties, where the properties change throughout the lifetime of the well due to pressure decline. Most current decline curve analysis models were developed based on the observations of single-phase flow. With multiphase behavior, often in application the DCA model is applied to only the fluid of interest (*i.e.*, oil or gas production), assuming it is the only produced fluid, which is incorrect due to the other components and phases impacting the time-rate data. The increase of slickwater volume used in hydraulic fracturing treatments has been a general trend in industry over the past few years, which has led to an increase in high water production from the induced fractures during flowback conditions. During late-life production periods the effects of liquid-loading become apparent, which can be identified by irregularity in bottomhole pressure during this time. Decline curve models all empirical, but they are based on observations from "perfect" reservoirs with many simplifying assumptions and homologations, therefore it is difficult for them to accurately represent the aforementioned non-mechanistic reservoir conditions.

1.2. Research Objectives

The main objectives of this thesis are:

- Validation and ranking of numerous declined curve analysis models.
- Provide best practice guidelines for a given decline curve analysis model.
- Develop a specialty (fit-for-purpose) multi-fractured horizontal well mechanistic model to be used as a validation tool.

1.3. Basic Concepts

In this section the fundamental concepts of this work are defined. The purpose of this section is to not discuss the concepts in depth, but rather to establish a foundation that can assist with the understanding the fundamental theory behind this research.

Unconventional Reservoirs

These resources plays are hydrocarbon bearing reservoirs that require special operations outside of conventional oil and gas operating practices in order to produce in an economic manner. The most common operation, and the focus of this research, is hydraulic fracturing, where the reservoir is stimulated by pumping fluid and proppant at high rates and pressures into the reservoir. Unconventional reservoirs include resources plays such as shale oil/gas reservoirs, tight-gas reservoirs, coalbed methane, gas-hydrate deposits, and heavy oil tar sands.

Decline Curve Analysis

Decline curve analysis (DCA) is a practice in which future oil or gas well production is estimated using previous time-rate data as a proxy. Oil and gas production typically declines as a function of time due to a loss in reservoir pressure. The basis of DCA is calibrating a line through the performance history and assuming that the same trend will continue in the future.

Mechanistic Model

The mechanistic model mentioned in this thesis is referring to the fit-for-purpose fully implicit numerical reservoir simulator built for this research. The mechanistic model is used to model fluid flow though porous media. The fundamental assumption of a mechanistic model is that the complex system can be represented by evaluating the workings of individual parts.

CHAPTER II

LITERARY REVIEW

The primary objective of this work is to validate and rank decline curve analysis models on their ability to represent and forecast production from unconventional reservoirs. Prior to discussion on the work performed to address the aforementioned primary objective, a discussion of both classical and modern production forecasting methodologies is warranted. Special emphasis will be placed on relations that were developed with the primary objective of forecasting production from unconventional reservoir systems. This section will discuss the origins of decline curve analysis, the classical equations (*i.e.,* Arps' equations), and new and evolving methods developed specifically to address the unique features seen in time-rate data obtained from unconventional reservoirs.

Decline curve analysis is the practice of extrapolating "time-rate" production data. It is used throughout the petroleum industry to estimate ultimate recovery (EUR) of producing wells in which the production decays over time (*i.e.,* non-constant rate production). Decline curve analysis is referring to calibrating a time-rate model to a producing wells historical production history in order to predict future production to an abandonment limit.

With the advancement of technology, numerical simulation can now be used extrapolate future production by calibrating input properties and parameters to represent historical production data. However, this has not replaced the need for traditional decline curve analysis due to the time-consuming process of numerical simulation. The initial goal of "production data analysis" was to estimate reserves for tax purposes. Taxes are still a primary reason why decline curve analysis is so widely performed today within the petroleum industry. Lewis and Beal (1918) are some of the

earliest individuals to recognize and publish on the need for quick and accurate forecasting methods to estimate reserves at an early time of a well's producing life (or field). They acquired data from the Nowata and Osage producing fields and observed that on a log-log plot of the percentage rate of decline versus time, the data exhibited a power-law relationship (*i.e.*, straight-line). They suggested that using this power-law behavior along with plots of cumulative percentage decline could be used to accurately forecast future production. Lewis and Beal (1918) also acknowledged in their original paper the limitations of estimating reserves using volumetrics and production curve forecasting.

Cutler (1924) concluded that using percentage rate decline, as suggested by Lewis and Beal, was too variable to observe straight-line behavior as they had proposed. He suggested that rate decline could be represented by a hyperbolic equation. However, this would need to be done using a trail-and-error method that involved shifting production data until a straight-line trend becomes apparent.

Johnson and Bollens (1927) were the first to mathematically explain the observations that have been previously stated. They introduced the concept of "loss-ratio" and "derivative of the loss-ratio", which are defined as:

$$\frac{1}{D} \equiv -\frac{q(t)}{dq(t)/dt}$$ (Definition of the loss-ratio) …………………………..(2.1)

$$b \equiv \frac{d}{dt}\left[\frac{1}{D}\right] \equiv \frac{d}{dt}\left[\frac{q(t)}{dq(t)/dt}\right]$$ (Derivative of the loss-ratio) ………………………….(2.2)

Where $(1/D)$ is the loss-ratio, b is the derivative of the loss-ratio, q is the flowrate, and t is the producing time. This was quite an advancement in production forecasting because it did not

require logarithmic extrapolation. Their proposed methodology was to tabulate the ratios presented in **Eq. 2.1** and **Eq. 2.2** of the time-rate data by using a finite difference numerical differentiation method, then extrapolating the observed loss-ratio behavior, and finally forecasting future production. They noted that the loss-ratio displays power-law behavior, as previously suggested.

The most well-known decline curve analysis models were originally presented by Arps in 1945. Prior attempts at forecasting production primarily focused on determining a straight-line behavior and extrapolating. Arps was the first to publish the equations for hyperbolic, exponential, and harmonic decline in oil and gas producing wells, as well as their corresponding cumulative production equations. All of these equations are based off observations of time-rate data and therefore are entirely empirical. However, Camacho and Raghavan (1989) later showed that the exponential decline relationship could be derived from pseudo-steady state production of a slightly compressible fluid at a constant pressure. The hyperbolic decline equation is the foundation for all three presented decline curve analysis models and is defined as:

$$q(t) = \frac{q_i}{(1+bD_i t)^{1/b}} \quad \text{.....(2.3)}$$

Where q_i is the initial flowrate, D_i is the initial rate of decline, b is the hyperbolic decline exponent, and t is producing time. This equation is the mathematical representation of non-constant percentage decline behavior, as first introduced by Cutler (1924). The hyperbolic equation is based off the observation that the loss-ratio derivative is constant. When the hyperbolic decline exponent (b) is equal to zero, **Eq. 2.3** becomes the exponential relationship, which is defined as:

$$q(t) = q_i \exp[-D_i t] \quad \text{.....(2.4)}$$

This equation is the mathematical representation of constant decline behavior, as alluded to by Lewis and Beal (1918). Thus, it represents the observation that the loss-ratio yields near constant behavior. Another special case for the hyperbolic decline equation is when the hyperbolic decline exponent (b) is equal to 1, this is referred to as harmonic decline at is defined as:

$$q(t) = \frac{q_i}{(1 + D_i t)} \quad \text{.....(2.5)}$$

Harmonic decline is not commonly observed in unconventional reservoir systems, but was included for completeness.

Lee and Wattenbarger (1996) discuss the primary assumptions pertaining to Arps' equations, which include:

- The well is being produced at a constant bottomhole pressure.
- The well is being produced from an unchanging drainage area with no flow boundaries.
- The well is being produced from a reservoir with constant permeability and constant skin factor.
- Historical production data used to calibrate the time-rate model is representative of future production trends.

Arps (1945) suggested in his original paper that the hyperbolic parameter should be less than one. When it is greater than one **Eq. 2.3** becomes unbounded and therefore can greatly overestimate reserves. Maley (1985) however showed that a b-parameter greater than one could accurately represent time-rate data from tight gas wells. This empirical observation is one of the first indications that the classical decline curve methods do not accurately represent time-rate data from unconventional reservoirs. Rushing et al. (2007) continued the work previously performed by

Maley and further provided evidence that using a hyperbolic exponent greater than one yields a significant over estimate of EUR. The authors also made the important observation that the *b*-parameter tends to decrease with time. These observations were further confirmed by Lee and Sidle (2010).

Fracture conductivity greatly influences the type of flow regimes observed in an unconventional reservoir system that has been stimulated by a hydraulic fracturing treatment. Fracture conductivity, in its dimensionless form is defined as:

$$F_{CD} = \frac{k_f w_f}{k X_f} \quad \text{.....(2.6)}$$

Where F_{CD} is dimensionless fracture conductivity, k_f is fracture permeability, w_f is width of the fracture, k is matrix permeability, and x_f is fracture half-length. In the traditional sense, a high fracture conductivity yields a linear flow response and a low fracture conductivity yields a bilinear flow response. Okouma *et al.* (2012) discusses that multi-fractured horizontal wells typically exhibit linear, bilinear, and multi-fractured flow. The authors provide a comprehensive review of decline curve analysis methods used for forecasting production from multi-fractured horizontal wells. The authors discuss that when the *b*-parameter is greater than one, power-law flow regime equations can be developed from Arp's hyperbolic relation. When the time-rate data exhibits a half-slope (1:2) on a logarithmic axis, it corresponds to linear flow. Linear flow is indicative of high conductivity fractures. The corresponding power-law flow regime equation is defined as:

$$q(t) = \frac{a_{LF}}{\sqrt{t}} \quad \text{.....(2.7)}$$

Where a_{LF} is a constant linear flow parameter. When the time-rate data exhibits a quarter-slope (1:4) on a logarithmic axis, it corresponds to bilinear flow. Bilinear flow is indicative of low / very low conductivity fractures. The corresponding power-law flow regime equation is defined as:

$$q(t) = \frac{a_{BLF}}{\sqrt[4]{t}} \quad \text{.....(2.8)}$$

Where a_{BLF} is a constant bilinear flow parameter. When the time rate-data exhibit a one-third slope (1:3) on a logarithmic axis, we believe this corresponds to a multi-fracture flow scenario. This is occasionally observed in practice as well as simulations with multiple vertical and horizontal fractures. The corresponding (one-third) power-law flow regime equation is defined as:

$$q(t) = \frac{a_{MFF}}{\sqrt[3]{t}} \quad \text{.....(2.9)}$$

Where a_{MFF} is a constant multi-fracture flow parameter. Okouma *et al.* (2012) made the observation that **Eqs. 2.7 – 2.9** could all be obtained from Arp's hyperbolic equation (**Eq. 2.3**) when a *b*-parameter greater than one was used, along with a simplifying assumption. These observations are summarized below:

- Substituting b=2 into **Eq. 2.3** (assuming $bD_it >> 1$) yields the linear flow relation (**Eq. 2.7**)
- Substituting b=4 into **Eq. 2.3** (assuming $bD_it >> 1$) yields the bilinear flow relation (**Eq. 2.8**)
- Substituting b=3 into **Eq. 2.3** (assuming $bD_it >> 1$) yields the multi-fracture flow relation (**Eq. 2.9**)

It needs to be noted that in multi-fractured horizontal wells these aforementioned flow regimes are only observed during early and transient periods. They are not observed during transitional and

late-life producing periods. This further enforces the ideology that extrapolation of the Arps' hyperbolic relation for cases where $b > 1$ yields over estimations of EUR and future production performance. However, if properly constrained (*i.e.*, using an exponential terminal decline), the hyperbolic relation can accurately represent time-rate data from multi-stage hydraulically fractured horizontal wells. As mentioned before, this needs to be done with extreme care because it can lead to highly variant estimates for ultimate recovery.

The technique of "constraining" the hyperbolic relation with an exponential terminal decline is commonly referred to as the modified hyperbolic decline curve model. It was introduced by Robertson (1988) and is by far the most commonly applied decline curve model within the petroleum industry for multi-fractured horizontal unconventional wells. This method allows for Arps' hyperbolic relation to represent the transient portion of the data with a *b*-parameter greater than one and then use Arps' exponential decline relation during late life production to constrain the forecast. The issue arises on determining at what point to change from hyperbolic decline to exponential decline, which was investigated as a part of this research. Robertson's (1988) modified hyperbolic time-rate equation is defined as:

$$q(t) = \begin{Bmatrix} \dfrac{q_i}{(1+bD_i t)^{1/b}} & (t < t^*) \\ q_i^* \exp[-D_{\min}(t - t^*)] & (t > t^*) \end{Bmatrix} \quad \text{.....(2.10)}$$

Where $q(t)$ is flowrate, q_i is the theoretical initial flowrate, b is the hyperbolic decline constant, D_i is the initial rate of decline, t^* is the time at which the function changes to exponential decline, q_i^* is the flowrate at t^*, and D_{min} is the minimum loss-ratio.

The power-law exponential decline curve model was presented by Ilk *et al.* (2008, 2009) as a better model to accurately represent fracture-dominated flow in high pressure, high temperature tight gas

wells. The model is derived from the observation that the *D*-parameter (reciprocal loss-ratio) exhibits power-law behavior. The power-law exponential time-rate model is defined as:

$$q(t) = \hat{q}_i \exp[-\hat{D}_i t^n - D_\infty t] \quad \text{.....(2.11)}$$

Where $\hat{q}_i$ is the initial rate parameter, $\hat{D}_i$ is the initial decline parameter, *n* is the time exponent, and D_∞ is the terminal decline parameter. To properly use the power-law exponential the loss-ratio (**Eq. 2.1**) and loss-ratio derivative (**Eq. 2.2**) must be calculated for the data. If power-law behavior is observed in the *D*-parameter, the model is calibrated to the data by varying the $\hat{D}_i$ and *n* parameters. Once the decline parameters are calibrated, the time-rate data projection is obtained by varying the $\hat{q}_i$ parameter. If a non-zero D_∞ value is used, there is no direct integration for the power-law exponential and therefore the cumulative production must be calculated numerically.

The stretched exponential was introduced by Valkó (2009) around the same time of the power-law exponential was initially proposed, although these relations were created independently. Valkó (2009) developed the stretched exponential model from analysis of monthly production from the Barnett Shale. It is almost identical to the power-law exponential; however, it does not include a terminal decline parameter. Therefore, there is a direct integration for calculating cumulative production. The equation itself is a historic statistical function and has been used for other engineering applications before being applied to forecasting time-rate data from oil and gas production wells. It was first introduced in physics literature by Kohlrausch (1847) and also mentioned by Phillips (1996) and Kisslinger (1993) in their respective articles. It is generally used to represent decay in chaotic heterogeneous systems, such as aftershock and decay rates. The time-rate equation for the stretched exponential is defined as:

$$q(t) = q_o \exp[-(t/\tau)^n] \quad \text{.....(2.12)}$$

Where q_o is the initial rate parameter, n is the time exponent, and τ is the time parameter. Valkó (2009) states that first a value for n needs to be assumed, and then the recovery potential is calculated using the following equation:

$$rp = 1 - \frac{Q(t)}{EUR} = \frac{1}{\Gamma\left[\frac{1}{n}\right]} \Gamma\left[\frac{1}{n}, -\ln\frac{q}{q_o}\right] \quad \text{.....(2.13)}$$

Where Γ is the complete and incomplete Gamma Function. A cartesian plot of recovery potential versus dimensionless cumulative production is then generated. The n-parameter is adjusted until a straight line appears and the y-intercept is 1. Estimated ultimate recovery is the x-intercept of the straight line. The τ-parameter is then adjusted to obtain the rate profile.

Duong (2011) developed his method to attempt to describe long-term transient flow performance. The respective time-rate equation for Duong's Method is defined as:

$$q(t) = q_1 t^{-m} \exp\left[\frac{a}{1-m}\left(t^{1-m} - 1\right)\right] \quad \text{.....(2.14)}$$

Where q_1 is the initial rate parameter, m is the time exponent, and a is a model parameter. A logarithmic plot of production rate divided by cumulative production versus time is generated to determine the a- and m-parameters. Power-law behavior must be observed in order to correctly estimate values for a and m. The a-parameter is the intercept of the straight line and the m-parameter is the slope. If this plot does not yield a straight-line then Duong's method does not apply to this data set. The a- and m-parameters are then used to calibrate the q_1-parameter.

Clark *et al.* introduced the logistical growth model in 2011. This model is a hyperlogistic form of the generalized logistical growth model [Blumberg 1968]. The form that is used for modeling time-rate data was adapted from Spencer and Coulombe (1966), who used it to model the regrowth of livers. The foundation of the logistical growth model is the cumulative production relation, which was then differentiated to obtain the time-rate relation. The cumulative production relation for the logistical growth model is defined as:

$$Q(t) = \frac{Kt^n}{a + t^n} \quad \text{.....(2.15)}$$

Where K is the carrying capacity, n is the hyperbolic exponent, and a is a model parameter. **Eq. 2.15** is a growth equation and therefore is used for calculating cumulative oil or gas production, as mentioned before. The derivative of **Eq. 2.15** yields the time-rate form of the logistical growth model, which is defined as:

$$q(t) = \frac{dQ(t)}{dt} = \frac{Knat^{n-1}}{(a + t^n)^2} \quad \text{.....(2.16)}$$

The logistical growth model is suitable for modeling transient and transitional flow remines, due to the shift in the loss-ratio derivative (see **Appendix E**).

The development of all of the decline curve models mentioned above is included in the **Appendix**. All of these models are be entirely empirical, with the exception of the Arps' exponential decline which Camacho and Raghavan (1989) later showed could be derived from pseudo-steady state production of a slightly compressible fluid at a constant pressure. The aforementioned decline curve analysis models attempt to accurately represent a particular observation made within the data, such as power-law behavior, boundary dominated flow, or long-term transient flow. Okouma

et al. (2012) provides an exhaustive review of the practical applications for each of the presented time-rate models.

CHAPTER III

MODEL DEVELOPMENT

The purpose of this chapter is to outline the workflow performed for this research in order to validate and provide an exhaustive review of the investigated decline curve analysis models. A general overview of the mechanistic model, the validation cases performed, and how each decline curve was analyzed is first presented. Next, the discretization of the reservoir system used in the mechanistic model is discussed. Finally, the mechanistic model used is validated by comparing it to known analytical solutions. This is performed to ensure accurate results are provided and to confirm that they can be used to validate the decline curve analysis models.

3.1. Overview

In this section we will discuss the capabilities and process of the built-for-purpose mechanistic model that was developed in order to validate the decline curve analysis models. This reservoir simulator was developed using the FORTRAN programing language. The code is based on the TOUGH+ single-phase non-isothermal mechanistic model developed at the Lawrence National Laboratory. It was then expanded in order to represent non-isothermal, three-component (oil, water, and gas) flow in porous media.

With the mechanistic model, an array of different input properties and parameters were used to accurately represent different prolific unconventional resource plays in the United States. The following unconventional plays were focused on to provide "typical" input properties and parameters for the mechanistic model:

- Haynesville Shale – Texas-Louisiana Salt Basin

- Eagle Ford Shale – Western Gulf Basin
- Wolfcamp Shale – Permian Basin

The ability of the decline curve analysis models to properly represent both mechanistic and non-mechanistic behaviors exhibited by these reservoirs was investigated, including:

- Pressure-dependent reservoir and fracture properties.
- Multiphase behavior of black oil, compositional, and dry gas reservoirs.
- Non-constant pressure production.
- Flowback conditions, where there is high water production through the fractures.

The mechanistic model was developed to accurately represent each of these non-mechanistic behaviors.

Each of the decline curve models were calibrated to each mechanistic validation simulation. In the validation cases, the entire simulated production history was used to calibrate each of the decline curve analysis models in order to obtain insight into late-life behaviors. The effect of the amount of producing time use to calibrate each decline curve relation was also investigated as part of this research in order to evaluate which decline curves can most accurately forecast future performance with the least amount of data. The decline curve models will each be calibrated using the technique described in their respective original papers. The use of "*qDb*" plots was also implemented into this research to allow for a higher resolution analysis of how well the decline curve model represented the time-rate data. The creation of these "*qDb*" plots is based on the original definitions of loss-ratio and loss-ratio derivative, which were introduced by Johnson and Bollens (1927), and then highlighted by Ilk (2008).

The definitions of "loss-ratio" and the "derivative of loss-ratio" are given as:

$$\frac{1}{D} \equiv -\frac{q(t)}{dq(t)/dt} \qquad \text{(Definition of the loss-ratio) ……..(3.1)}$$

$$b \equiv \frac{d}{dt}\left[\frac{1}{D}\right] \equiv \frac{d}{dt}\left[\frac{q(t)}{dq(t)/dt}\right] \qquad \text{(Derivative of the loss-ratio) …….(3.2)}$$

In this research, we work in terms of the reciprocal of Eq. 3.1 (i.e., we want to solve for the $D(t)$-parameter), which is defined as:

$$D(t) \equiv -\frac{1}{q(t)}\frac{dq(t)}{dt} \qquad \text{(Definition of the reciprocal loss-ratio) …….(3.3)}$$

Once all of this analysis was completed, each decline curve was individually analyzed for all production periods that have been mentioned previously. This in-depth analysis is the foundation for the validation and ranking for each of the respective decline curve analysis models. **Fig. 3.1** is a visual representation of the workflow that has been described above.

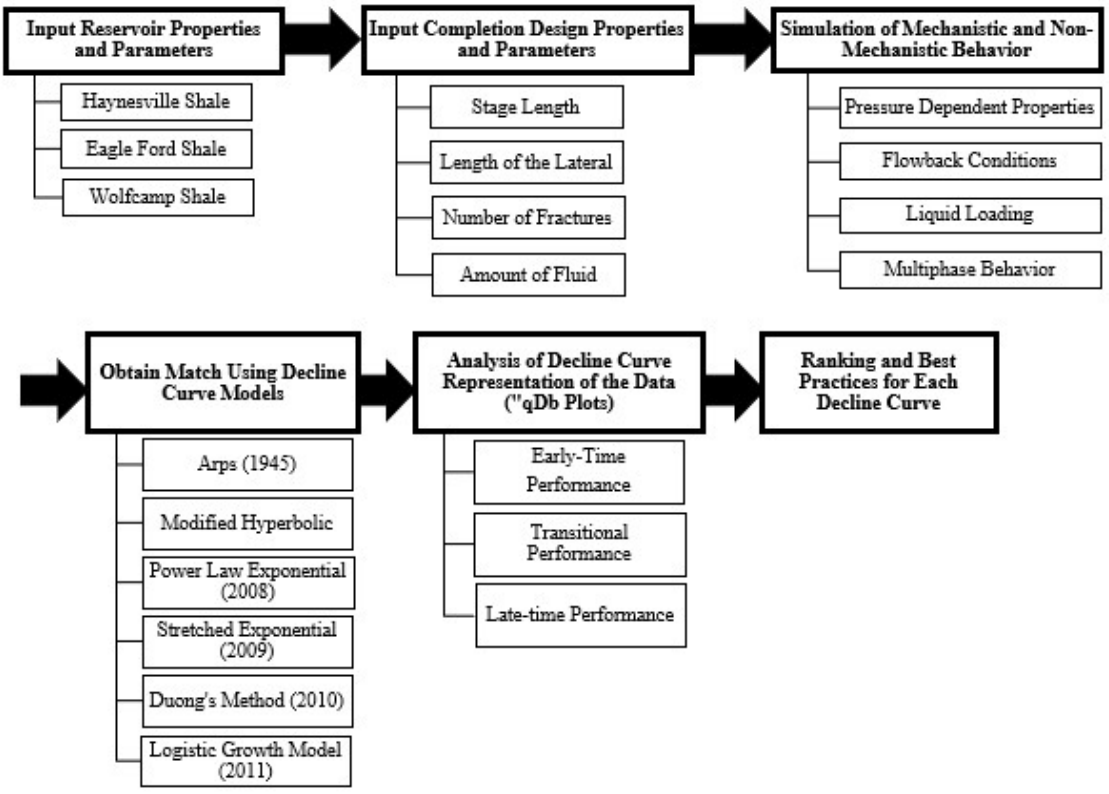

Figure 3.1 — Workflow for mechanistic model validation of decline curve analysis models for unconventional reservoirs.

3.2. Geometry and Discretization of the Simulated System

Similar to Moridis *et al*. (2010) the behavior of the unconventional reservoirs and the associated hydraulic fracture was represented by a stencil, which is defined as the minimum repeatable and symmetric element in which the system is subdivided by the horizontal well and the hydraulic fractures. The production simulated data from the discretized stencil was then upscaled until the entire horizontal well and the associated hydraulic fractures were represented. **Fig. 3.2** is a representation of what each stencil looks like that was used within the mechanistic model.

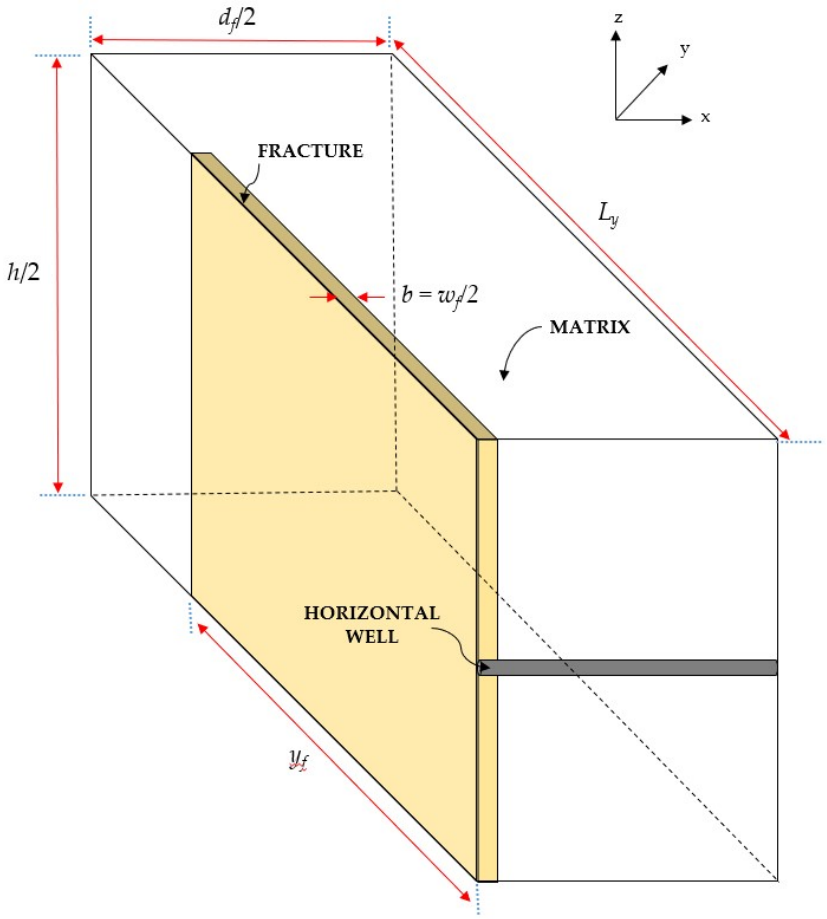

Figure 3.2 — Schematic diagram of a stencil used to represent a fracture in a multi-fractured horizontal well.

In the *x*-direction, the gridblocks were finely discretized logarithmically, increasing in size in the direction moving away from the fracture face (approximately 50 gridblocks). In the *y*-direction it was finely discretized increasing in size moving away from the horizontal well (approximately 50 gridblocks). In the *z*-direction, it was discretized with uniform-size subdivisions except near the wellbore (approximately 30 gridblocks).

3.3. Mechanistic Model Validation

Each of the three-components (oil, water, and gas) within the mechanistic model were validated independently using respective analytical flow equations. The governing equations for the

mechanistic model can be found in **Appendix I**. Further information regarding the thermophysical properties used within the mechanistic model can be found in **Appendix J**.

3.3.1. Validation of the Oil Component Module

To validate the simulated results for the oil component module of the mechanistic model it was compared to the analytical flow solution for a slightly compressible fluid produced from a vertical well at a constant rate in a closed homogeneous, isotropic reservoir. The analytical solution in the Laplace domain for pressure distribution in the reservoir is defined as:

$$\mathcal{L}\left\{\bar{p}_D(r,s)\right\} = \frac{K_1(r_{eD}\sqrt{s})\times I_0(r_D\sqrt{s}) + I_1(r_{eD}\sqrt{s})\times K_0(r_D\sqrt{s})}{s^{3/2}[I_1(r_{eD}\sqrt{s})\times K_1(\sqrt{s}) - I_1(\sqrt{s})\times K_1(r_{eD}\sqrt{s})]} \quad \text{.....(3.4)}$$

Where

$$p_D = \frac{2\pi kh[p_i - p(r,t)]}{q\mu} \quad \text{.....(3.5)}$$

$$t_D = \frac{kt}{\phi\mu c_t r_w^2} \quad \text{.....(3.6)}$$

$$r_D = \frac{r}{r_w} \quad \text{.....(3.7)}$$

$$r_{eD} = \frac{r_e}{r_w} \quad \text{.....(3.8)}$$

This analytical solution was first presented by Muskat in 1934 and then by Van Everdingen in 1949. In order to obtain the analytical solution in the real domain the Gaver-Stehfest algorithm was applied to **Eq. 3.4**.

The properties and parameters used in this validation case for the oil component in the mechanistic model can be found in **Table 3.1**.

Table 3.1 — Reservoir and fluid properties used for the validation of the oil component in the mechanistic model. Closed circular reservoir containing a slightly compressible fluid being produced at a constant rate.

Reservoir Properties:		
Net pay thickness, h	=	65 ft
Formation permeability, k	=	150 mD
Wellbore radius, r_w	=	0.23 ft
Reservoir radius, r_e	=	3280 ft
Formation compressibility, c_f	=	7×10^{-6} psi^{-1}
Porosity, ϕ	=	0.16 (fraction)
Initial reservoir pressure, p_i	=	4640 psi
Skin factor, s	=	0.00 (dimensionless)
Reservoir Temperature, T_r	=	160 °F
Fluid Properties:		
Oil specific gravity, γ_o	=	0.75 (water = 1)
Oil compressibility, c_f	=	1.7×10^{-5} psi^{-1}
Oil viscosity, c_f	=	1.0 cP
Production Parameters:		
Constant production rate, q_0	=	82 BOPD

Fig. 3.3 is the pressure distribution throughout the reservoir for both the analytical solution and the mechanistic model at 10 days, 100 days, 1 year, and 10 years. The mechanistic model was able to produce near identical results as the analytical solution, validating the oil component module used within the mechanistic model.

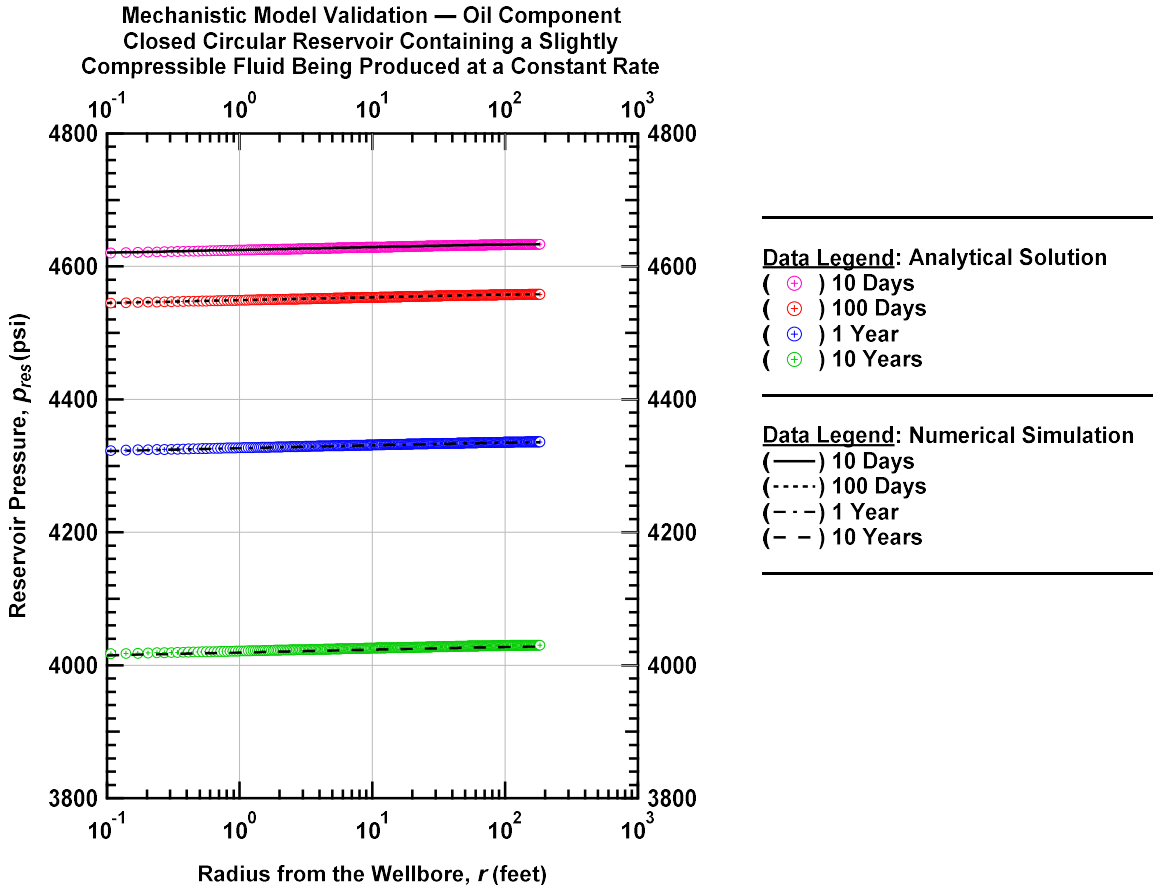

Figure 3.3 — Reservoir pressure (p_{res}), versus radius from the wellbore (r) at different producing times. Mechanistic Model Validation – Oil Component. Closed circular reservoir containing a slightly compressible fluid being produced at a constant rate.

3.3.2. Validation of the Gas Component Module

To validate the simulated results for the gas component module of the mechanistic model it was compared to the analytical solution for gas flow in a finite circular homogeneous, isotropic reservoir that is being produced at a constant rate. The diffusivity equation for this situation can be represented by the following equation:

$$p_D(t_D, r_D) \frac{1}{2} E_1 \left[\frac{r_D^2}{4t_D} \right] \quad \text{.....(3.9)}$$

Where

$$p_D = \frac{kh[p_{pi} - p_p(r,t)]}{q\mu} \quad \text{.....(3.10)}$$

$$t_D = \frac{kt}{\phi\mu c_t r_w^2} \quad \text{.....(3.11)}$$

$$r_D = \frac{r}{r_w} \quad \text{.....(3.12)}$$

$$p_p = 2\int_{p_r}^{p} \frac{p}{\mu z} dp \quad \text{.....(3.13)}$$

The properties and parameters used in this validation case for the gas component in the mechanistic model can be found in **Table 3.2**.

Table 3.2 — Reservoir and fluid properties used for the validation of the gas component in the mechanistic model. Closed circular reservoir containing a slightly compressible fluid being produced at a constant rate.

Reservoir Properties:

Net pay thickness, h	=	72 ft
Formation permeability, k	=	150 mD
Wellbore radius, r_w	=	0.23 ft
Reservoir radius, r_e	=	180ft
Formation compressibility, c_f	=	7 x 10^{-6} psi^{-1}
Porosity, ϕ	=	0.15 (fraction)
Initial reservoir pressure, p_i	=	4640 psi
Skin factor, s	=	0.00 (dimensionless)
Reservoir Temperature, T_r	=	160 °F

Fluid Properties:

Gas specific gravity, γ_g	=	0.65 (air = 1)

Production Parameters:

Constant production rate, q_g	=	0.3 kg/s

Fig. 3.4 is the pressure distribution throughout the reservoir for both the analytical solution and the mechanistic model at 10 days, 100 days, 1 year, and 10 years. The mechanistic model was able to produce near identical results as the analytical solution, validating the gas component module used within the mechanistic model.

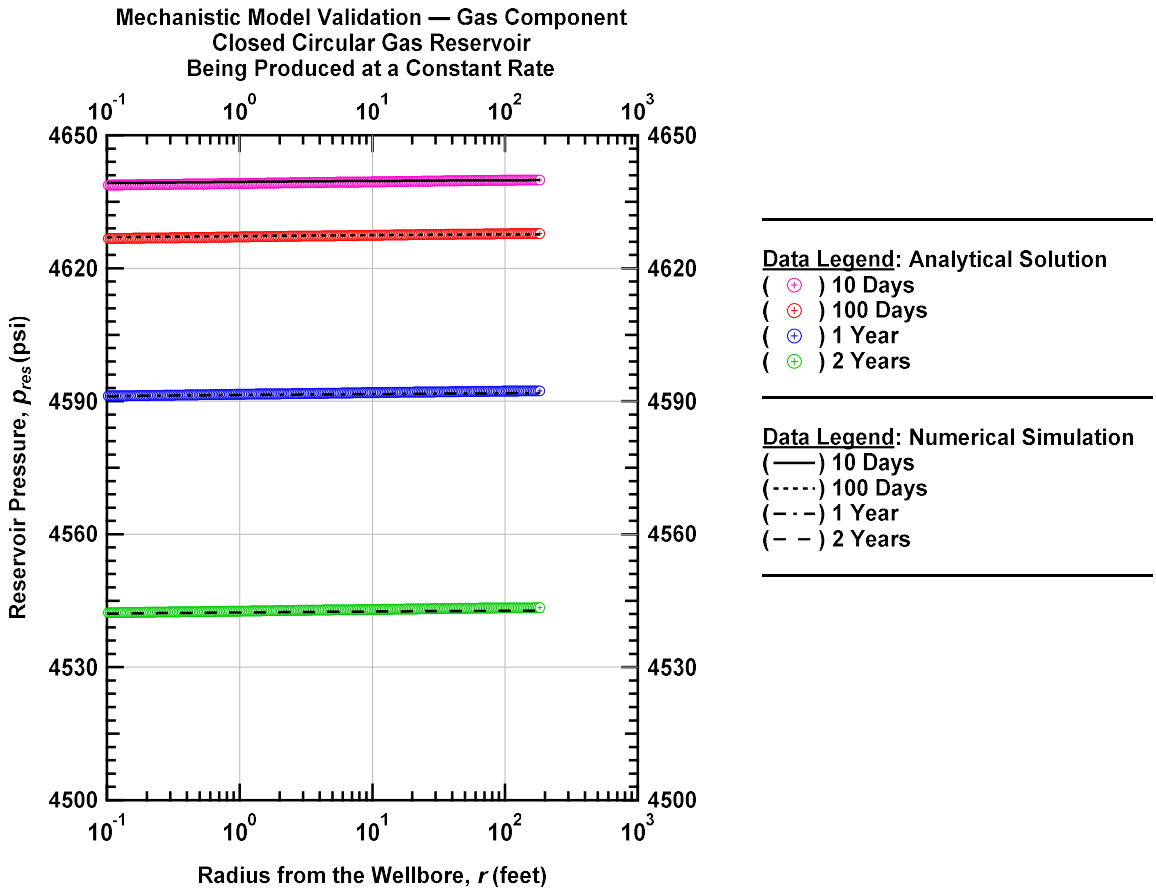

Figure 3.4 — Reservoir pressure (p_{res}), versus radius from the wellbore (r) at different producing times. Mechanistic Model Validation – Gas Component. Closed circular reservoir containing a slightly compressible fluid being produced at a constant rate.

3.3.3. Validation of the Water Component Module

To validate the simulated results for the water component module of the mechanistic model they were compared to the Geothermal Model Intercomparison Study (1980). In this study the

simulated results from multiple "bench mark" simulators were compared to the analytical solution for a slightly compressible fluid being produced at a constant rate from an infinite acting homogeneous, isotropic reservoir. This is also referred to as the line-source solution, which is defined as:

$$p_D(t_D, r_D)\frac{1}{2}E_1\left[\frac{r_D^2}{4t_D}\right] \quad \text{.....(3.9)}$$

Where

$$p_D = \frac{2\pi kh[p_i - p(r,t)]}{q\mu} \quad \text{.....(3.5)}$$

$$t_D = \frac{kt}{\phi\mu c_t r_w^2} \quad \text{.....(3.6)}$$

$$r_D = \frac{r}{r_w} \quad \text{.....(3.7)}$$

The properties and parameters used in this validation case for the water component in the mechanistic model can be found in **Table 3.3**.

Table 3.3 — Reservoir and fluid properties used for the validation of the water component in the mechanistic model. Infinite acting reservoir containing a slightly compressible fluid being produced at a constant rate.

Reservoir Properties:		
Net pay thickness, h	=	328 ft
Formation permeability, k	=	150 mD
Reservoir radius, r_e	=	5000ft ("infinite" acting)
Formation compressibility, c_f	=	0 psi^{-1}
Porosity, ϕ	=	0.20 (fraction)
Initial reservoir pressure, p_i	=	1305 psi
Skin factor, s	=	0.00 (dimensionless)
Reservoir Temperature, T_r	=	500 °F
Production Parameters:		
Constant production rate, q_g	=	1400 kg/s

Fig. 3.5 is a recreation of Figure 1 from the Geothermal Model Intercomparison Study (1980) along with the simulated results using the mechanistic model from this study. The mechanistic model was able to produce near identical results as the analytical solution and the other numerical simulators validating the water component module used within the mechanistic model.

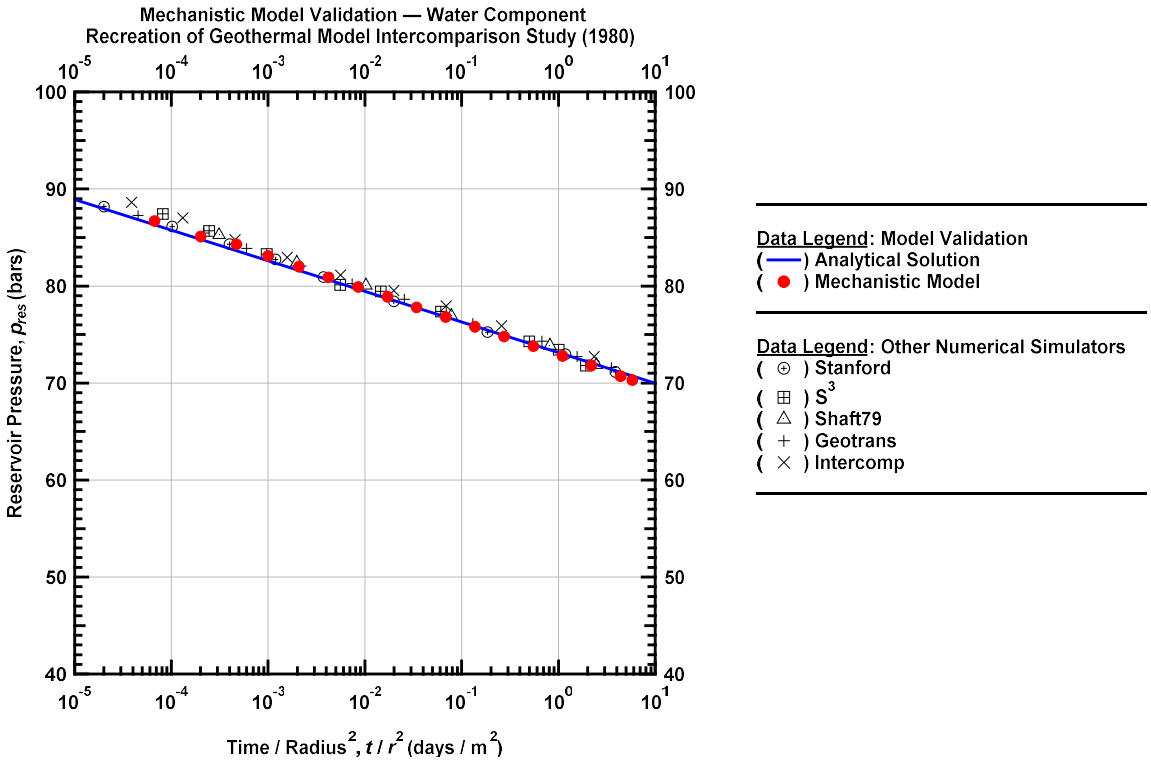

Figure 3.5 — Reservoir pressure (p_{res}), versus time / radius^2 (t / r^2) at different producing times. Mechanistic Model Validation – Water Component. Recreation of Geothermal Model Intercomparison Study (1980).

CHAPTER IV

FIELD PRODUCTION DATA VALIDATION

In this chapter, the difficulty of applying decline curve analysis to unconventional reservoirs time-rate data is discussed. Time-rate data for an unconventional South Texas oil well is presented and decline curve analysis is performed. The same methodology applied here will also be used with the validation cases from the mechanistic model. The estimated ultimate recovery (EUR) values for each DCA model is compared to demonstrate the non-uniqueness of this type of analysis.

4.1. South Texas Well F

Production data from horizontal hydraulically fractured wells is often quite erratic, due to a magnitude of factors, including the non-mechanistic behaviors mentioned previously, as well as offset production and operations. **Fig. 4.1** and **Fig. 4.2** are the production history plots for South Texas Well F. This well was hydraulically fractured in an unconventional reservoir. There is approximately 400 producing days of time-rate data available, however, there is no clear trend within the data after about 320 days, therefore none of the time-rate data after this point was used for analysis. The inconsistent behavior can easily be identified within the production data of not only oil, but also gas and water. This behavior may be caused by offset operations or the effects of liquid loading. **Fig. 4.2** shows that once gas evolves before reaching the wellhead (*i.e.,* pressure falls below bubble point), there is a clear change in the production decline profile of the well, along with more noise in the data. Prior to analysis, the data set was edited to remove any erroneous data points in the data set. To develop the "*qDb*" plots the Bourdet (1989) derivative algorithm was applied using the rate-time production data.

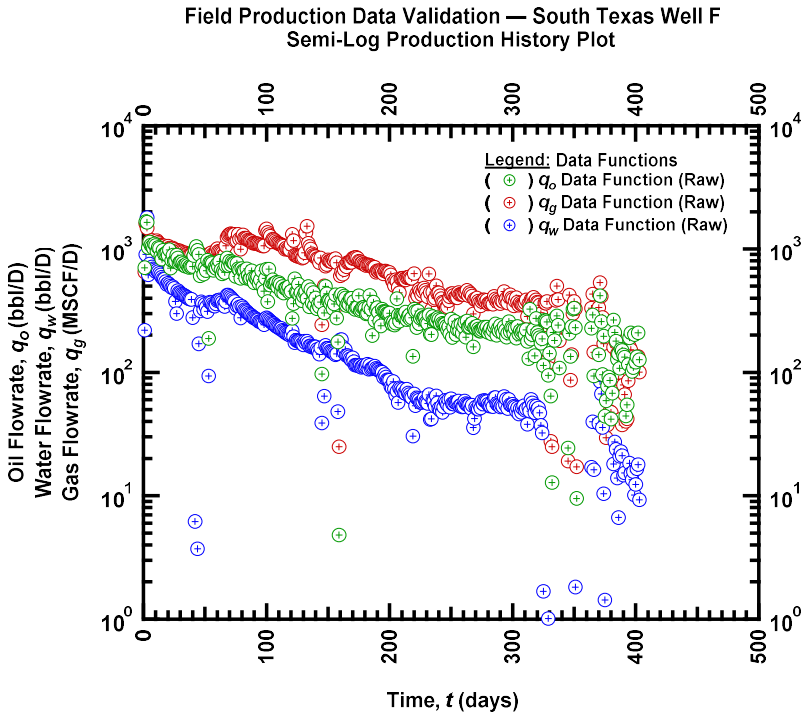

Figure 4.1 — (Semi-log Plot) Oil flowrate (q_o), water flowrate (q_w), and gas flowrate (q_g) versus producing time (t). Production history plot – South Texas Well F.

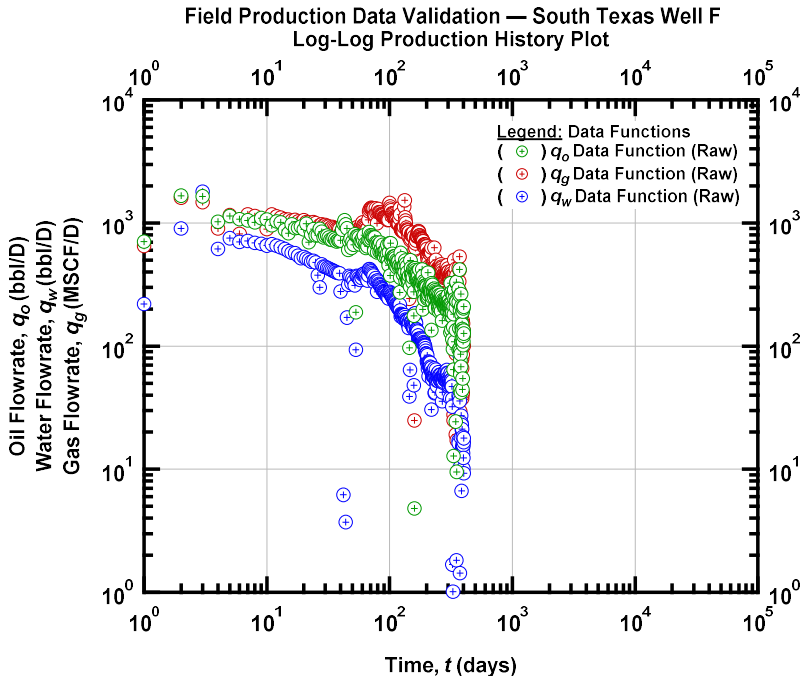

Figure 4.2 — (Log-log Plot) Oil flowrate (q_o), water flowrate (q_w), and gas flowrate (q_g) versus producing time (t). Production history plot – South Texas Well F.

Fig. 4.3 is the flowing tubing pressure for this well. This is included to demonstrate that using the assumption of constant pressure production throughout an entire wells production history is not valid for modeling unconventional reservoirs. Simulating constant-rate production has been used as a proxy for non-constant pressure production. If this is methodology is implemented then rate-normalized pressure needs to be used for the analysis [Collins 2014]. In **Fig. 4.3** there is a clear pressure decline, which constant-rate with rate-normalized pressure can accurately represent. However, the well is then produced at near constant pressure production. If the constant-rate solution is applied, the bottomhole pressure will continue to decline (asymptotically). This does not properly represent the actual production pressure file of many unconventional oil wells. Constant pressure production often occurs once a rod-pump is used for artificial lift. In **Fig. 4.3**, both edited and non-edited data is included for Well F. You can clearly see the "sporadic" behavior of the pressure during this "constant" pressure production phase, this is likely due to liquid-loading.

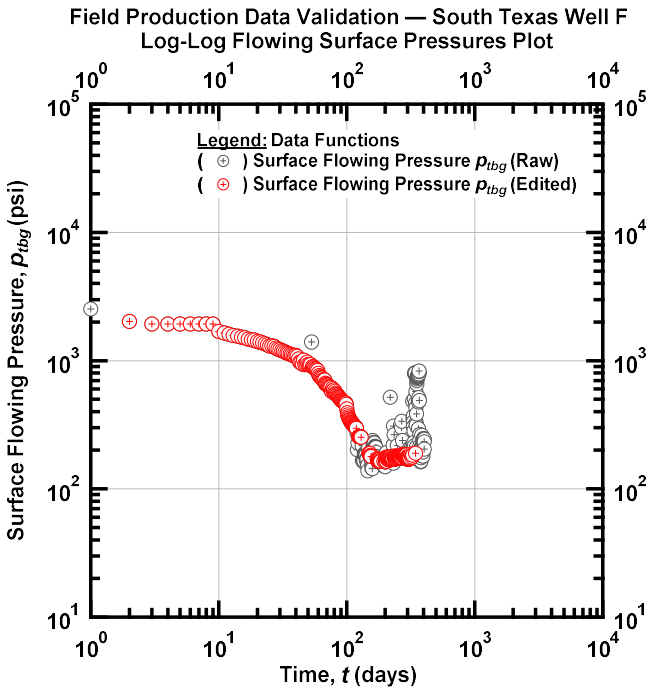

Figure 4.3 — (Log-log Plot) Surface flowing pressure (p_{tbg}) versus producing time (t). Production pressure history plot – South Texas Well F.

The calibrated decline curve analysis models for Well F can be seen in **Fig. 4.4**. **Fig. 4.4** is referred to as a "*qDb*" plot and the oil-rate data, *D*-parameter, and *b*-parameter are included on it to assist with decline curve analysis. This plot will be the standard for the comparison and validation of the decline curve models in this research. The equations for time-rate, *D*-parameter, and *b*-parameter for each of the decline curves investigated in this study can be found in the **Appendix**. The calculated *D*-parameter exhibits power-law behavior, which is expected and common in unconventional reservoirs. By observing **Fig. 4.4** it is evident that each of the decline curve analysis models adequately represent the oil production time-rate data, but there is large degree of variation with their respective projections of future performance.

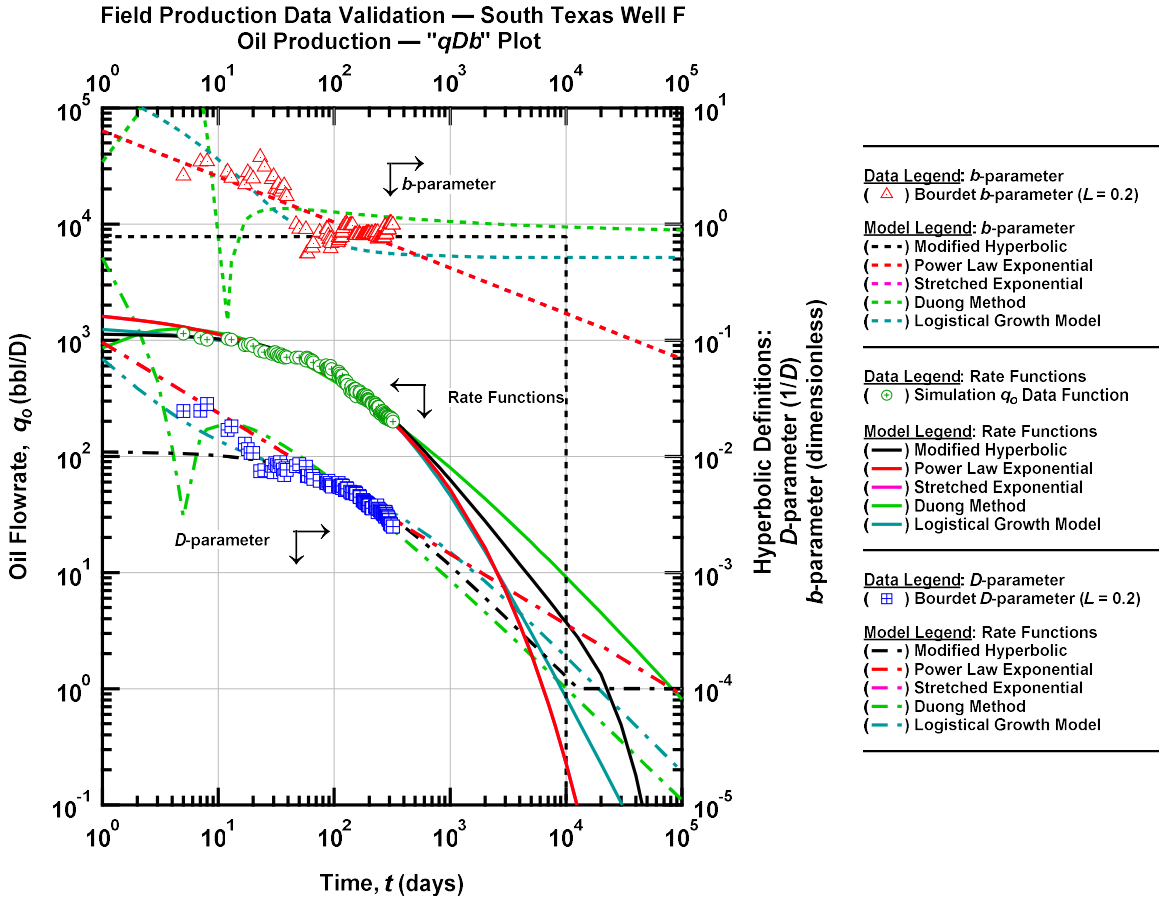

Figure 4.4 — (Log-log Plot) "*qDb*" plot – South Texas Well F. Decline curve analysis methods representation of the time-oil rate data.

4.1.1. Modified Hyperbolic

The modified hyperbolic is the standard decline curve analysis model in the oil and gas industry for forecasting time-rate data from unconventional reservoirs. The model projected the second highest EUR for this validation example. A common assumption for D_{min} of 10 percent/year was used. The issue with this assumption is that if did not affect the flowrate projection until after 12,000 days (32.8 years). Typically wells production is forecasted for 30 years, therefore this assumption made no difference in the EUR projection. Using the mechanistic model, we can and will evaluate a better assumption for D_{min}. This will allow engineers to better predict when the modified hyperbolic model will transition from hyperbolic to exponential decline.

4.1.2. Power-Law Exponential and Stretched Exponential

Due to the short producing time of Well F, no late-life effects can be seen within the time-rate data. The power-law exponential and stretched exponential are very similar, but the power-law exponential has a D_∞-parameter that is a terminal decline term to account for late-life producing effects. Determining proper value for D_∞ is one of the objectives of validating these decline curve models with the mechanistic model. In this field data validation case, D_∞ was assumed to be zero, therefore the power-law exponential provides nearly the exact same solution as the stretched exponential. The decline curves models were calibrated to represent the power-law behavior observed in the *D*-parameter. Once the decline parameters were calibrated, the initial flowrate was adjusted so that the models accurately represented the available time-rate data. The *b*-parameter projection for both the power-law exponential and the stretched exponential is decreasing with time, rather than being essentially constant as suggested by the other decline curve analysis models. All of the other decline curve analysis models forecast that the *b*-parameter will be

relatively constant for the entire producing life of the well. The power-law exponential and stretched exponential suggest that the horizontal trend seen within the numerically calculated *b*-parameter of the time-rate data from Well F will not continue, but rather decrease as time goes on. This further validates the necessity of this research to determine if during late-time production the *b*-parameter remains relatively constant or if it decreases with time, as the power-law exponential and stretched exponential are suggesting in this field production data validation case.

4.1.3. Duong's Method

Due to the nature of Duong's Method the oil rate increases initially. This is emphasized in the *b*- and *D*-parameters. Once the forecasted rate projection of Duong's Method begins to decrease the *b*-parameter because roughly constant, but at a higher value relative to the other decline curve models being presented in this validation case. Duong's Method also yielded the highest estimate for EUR. Following the procedure outlined in Duong's original paper, a log-log plot of $q(t)/Q(t)$ versus time is used to determine the *a*- and *m*-parameters within the model. This is a unique approach to determining the decline parameters. The *D*- and *b*-parameter projections of Duong's method are similar to other methods after the initial non-physical behavior in the time-rate model.

4.1.4. Logistical Growth Model

The logistical growth model has a shift in the *b*-parameter, however, unlike Duong's Method this shift may be physical and supported by the data. Looking at the numerically calculated *b*-parameter of the time rate data, the initial values are higher, and then go to a constant value for the remainder of the available time-rate data. The logistical growth model captures this feature, and provides the third lowest estimate for EUR.

Table 4.1 contains all of the parameters used for the decline curve models that are featured in **Fig. 4.4**. As expected, with no D_∞-parameter used for the power-law exponential it yielded nearly identical results to the stretched exponential.

Table 4.1 — Summary of decline curve analysis models parameters for South Texas Well F

Decline Model	q_i or K (STB/D)	D_i or $\hat{D}_i$ or a (1/D)	n or b or m (dim. less)	D_{min} or D_∞ (% / year) or (1/D)
M.HYP	1138.4	0.011	0.780	10
PLE	2055.3	0.244	0.393	0
SEM	2056.3	36.13	0.393	-
DNG	856.41	1.740	1.225	-
LGM	27095	250.0	0.800	-

Table 4.2 contains the EUR estimate for all of the decline curve models. It was assumed that the well is abandoned at 30 years. Duong's Method yielded the highest estimate for EUR, while the power-law exponential forecasted the lowest.

Table 4.2 — Summary of 30-year EUR values determined using different decline curve analysis models parameters for South Texas Well F

Decline Model	EUR_{30yr} Estimate (Mbbl)
M. HYP	339
PLE	258
SEM	258
DNG	428
LGM	262

CHAPTER V

SOLUTION AND RESULTS

In this section three different mechanistic models of prolific onshore U.S. unconventional reservoirs are analyzed using decline curve analysis. First, a single-phase gas mechanistic model representing Haynesville shale located in Louisiana is analyzed. This is a tight-gas reservoir that produces almost entirely methane. Next, a three-phase mechanistic model representing the Eagle Ford shale located in South Texas is analyzed. This reservoir has a broad gas-oil-ratio (GOR) spectrum found within it, but the volatile oil region was the primary focus for this research. Finally, a three-phase mechanistic model representing the Wolfcamp shale is analyzed. The Wolfcamp generally has a lower producing GOR and much higher water-cut as compared the Eagle Ford shale.

5.1. Haynesville Shale Mechanistic Model Validation Case

A single-phase reservoir simulation was completed using the mechanistic model developed for the validation and ranking of the decline curve models in this research. This particular mechanistic model validation case is intended to mimic typical reservoir characteristics and completion design of a well completed in the Haynesville shale. All of the system properties can be found in **Table 5.1**.

Table 5.1 — Reservoir and fluid properties for numerical simulation case – hydraulically fractured well with typical Haynesville shale properties and parameters.

Reservoir Properties:		
Net pay thickness, h	=	200 ft
Formation permeability, k	=	10 nD
Wellbore radius, r_w	=	0.3 ft
Formation compressibility, c_f	=	2 x 10^{-5} psi^{-1}
Porosity, ϕ	=	0.1 (fraction)
Initial reservoir pressure, p_i	=	10,000 psi
Skin factor, s	=	0.00 (dimensionless)
Wellbore storage coefficient, C_D	=	0 (dimensionless)
Reservoir Temperature, T_r	=	300 °F
Fluid Properties:		
Gas specific gravity, γ_o	=	0.68 (air = 1)
Hydraulically Fractured Well Model Parameters:		
Fracture half-length, X_f	=	180 ft
Number of fractures, n_f	=	210
Fracture spacing, s_f	=	40 ft
Horizontal well length, L_w	=	5200 ft
Fracture permeability, k_f	=	20 md
Fracture conductivity, F_{CD}	=	2 (dimensionless)
Production Parameters:		
Flowing Pressure, p_{wf}	=	500 psi

Fig. 5.1 is a log-log plot of all of the simulated gas flowrate data for this well, which spans 30 years of simulated production. **Fig. 5.2** is the same data represented in semi-log format. The production exhibits linear flow (1:2 slope) initially. A boundary-dominated/depletion flow regime begins around 1000 days. The purpose of this simulation is to analyze how well the decline curve analysis models can accurately represent time-rate data that has a long transient period of linear flow, along with a terminal decline behavior.

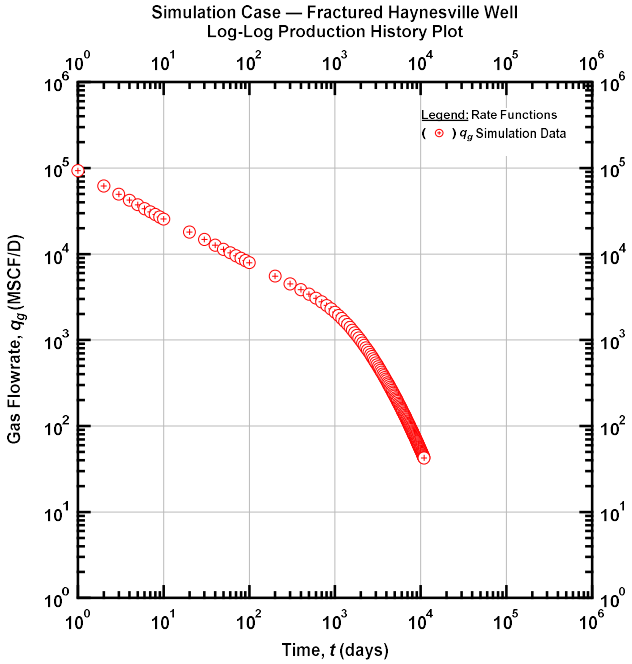

Figure 5.1 — (Log-log Plot) Oil flowrate (q_o), water flowrate (q_w), and gas flowrate (q_g) versus producing time (t). Production history plot – Simulation case fractured Haynesville shale well.

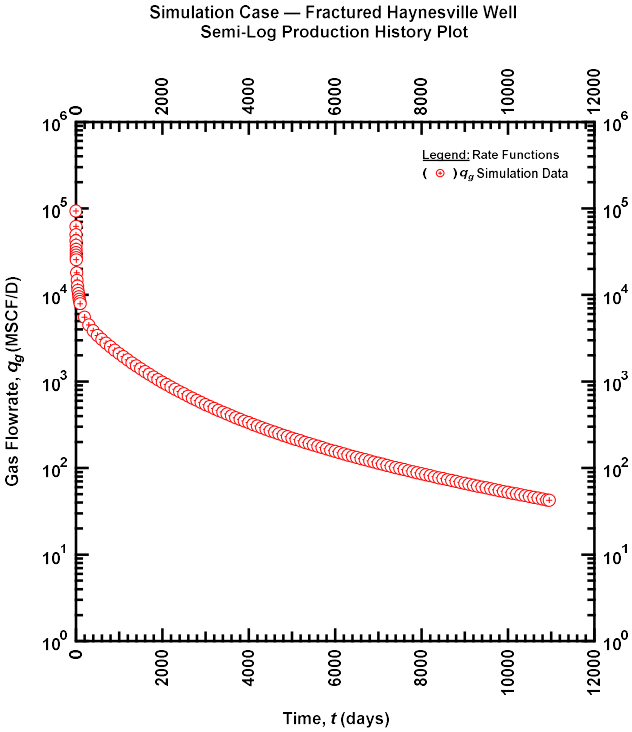

Figure 5.2 — (Semi-log Plot) Oil flowrate (q_o), water flowrate (q_w), and gas flowrate (q_g) versus producing time (t). Production history plot – Simulation case fractured Hayneville shale well.

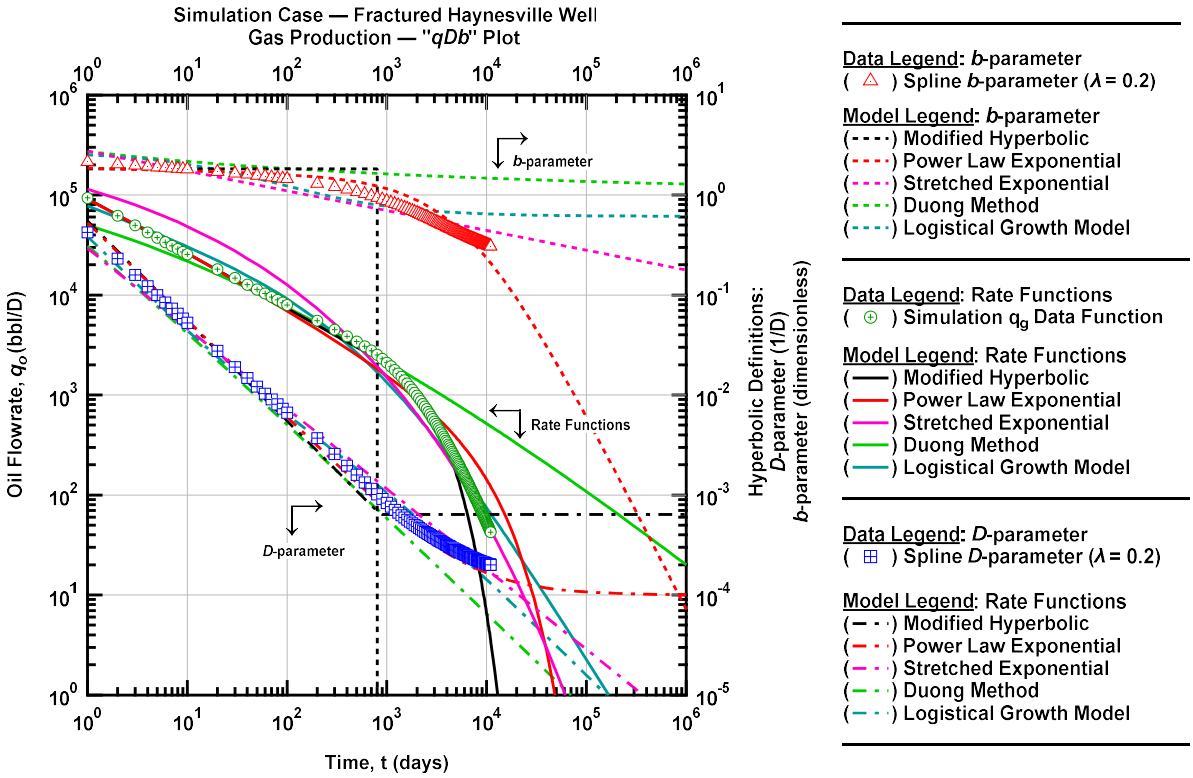

Figure 5.3 — (Log-log Plot) "*qDb*" plot – Haynesville shale simulation case. Decline curve analysis methods representation of the time-oil rate data.

For this validation case, as well as the other mechanistic model validations, a spline was applied to the oil-rate to compute the *D*- and *b*-parameters as a function of time, these results are presented in the "*qDb*" plot (log-log format) in **Fig. 5.3** [Ilk, 2010]. The same decline curves were matched to the data, as were used in the field production data validation example. The entire simulated production history was used to calibrate the decline parameters for each of the decline curve analysis models. The purpose of this is to investigate how accurately each of the decline curve models is able to represent the entirety of the wells production profile. Also, this effort provides insight into determining proper late-life parameters values to be applied to field data cases. Proper values for late-life parameters is vital in obtaining accurate estimates for ultimate recovery. Power-law behavior is observed in the *D*-parameter, as suggested by Ilk (2008). It starts to deviate from

this straight-line once terminal decline characteristics begin to become evident in the time-rate data. By observing **Fig. 5.3** it is clear that each of the models adequately represent the simulated production data, but some represent the reciprocal loss-ratio and loss-ratio derivative more appropriately.

5.1.1. Modified Hyperbolic

The modified hyperbolic over all represented the simulated time-rate data quite well. The exponential tail attached to the hyperbolic equation may be too "aggressive" for this validation case, as noted by the predicted rate projection made by the modified hyperbolic begins to fall below the simulated data during terminal decline. The D_{min}-parameter used in this particular validation case was 6.4% / year, less than the common assumption of 10% / year.

5.1.2. Power-Law Exponential

The power-law exponential predicted the EUR at 30 years for this simulation within a 2% error. In this validation case, unlike field production data example, a value of 1.0E-4 was used for D_∞, instead of a value of 0. A common assumption made for the power-law exponential is to assume that the D_∞-parameter is zero. There are multiple reasons for doing this, one being not a good estimate for the value is known. Another reason is when it is assumed to be zero the time-rate equation for the power-law exponential has a direct integration so cumulative production can be calculated analytically rather than numerically. This validation case suggests that a non-zero D_∞-parameter is useful in correctly representing late-life production behavior. Referring back to field data validation example, it was noted that the b-parameter projection for the power-law exponential was decreasing with time, while other decline curve models (excluding the stretched exponential) suggested that it should remain approximately constant though late-life production.

This validation example confirms that the suggestion of a decreasing *b*-parameter, over the producing life of the well, is a more accurate representation of the time-rate data.

5.1.3. Stretched Exponential

The stretched exponential decline curve model is essentially the same as the power-law exponential without a terminal decline parameter and using different notation. The stretched exponential yielded about the same amount of error in its EUR projection as the power-law exponential, however it represented the time-data differently due to it not including a terminal decline parameter within the model. The power-law exponential *b*-parameter better represented the shape of the simulated time-rate data's calculated *b*-parameter, but the stretched exponential suggests that the *b*-parameter can also be represented as a straight-line and the terminal decline parameter is not necessary. However, the time-rate projection of the stretched exponential does not appear to represent the simulated time-rate data as well. It may yield a small error in EUR, but it does not correctly represent the transient data portion of the simulated time-rate data.

5.1.4. Duong's Method

Duong's Method once again yielded the highest time-rate projection out of all of the models. Due to the nature of the equation the early-time data is not properly represented. The transient flow period observed in the time-rate data is represented well by Duong's Method, however; the decline curve model projects this transient state into the late-life period of the simulated time-rate data and therefore it yields too high of an estimate for rate. This is a general issue when applying Duong's Method.

5.1.5. Logistical Growth Model

The logistical growth model yields a reasonable estimate for EUR. The *b*-parameter for the logistical growth model allows it to decrease during transient flow, but then it remains constant during late-life production. Overall, the logistical growth model appears to follow the correct observed behavior trends, however in practice the equation itself appears too "stiff" to accurately represent the simulated results in the desired fashion.

Table 5.2 contains all of the parameters used for the decline curve models that are featured in **Fig. 5.3**. **Table 5.3** contains the EUR for all of the decline curve models. The stretched exponential had the least amount of error in determining EUR. However, the power-law exponential was only slightly less accurate in terms of EUR but it was better able to represent the transient/transitional flow regimes, as well as the terminal decline.

Table 5.2 — Summary of decline curve analysis models parameters for Haynesville Shale mechanistic model.

Decline Model	q_i or K (STB/D)	D_i or $\hat{D}_i$ or a (1/D)	n or b or m (dim. less)	D_{min} or D_∞ (% / year) or (1/D)
M.HYP	7.61E+6	1.68E+3	1.817	6.4
PLE	8.01E+13	20.59	5.22E-2	1.0E-4
SEM	5.00E+5	0.138	0.198	-
DNG	5.00E+4	0.756	1.065	-
LGM	8.52E+6	67.44	0.634	-

Table 5.3 — Summary of 30-year EUR values determined using different decline curve analysis models for the Haynesville Shale mechanistic model.

Model	EUR_{30yr} (BSCF)	Percent Error
SIM	7.85	
M. HYP	7.20	- 8.19%
PLE	7.75	- 1.16%
SEM	7.86	0.21
DNG	12.5	59.47%
LGM	6.61	- 15.74%

5.2. Eagle Ford Shale Mechanistic Model Validation Case

A three-phase reservoir simulation was completed using the mechanistic model developed for the validation and ranking of the decline curve models in this research. This particular mechanistic model validation case is intended to mimic typical reservoir characteristics and completion design of a well completed in the Eagle Ford shale. It was assumed that all production was coming from the Eagle Ford, and there was no production from surrounding formations such as the Austin Chalk. From a simulation standpoint this means that the discretized system is not as tall as compared to the Wolfcamp model that will be discussed next. This simulation evaluates the decline curve analysis model's ability to accurately represent the time-rate data when linear and bilinear flow regimes cannot be easily identified during transitional flow. It also evaluates the decline curve models ability to accurately represent terminal decline. All of the mechanistic model properties and parameters can be found in **Table 5.4**.

Table 5.4 — Reservoir and fluid properties for numerical simulation case – hydraulically fractured well with typical Eagle Ford shale properties and parameters.

Reservoir Properties:		
Net pay thickness, h	=	200 ft
Formation permeability, k	=	200 nD
Wellbore radius, r_w	=	0.3 ft
Formation compressibility, c_f	=	2 x 10^{-5} psi^{-1}
Porosity, ϕ	=	0.1 (fraction)
Initial reservoir pressure, p_i	=	7,500 psi
Oil saturation, S_o	=	0.58 (fraction)
Skin factor, s	=	0.00 (dimensionless)
Wellbore storage coefficient, C_D	=	0 (dimensionless)
Reservoir Temperature, T_r	=	270 °F
Fluid Properties:		
Oil specific gravity, γ_o	=	0.84 (water = 1)
Gas-Oil-Ratio, GOR	=	1200 scf/bbl
Gas specific gravity, γ_g	=	0.68 (air = 1)
Water specific gravity, γ_w	=	1.0 (water = 1)
Hydraulically Fractured Well Model Parameters:		
Fracture half-length, X_f	=	180 ft
Number of fractures, n_f	=	210
Fracture spacing, s_f	=	40 ft
Horizontal well length, L_w	=	5200 ft
Fracture permeability, k_f	=	20 md
Fracture conductivity, F_{CD}	=	2 (dimensionless)
Production Parameters:		
Flowing Pressure, p_{wf}	=	1325 psi
Producing time, t	=	30 years

Fig. 5.4 is a log-log plot of all of the simulated production flowrate data for this well (oil, water, and gas), spanning 30 years of simulated production. **Fig. 5.5** is the same data represented in semi-log format. The production exhibits a steep decline initially. Linear and bilinear flow regimes are not directly observed. The decline profile of the simulated time-rate data has three apparent different production periods. The first being an initial decline to about 10 days. Then a transitional phase exists to about 500 days, at which terminal decline effects begin to become apparent.

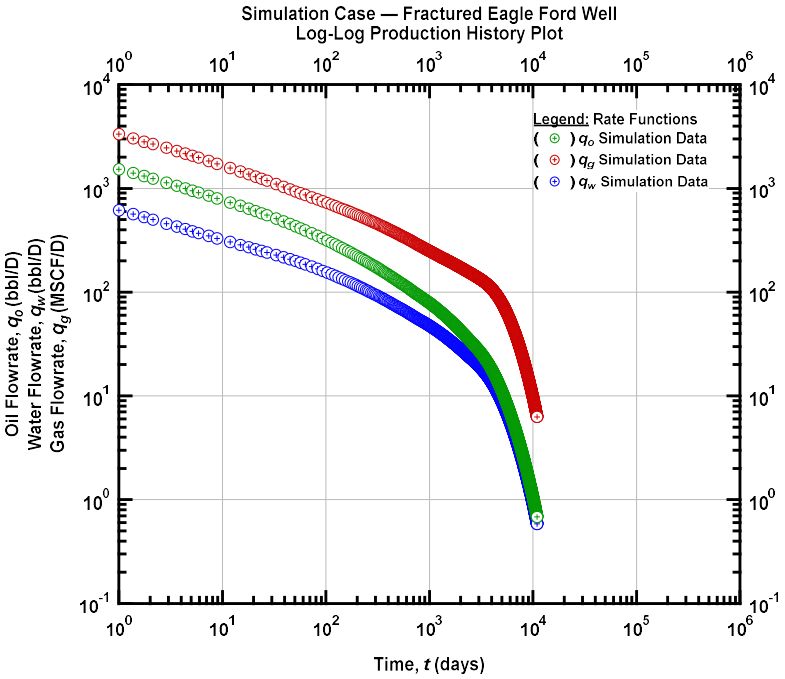

Figure 5.4 — (Log-log Plot) Oil flowrate (q_o), water flowrate (q_w), and gas flowrate (q_g) versus producing time (t). Production history plot – Simulation case fractured Eagle Ford shale well.

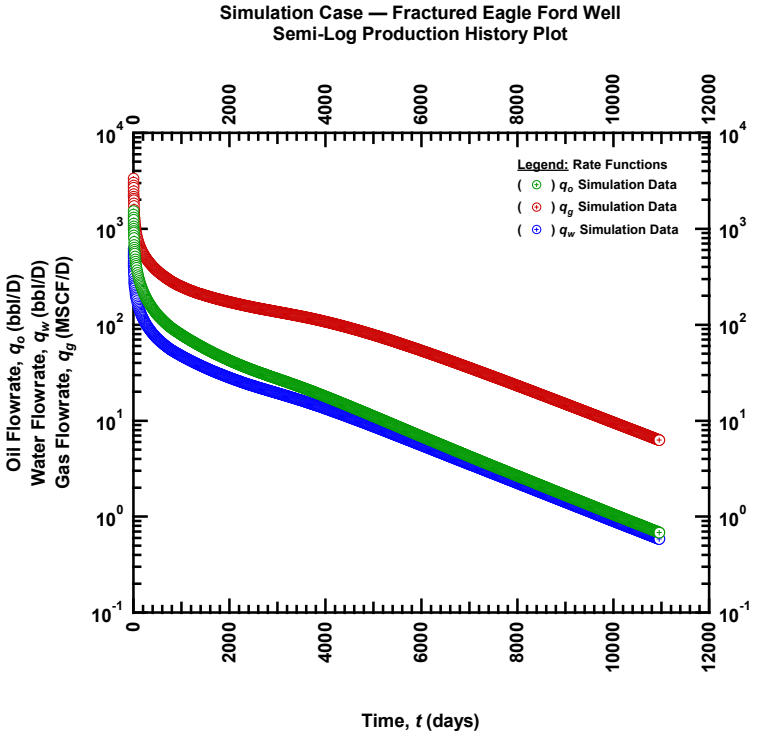

Figure 5.5 — (Semi-log Plot) Oil flowrate (q_o), water flowrate (q_w), and gas flowrate (q_g) versus producing time (t). Production history plot – Simulation case fractured Eagle Ford shale well.

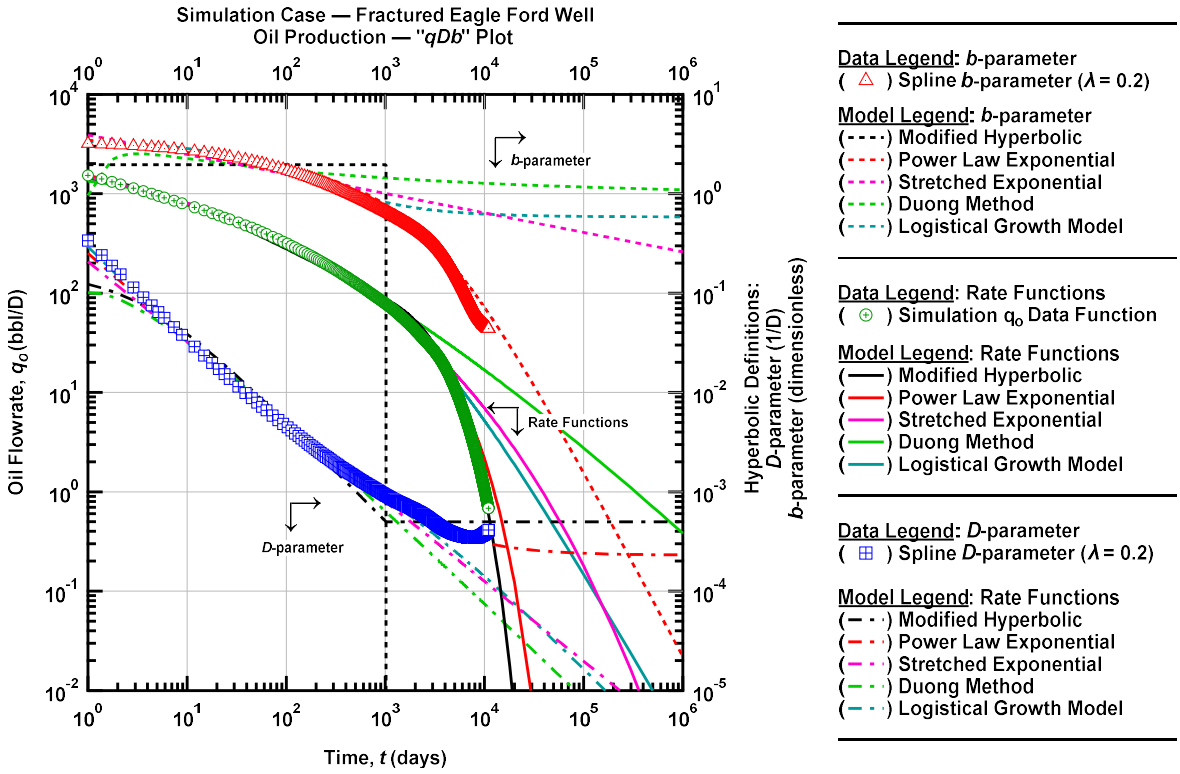

Figure 5.6 — (Log-log Plot) "*qDb*" plot – Eagle Ford shale simulation case. Decline curve analysis methods representation of the time-oil rate data.

A spline was applied to the oil-rate data in order to compute the *D*- and *b*-parameters as a function of time, these results are presented in the "*qDb*" plot (log-log format) in **Fig. 5.6** [Ilk, 2010]. The same decline curves were matched to the data, as were used in the previous validation cases. The entire production history was used to obtain a match for each of the decline curve models. Power-law behavior is observed in the *D*-parameter, as suggested by Ilk (2008). It starts to deviate from this straight-line once terminal decline characteristics begin to become evident in the time-rate data. By observing **Fig. 5.6** it is clear that each of the models adequately represent the simulated production data, but some represent the *D*- and *b*-parameters more appropriately. In this example, as compared to the Haynesville shale example, linear flow and bilinear flow regimes cannot be clearly identified. The time-rate data decreases gradually, and does not have any extended periods

of transient flow. Terminal decline effects begin to take place around 500 days into the producing history. This is due to the size of the stimulated rock volume (SRV). It is apparent in working with the mechanistic model, the size of the SRV, which correlates to the amount of reservoir volume the hydraulic fractures are accessing, greatly impacts when terminal decline effects become evident in the data. It should be noted that in the numerically calculated *D*-parameter begins to increase in very late time. This is an end-point effect of the spline and not representative of the data.

5.2.1. Modified Hyperbolic

The modified hyperbolic represented the simulated time-rate data quite well. Looking at the time-rate data it appears that the modified hyperbolic represents it almost perfectly, however looking at the *b*-parameter it becomes apparent that the model is representing declining *b*-parameter with an average, rather than mimicking the actual trend within the data. If decline curve analysis is performed early in a well's producing life, then the modified hyperbolic relation will likely lead to an overestimate of EUR. This occurs because the production data *b*-parameter decreases with time, and since the modified hyperbolic decline curve is taking an average of the available data, a *b*-parameter may be selected that is too high for the future production of the well. The selected *b*-parameter would be representative of the available data but not future production. The D_{min} value used to obtain this match was 5.0% / year.

5.2.2. Power-Law Exponential

The power-law exponential predicted the EUR at 30 years for this simulation almost exactly. In this validation case, unlike field production data example a value of 2.3E-4 was used for D_{∞}, rather than assuming it was zero. This validation case confirms the observations and lessons-learned

from the Haynesville validation case, specifically, that the D_∞-parameter is useful in correctly representing late life production for time-rate data from unconventional wells. It is most apparent in the *b*-parameter that the power-law exponential is the superior decline curve for forecasting time-rate data exhibiting production trends similar to those presented in this validation case. The *b*-parameter is decreasing with time, but not at a constant rate (*i.e.*, a straight line). The inclusion of the terminal decline parameter within the power-law exponential allows it to correctly represent the simulated data throughout all periods of production.

5.2.3. Stretched Exponential

As previously mentioned, the stretched exponential equation is essentially the same as the power-law exponential without a terminal decline parameter. The stretched exponential did not represent the simulated Eagle Ford data as well as the power-law exponential due to it lacking the terminal decline parameter. Initially the stretched exponential was representative of the time-rate data, the reciprocal loss-ratio, and the loss-ratio derivative. However, once the terminal decline effects began to influence the simulated data the stretched exponential was not able to accurately represent it.

5.2.4. Duong's Method

Duong's Method once again yielded the highest forecast for all of the decline curve models. Since this particular validation case had such a short period of transient flow, Duong's method is not valid for a long-term extrapolation. Looking at the calculated *b*-parameter for the simulated data, it falls below 1.0 in less than 100 days. Duong's method never estimates a *b*-parameter below 1 for the entire 30 years of production.

5.2.5. Logistical Growth Model

The logistical growth model yielded an EUR estimate similar to the modified hyperbolic model. However, the modified hyperbolic yielded an estimate that was about 5% too low and the logistical growth model estimate was about 5% too high compared to the simulated EUR value from the mechanistic model. Overall, we believe that the logistical growth model is a quality decline curve model due to the shift that is apparent in the *b*-parameter. However, in late-life when terminal decline is experienced, this model cannot represent the production rate data as well as other models that include terminal decline parameters.

Table 5.5 contains all of the parameters used for the decline curve models that are featured in **Fig. 5.6**. **Table 5.6** contains the EUR estimate for all of the decline curve models. All of the decline curve analysis models (excluding Duong's method), were able to provide reasonable estimates for EUR. The modified hyperbolic and the power-law exponential stood out in this validation case due to each of them including a terminal decline parameter.

Table 5.5 — Summary of decline curve analysis models parameters for Eagle Ford Shale mechanistic model.

Decline Model	q_i or K (STB/D)	D_i or $\hat{D}_i$ or a (1/D)	n or b or m (dim. less)	D_{min} or D_∞ (% / year) or (1/D)
M.HYP	1.65E+3	0.162	1.960	5.0
PLE	1.23E+4	2.088	0.121	2.3E-4
SEM	4.20E+3	0.767	0.196	-
DNG	1.33E+3	1.001	1.110	-
LGM	4.31E+5	196.6	0.714	-

Table 5.6 — Summary of 30-year EUR values determined using different decline curve analysis models for the Eagle Ford Shale mechanistic model.

Model	EUR_{30yr} (MSTB)	Percent Error
SIM	323	
M. HYP	338	- 4.72 %
PLE	326	- 1.03 %
SEM	349	8.04 %
DNG	470	45.55 %
LGM	339	4.96 %

5.3. Wolfcamp Shale Mechanistic Model Validation Case

A three-phase reservoir simulation was completed using the mechanistic developed for the validation and ranking of the decline curve models. This particular synthetic validation case is intended to mimic typical reservoir characteristics and completion design of a well completed in the Wolfcamp shale. As compared to the previous Eagle Ford validation example, the height of the fracture in this mechanistic model validation was greater and therefore able access a larger reservoir volume. A characteristic highlighted in this validation case is the impact of high-water production. Unlike the previous example, the water-rate is greater than the oil-rate throughout the wells production history and the reservoir has a lower-initial pressure and temperature. The gas-to-oil ratio (or GOR) is more representative of a black oil, rather than a volatile oil, as investigated in the Eagle Ford validation case. This simulation evaluates the ability of the decline curve analysis relation to accurately model the time-rate data when linear and bilinear flow regimes can be easily identified during transient flow. Terminal decline effects are still observed, but not until much later in the wells producing life due to the increased reservoir volume. All of the system properties can be found in **Table 5.7**.

Table 5.7 — Reservoir and fluid properties for numerical simulation case – hydraulically fractured well with typical Wolfcamp shale properties and parameters.

Reservoir Properties:

Net pay thickness, h	=	470 ft
Formation permeability, k	=	47 nD
Wellbore radius, r_w	=	0.3 ft
Formation compressibility, c_f	=	2 x 10^{-5} psi^{-1}
Porosity, ϕ	=	0.1 (fraction)
Initial reservoir pressure, p_i	=	5760 psi
Oil saturation, S_o	=	0.45 (fraction)
Skin factor, s	=	0.00 (dimensionless)
Wellbore storage coefficient, C_D	=	0 (dimensionless)
Reservoir Temperature, T_r	=	170 °F

Fluid Properties:

Oil specific gravity, γ_o	=	0.78 (water = 1)
Gas-Oil-Ratio, GOR	=	1060 scf/bbl
Gas specific gravity, γ_g	=	0.68 (air = 1)
Water specific gravity, γ_w	=	1.0 (water = 1)

Hydraulically Fractured Well Model Parameters:

Fracture half-length, X_f	=	180 ft
Number of fractures, n_f	=	210
Fracture spacing, s_f	=	40 ft
Horizontal well length, L_w	=	5200 ft
Fracture permeability, k_f	=	20 md
Fracture conductivity, F_{CD}	=	2 (dimensionless)

Production Parameters:

Flowing Pressure, p_{wf}	=	1325 psi
Producing time, t	=	30 years

Fig. 5.7 is a log-log plot of all of the flowrate data for this well, which spans the entire 30 years of simulated production. **Fig. 5.8** is the same data represented in semi-log format. The production exhibits linear flow (1:2 slope) initially. Terminal decline effects occur much later in the wells producing life, due to the increased reservoir volume. The overall oil-production less than the Eagle Ford validation case, because of the lower reservoir pressure. The amount of gas produced is also less than the Eagle Ford, due to the oil having a lower GOR.

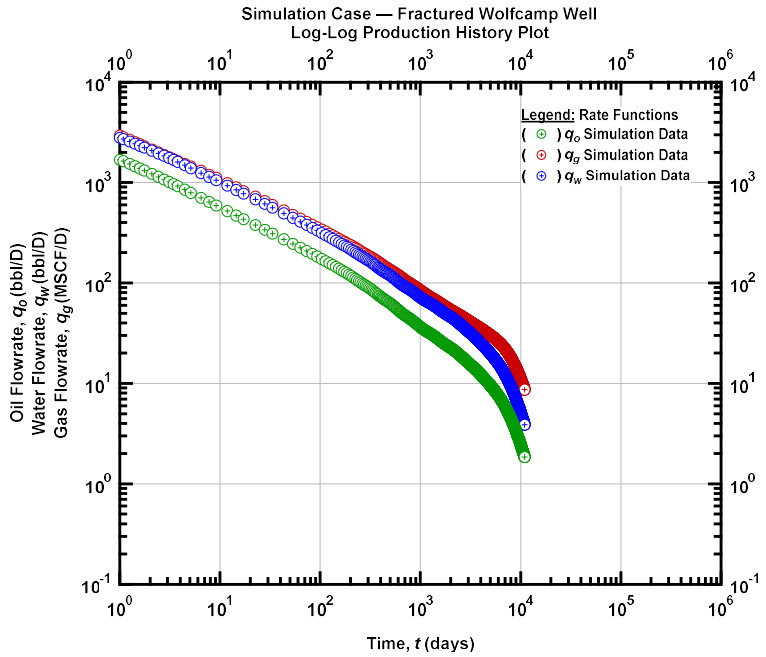

Figure 5.7 — (Log-log Plot) Oil flowrate (q_o), water flowrate (q_w), and gas flowrate (q_g) versus producing time (t). Production history plot – Simulation case fractured Wolfcamp shale well.

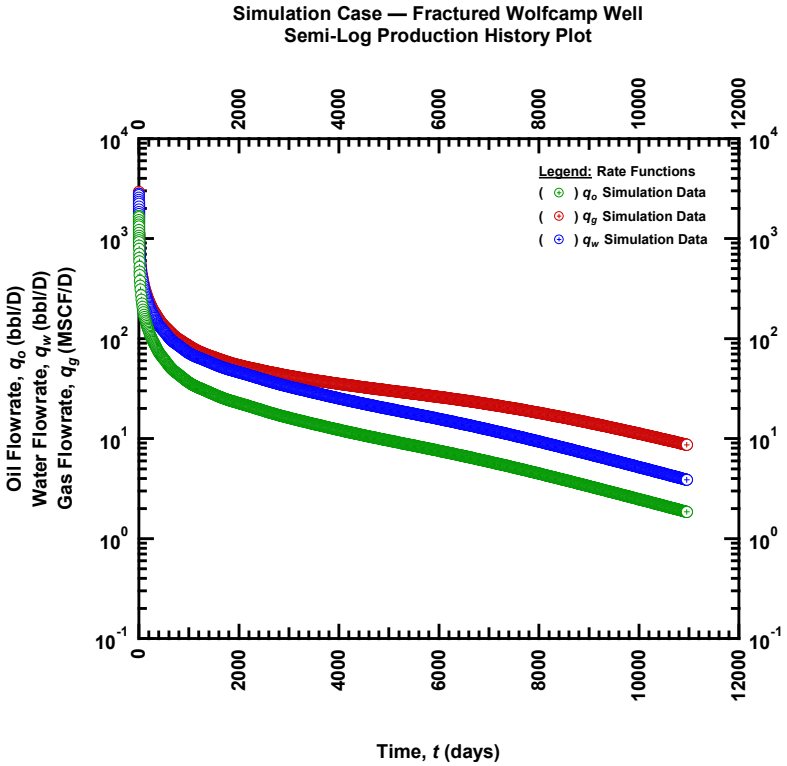

Figure 5.8 — (Semi-log Plot) Oil flowrate (q_o), water flowrate (q_w), and gas flowrate (q_g) versus producing time (t). Production history plot – Simulation case fractured Wolfcamp shale well.

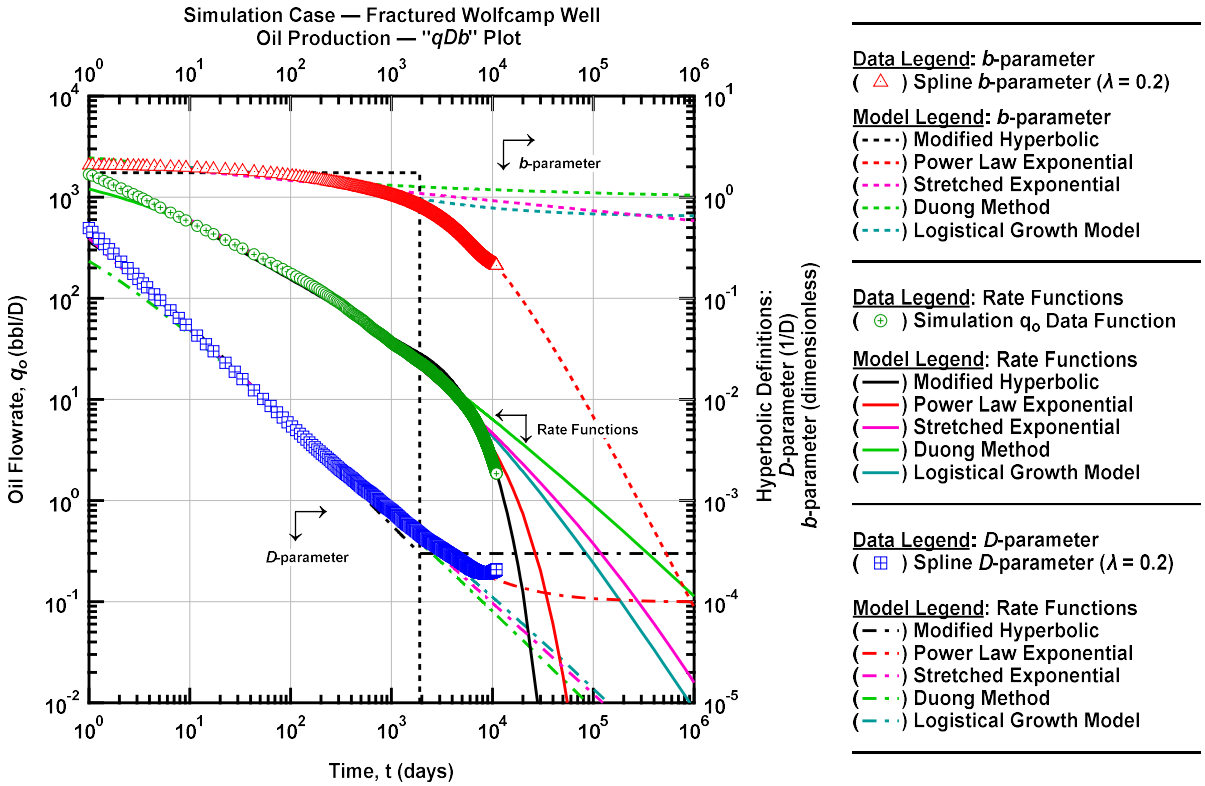

Figure 5.9 — (Log-log Plot) "*qDb*" plot – Wolfcamp shale simulation case. Decline curve analysis methods representation of the time-oil rate data.

The *D*- and *b*-parameters were numerically calculated as a function of time using a spline representation of the time-rate simulated data, these results are presented in the "*qDb*" plot (log-log format) in **Fig. 5.9** [Ilk, 2010]. The same decline curves were matched to the data, as were used in the Haynesville and Eagle Ford shale examples. The entire production history was used to calibrate each of the decline curve models. We observe power-law behavior in the *D*-parameter, as suggested by Ilk (2008). The trend starts to deviate from this straight-line once terminal decline characteristics begin to become evident in the time-rate data, however this occurs much later in the production history as compared to the Eagle Ford validation example due (we believe) to the increased reservoir volume. By observing **Fig. 5.9** it is clear that each of the models adequately represent the simulated production data.

5.3.1. Modified Hyperbolic

The modified hyperbolic over all represented the simulated time-rate data well, as observed in the previous examples. Due to the extended period of transient flow in this example, where linear flow can be easily identified, the modified hyperbolic is a valid model to apply to the time-rate data. Linear flow exhibits a *b*-parameter equal to two. The *b*-parameter used for the modified hyperbolic to obtain this match was 1.7. This makes sense because after this period of linear flow the *b*-parameter decreases. Once again, the use of the terminal decline parameter assists the modified hyperbolic in representing the data throughout its entire production history. A D_{min} value of 3.0% / year was used to obtain the decline curve match. It makes sense that this is less than the previous validation examples because transient flow is exhibit for a greater portion of the production history.

5.3.2. Power-Law Exponential

The power-law exponential predicted the EUR at 30 years for this simulation almost perfectly. This further validates the power-law exponential is valid forecasting method for unconventional reservoirs. This decline curve model was initially developed for high pressure, high temperature gas reservoirs but this research has validated that power-law behavior is still observed in the *D*-parameter for multi-phase unconventional reservoir time-rate data, which is the foundation for the power-law exponential model. However, in these multi-phase reservoir systems terminal decline effects are very apparent and the use of the D_{inf}-parameter allows for more flexibility in the power-law exponential model to accurately represent the entirety of the production history.

5.3.3. Stretched Exponential

Once again, the stretched exponential was able to represent the early-time, transient, and transitional flow of the simulated data. However, since this decline curve model lacks a terminal decline parameter (unlike the power-law exponential), it is not able to correctly model the late-life behavior of the simulated data.

5.3.4. Duong's Method

Duong's Method again yielded the highest forecast for all of the investigated decline curve models. However, it yielded a much more accurate estimate for EUR in this particular validation case as compared to the previous ones, most likely due to a longer transient behavior period being observed.

5.3.5. Logistical Growth Model

The logistical growth model once again provided a reasonable estimate for EUR. Even without a terminal decline parameter the logistical growth model is able to accurately represent most of the production history. This is a simple model, one which does not require a strong estimate for the terminal decline parameter, therefore if little is known about the reservoir, it is a viable option for decline curve analysis. Also, due to the nature of the equation and its origins, the *K*-parameter is the carrying capacity of the system (*i.e,* the original oil in place (OOIP) for our work). This artifact in the equation can assist engineers in determining not only decline parameters of the time-rate data, but *may* also give insight into the overall characteristics of the reservoir itself.

Table 5.8 contains all of the parameters used for the decline curve models that are featured in **Fig. 5.9**. **Table 5.9** contains the EUR estimate for all of the decline curve models. The power-law

exponential had almost an exact approximation of the simulated EUR. Overall all of the decline curve models has a smaller percent error in their respective estimate for EUR in this validation case as compared to the previous validation cases.

Table 5.8 — Summary of decline curve analysis models parameters for Wolfcamp Shale mechanistic model.

Decline Model	q_i or K (STB/D)	D_i or $\hat{D}_i$ or a (1/D)	n or b or m (dim. less)	D_{min} or D_∞ (% / year) or (1/D)
M.HYP	7.61E+6	1.68E+3	1.817	6.4
PLE	8.01E+13	20.59	5.22E-2	1.0E-4
SEM	5.00E+5	0.138	0.198	-
DNG	5.00E+4	0.756	1.065	-
LGM	8.52E+6	67.44	0.634	-

Table 5.9 — Summary of 30-year EUR values determined using different decline curve analysis models for the Wolfcamp Shale mechanistic model.

Model	EUR_{30yr} (MSTB)	Percent Error
SIM	196	
M. HYP	209	6.89 %
PLE	196	- 0.02 %
SEM	190	- 2.85 %
DNG	210	7.43 %
LGM	196	1.38 %

5.4 Non-Constant Pressure Production Mechanistic Model Validation

The purpose of this validation case is to address the issue of non-constant pressure production exhibited in unconventional reservoirs. All previous validation cases assumed a constant bottomhole pressure for the entirety of the simulated producing time, however, in practice this is often not valid. In reality, unconventional wells are completed and stimulated using hydraulic fracturing. Once the well is ready to be brought online, the fluid is produced through a choke.

How to optimize this early-life production period of an unconventional well is highly debated throughout the industry and is outside the scope for this research. Due to the hydraulic fracturing treatment, the reservoir is energized, and the hydraulic fracture, as well as the surrounding area is flooded with water. Choke management during this early-time production period is designed to not overwhelm the production facilities due to very high fluid production. After some time, the well will begin to produce hydrocarbons along with the water. The timing and volume of hydrocarbons produced depends on the reservoir, but it is not uncommon for it to take 1-2 weeks before the well produces significant hydrocarbons. This early-time production should not be used for long-term production analysis. Commonly, the well is considered "fully-open" once it is being produced though an open choke. Even once the well is fully-open, the well is still not produced at a constant bottomhole pressure immediately.

A typical well is produced with no assistance from artificial lift until hydrocarbon production begins to fall below expected trends. This can also be referred to as "loading-up". Once this occurs, artificial lift is installed on the well. For horizontal wells with large hydraulic fracturing treatments, the total fluid production volume is still too high for rod pumps to be an optimized form of artificial lift. Therefore, it is common for an electric submersible pump (ESP) or gas lift system to be installed. The purpose of installing artificial lift is to continue to drawdown the bottomhole pressure in the wellbore and maximize hydrocarbon production. The well itself will continue to decline and fluid volumes will continue to decrease. Due to the harsh downhole environment of unconventional wells, artificial lift systems have a limited lifespan. Once the initial form of artificial lift fails, or is no longer optimal, a new artificial lift design is installed. It is common at this point in a well's life that the total fluid volume has decreased enough for a rod pump to be installed. Rod pump is a common form of artificial lift for not only unconventional

reservoirs, but for many oil and gas reservoirs due to its low operating costs. Once rod pump has been installed on an unconventional well the bottomhole pressure is relatively constant for the remainder of the well's productive life. The purpose of this section it to attempt to capture this described production strategy, where a well is produced initially to drawdown the bottomhole pressure until it reaches a certain point at which the well is then produced at a constant bottomhole pressure for the remainder of its life.

A three-phase reservoir simulation was completed using the mechanistic model developed for this study. This particular synthetic case is used identical properties and parameters as the Eagle Ford validation case, besides the assumption of a constant bottomhole pressure throughout the entire production history. All of the system properties can be found in **Table 5.10**.

Table 5.10 — Reservoir and fluid properties for numerical simulation case – hydraulically fractured well with typical Eagle Ford shale properties and parameters.

Reservoir Properties:

Net pay thickness, h	=	200 ft
Formation permeability, k	=	200 nD
Wellbore radius, r_w	=	0.3 ft
Formation compressibility, c_f	=	2×10^{-5} psi^{-1}
Porosity, ϕ	=	0.1 (fraction)
Initial reservoir pressure, p_i	=	10,000 psi
Oil saturation, S_o	=	0.58 (fraction)
Skin factor, s	=	0.00 (dimensionless)
Wellbore storage coefficient, C_D	=	0 (dimensionless)
Reservoir Temperature, T_r	=	270 °F

Fluid Properties:

Oil specific gravity, γ_o	=	0.84 (water = 1)
Gas-Oil-Ratio, GOR	=	1200 scf/bbl
Gas specific gravity, γ_g	=	0.68 (air = 1)
Water specific gravity, γ_w	=	1.0 (water = 1)

Hydraulically Fractured Well Model Parameters:

Fracture half-length, X_f	=	180 ft
Number of fractures, n_f	=	210
Fracture spacing, s_f	=	40 ft
Horizontal well length, L_w	=	5200 ft
Fracture permeability, k_f	=	20 md
Fracture conductivity, F_{CD}	=	2 (dimensionless)

Production Parameters:

Flowing Pressure, p_{wf}	=	***See Fig. 5.11***
Producing time, t	=	30 years

To estimate the flowing bottom-hole pressure, the surface flowing pressures for 10 South Texas multi-fractured horizontal unconventional wells were used as a proxy. All of these wells were produced similarly, have similar PVT properties, and are in close proximity to one other. It can be observed in **Fig. 5.10** that all of the wells surface flowing pressures begin at a maximum and are drawn down until they are produced at a relatively constant pressure. The peaks/spikes during production are often due to offset operations, a shut-in of the well itself, or a variety of other reasons. The flowing bottomhole pressure for each of the well was calculated using the Hagedorn

and Brown (1965) bottomhole pressure correlation. The Hagedorn and Brown correlation is an empirical two-phase flow correlation; therefore, the oil and water phases were treated as a single phase, using a weighted average of their properties to represent the one fluid phase in the correlation. The calculated bottomhole pressures from the ten wells were then averaged, which can be seen in **Fig. 5.11**. The average calculated bottomhole pressure exhibited a near perfect logarithmic decline before the constant bottomhole pressure segment. The R^2 value for the logarithmic line of best fit was 0.99. After this logarithmic pressure decline period a constant bottomhole flowing pressure of 1325 psia was assumed. This constant flowing pressure determined from this study was used in the Eagle Ford and Wolfcamp validation examples that were previously investigated.

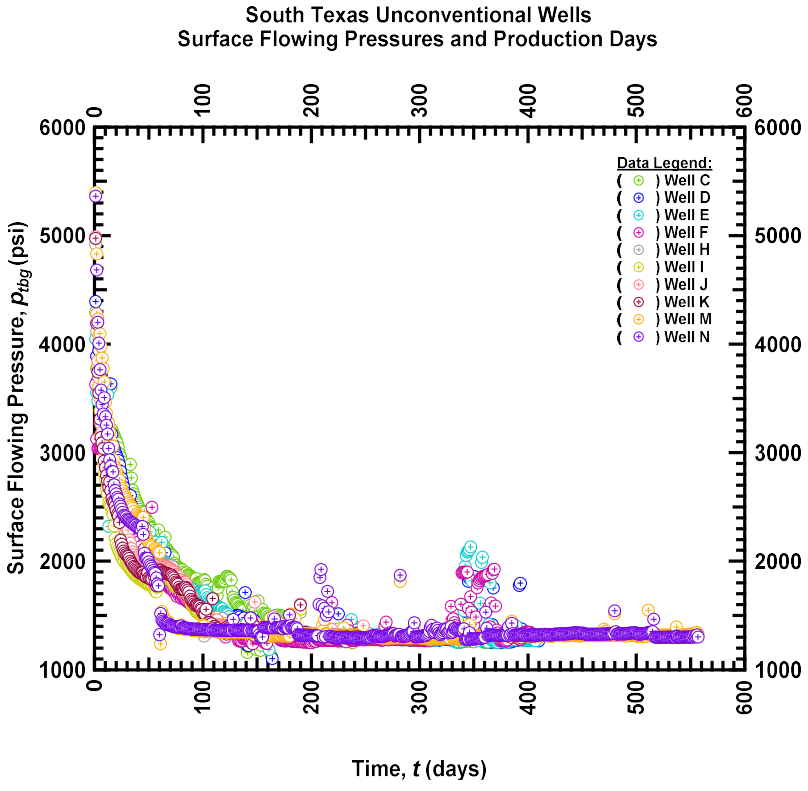

Figure 5.10 — (Cartesian Plot) Surface flowing pressure (p_{tbg}) versus producing time (t). Pressure production history plot – South Texas Unconventional Wells.

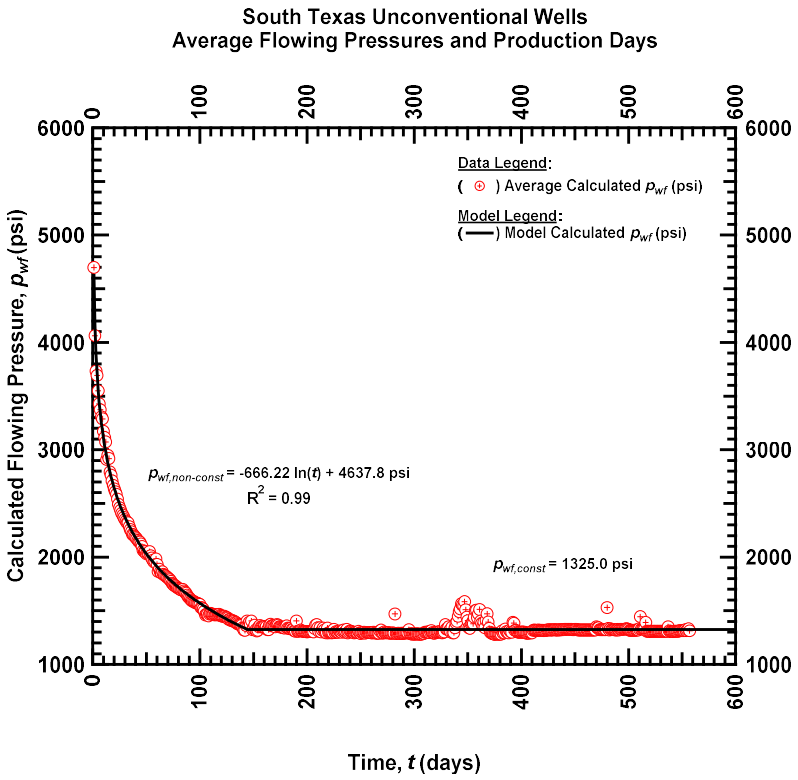

Figure 5.11 — (Cartesian Plot) Average calculated flowing bottomhole pressure (p_{wf}) versus producing time (t). Pressure production history plot – South Texas Unconventional Wells.

Fig. 5.12 is a log-log plot of all of the time-rate data (oil, water, and gas) for this well as well as the bottomhole pressure, which spans the entire 30 years of simulated production. **Fig. 5.13** is the same data represented in semi-log format. During the period of logarithmic bottomhole pressure production the production rate exhibited a near perfect constant-rate behavior. This is most apparent in the water and gas rates. The oil rate decreases slightly, but not as aggressively as the other validation cases that assumed constant pressure production. Once the well is produced at a constant pressure a 1:1 slope is observed in the oil rate simulated data. Similarly, the constant bottomhole production Eagle Ford validation case, terminal decline characteristics are observed around 500 days. The initial production rates are lower in this validation case, but the overall EUR is about the same. Reservoir pressure is the main drive mechanism in unconventional reservoirs.

By producing at a higher bottomhole pressure initially leaves more pressure in the reservoir for longer. Even though the high initial production (IP) rates are not observed, relatively the oil volume is eventually produced, thus there is a relatively small change in EUR. However, most oil exploration and production companies prefer higher initial production rates, because it makes the economics of the well more favorable since the initial investment to drill and complete the well is recuperated in a shorter amount of time. Due to the time-value of money this higher hydrocarbon production initially increases the rate of return for the investment for the well.

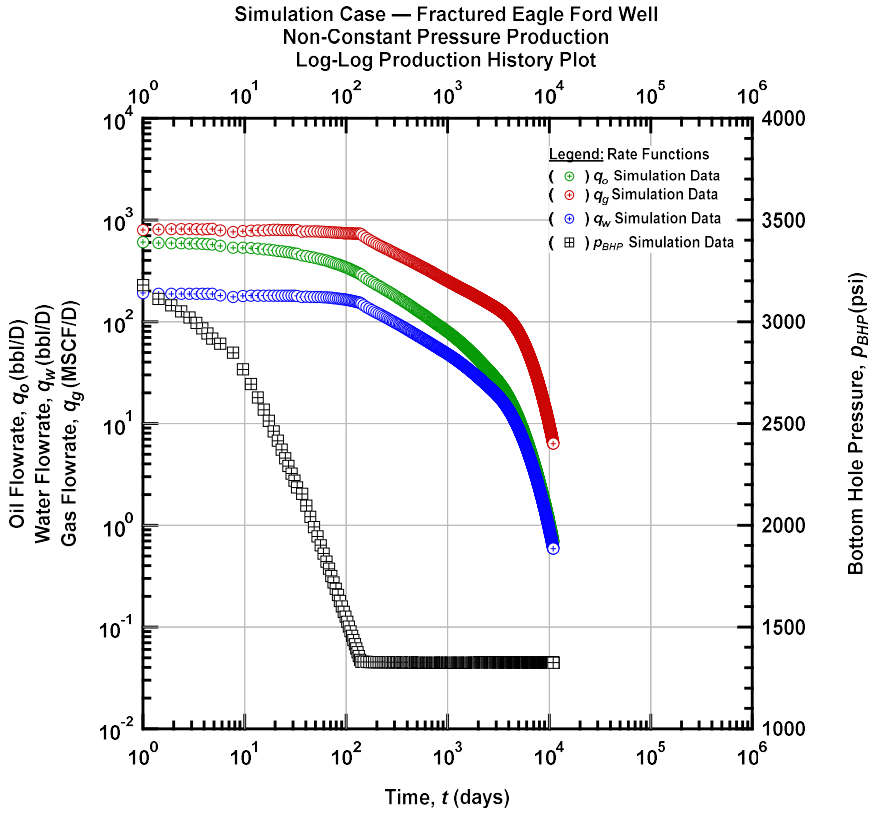

Figure 5.12 — (Log-log Plot) Oil flowrate (q_o), water flowrate (q_w), gas flowrate (q_g), and bottomhole pressure (p_{wf}) versus producing time (t). Production history plot – Simulation case fractured Eagle Ford shale well with non-constant pressure production.

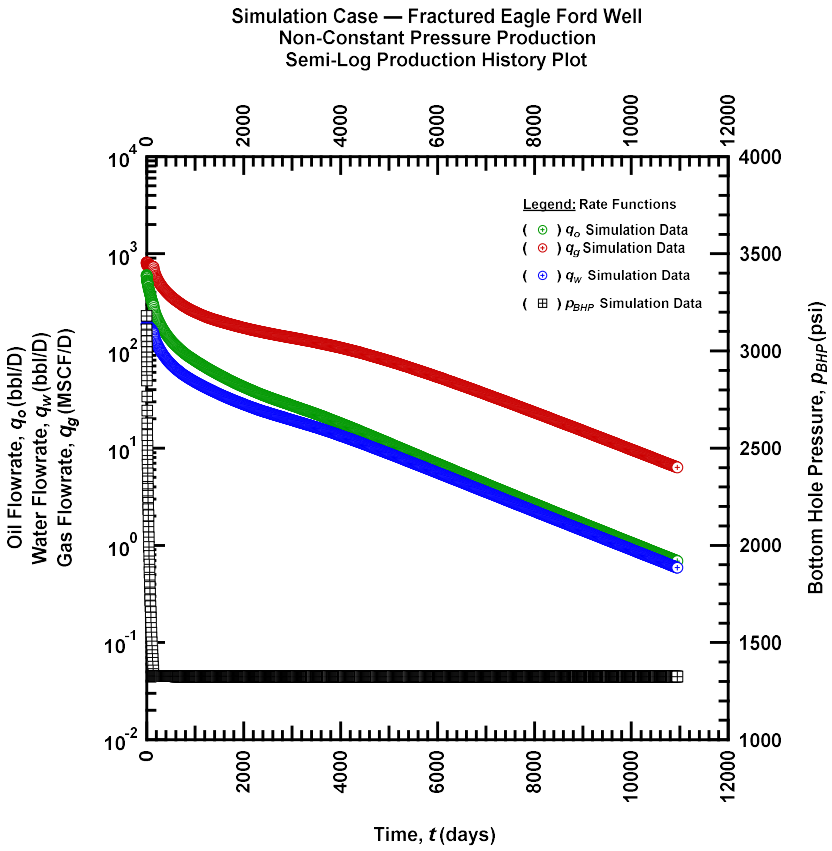

Figure 5.13 — (Semi-log Plot) Oil flowrate (q_o), water flowrate (q_w), gas flowrate (q_g), and bottomhole pressure (p_{wf}) versus producing time (t). Production history plot – Simulation case fractured Eagle Ford shale well with non-constant pressure production.

Once again, the D and b-parameters were computed numerically as a function of time using a smoothing spine on the time-rate data, these results are presented in the "qDb" plot (log-log format) in **Fig. 5.14** [Ilk, 2010]. The spline that was used to estimate the loss-ratio and loss-ratio derivative of the simulated data is subject to a smoothing factor. For consistency a smoothing factor of 0.2 was used, which is the same as the other validation cases. Unlike the other validation cases the b-parameter appears to be decreasing at a near constant rate, until terminal decline effects begin to take place.

One common approach to dealing with non-constant bottomhole pressure production in decline curve analysis is to use rate-normalized pressure. Therefore, the decline curve analysis model will be forecasting time-rate-pressure data rather than time-rate. The purpose of this research is to validate decline curve analysis models for time-rate data. Therefore rate-normalized pressure will not be used for this validation example.

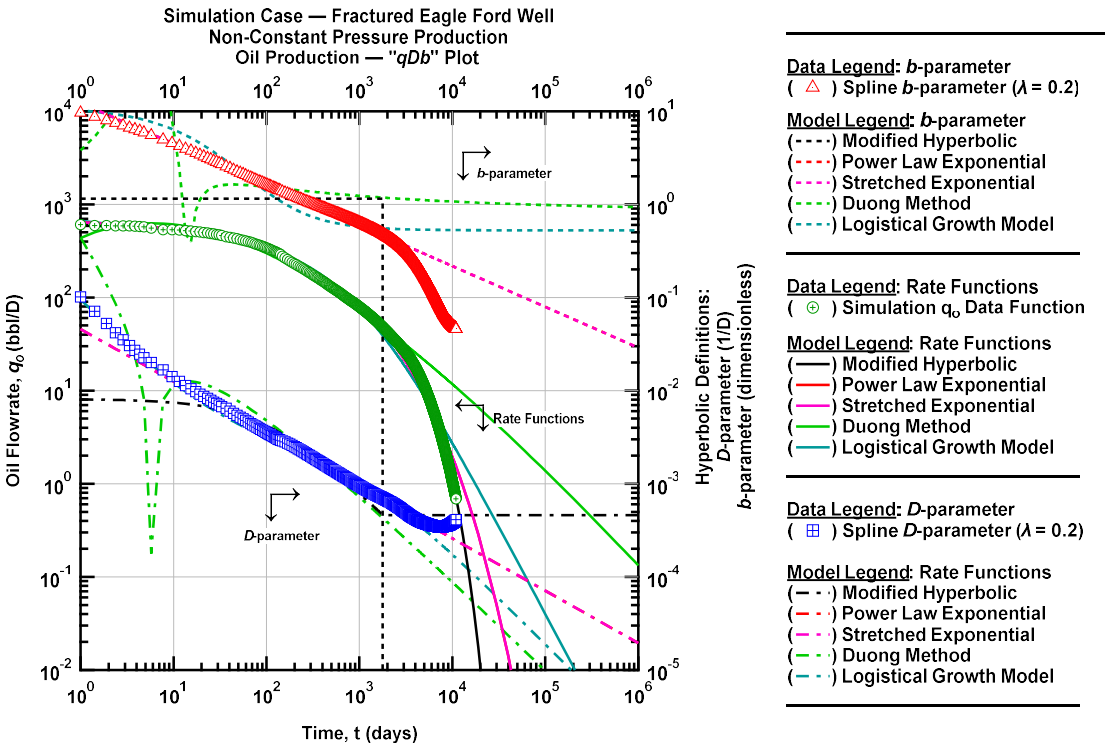

Figure 5.14 — (Log-log Plot) "*qDb*" plot – Eagle Ford shale simulation case with non-constant bottomhole pressure production. Decline curve analysis methods representation of the time-oil rate data.

5.4.1. Modified Hyperbolic

The modified hyperbolic once again give an excellent estimate for EUR. After the initial non-constant bottomhole pressure decline, the well exhibits a near perfect 1:1 slope. This is not reflected in numerically calculated *b*-parameter of the time-rate data in **Fig. 5.14** due to the smoothing property of the spline. But it can be observed in the time-rate data that this transient

behavior exists. The value of the *b*-parameter used for the modified hyperbolic in this validation case was 1.1. Therefore, it is suggested that with time-rate data, do not attempt to perform decline curve analysis with the modified hyperbolic until constant pressure production is established. The higher *b*-parameters experienced early in the wells production history is not representative of its long-term performance. The value of the D_{min} parameter used to obtain this match for the time-rate data was 4.6% / year.

5.4.2. Power-Law Exponential

The power-law exponential predicted the EUR at 30 years for this simulation almost exactly. Unlike in the other validation cases, a D_∞ parameter was not used. The analysis was performed with both a zero and non-zero D_∞ parameter, and a zero value D_∞ case yielded a better estimate for EUR. Therefore, it is recommended in cases where the time-rate data is more constant initially to not use a terminal decline parameter with the power-law exponential. However, ensure that the *b*-parameter estimate is decreasing with time. In the other validation cases, the *b*-parameter was decreasing with time, but to a lesser degree, therefore the terminal decline parameter was needed to further decrease the estimated *b*-parameter value during late-life production.

5.4.3. Stretched Exponential

Since the power-law exponential best fit the simulated data without a terminal decline parameter the stretched exponential yielded nearly the exact same time-rate projection and estimate for EUR.

5.4.4. Duong's Method

Although transient behavior was observed in the time-rate data, Duong's method once again provided the highest estimate for EUR. It did however provide a more accurate estimate for EUR

in this validation case as compared to the Eagle Ford validation case with constant pressure production. However, we do not recommend Duong's method to project time-rate data for wells in unconventional reservoirs. Even in cases where it does provide acceptable estimates for EUR other models that more accurately represent the time-rate data.

5.4.5. Logistical Growth Model

The logistical growth model yielded the least accurate estimate for EUR (with the exception of Duong's Method). Since the *b*-parameter is decreasing at a near constant rate throughout most of the wells production history the logistical growth model cannot accurately represent this behavior.

Table 5.11 contains all of the parameters used for the decline curve models that are featured in **Fig. 5.14**. **Table 5.12** contains the EUR estimate for all of the decline curve models. The power-law exponential and stretched exponential models yielded approximately the same estimate for EUR, since no terminal decline was incorporated into the power-law exponential. The modified hyperbolic yielded the most accurate estimate for EUR.

Table 5.11 — Summary of decline curve analysis models parameters for Eagle Ford Shale mechanistic model with non-constant pressure production.

Decline Model	q_i or K (STB/D)	D_i or $\hat{D}_i$ or a (1/D)	n or b or m (dim. less)	D_{min} or D_∞ (% / year) or (1/D)
M.HYP	591	8.11E-3	1.147	4.6
PLE	712	0.104	0.438	0
SEM	712	173.7	0.438	-
DNG	435	1.620	1.181	-
LGM	4.40E+5	465.4	0.909	-

Table 5.12 — Summary of 30-year EUR values determined using different decline curve analysis models for the Eagle Ford Shale mechanistic model with non-constant pressure production.

Model	EUR_{30yr} (MSTB)	Percent Error
SIM	321	
M. HYP	322	- 0.18 %
PLE	316	- 1.48 %
SEM	317	-1.47 %
DNG	391	22.01 %
LGM	307	-4.22 %

CHAPTER VI

PRODUCING TIME INFLUENCE ON EUR ESTIMATE

In all validation cases discussed prior to this chapter, the complete history (initial production to abandonment) of the time-rate data was used in order to perform the decline curve analysis. However, this is not possible in practice. The purpose of decline curve analysis is to forecast future production using historical production rate — therefore, a typical criteria used to define the "best decline curve analysis model" is the one that can most accurately predict future performance with the least amount of production history. **Table 6.1** contains the amount of production history used to perform decline curve analysis from different articles in the literature.

Table 6.1 — Summary of producing time to perform decline curve analysis in different available publications in the literature.

Reference	Number of Months Used in DCA Matching
Ali and Sheng (2015)	72 (average)
Berman (2014)	24 - 36
Clark (2011)	50 - 90
Hategan (2011)	> 36
Johanson (2013)	72 (average)
Joshi (2015)	30 - 40
Mishra (2010)	50 - 180
Patzek *et. al*. (2013)	> 36

It can be seen in **Table 6.1** that in the academic literature using less than 2 years of production data to perform decline curve analysis is very uncommon, with most using at least 3 years of data. The development of unconventional reservoirs is progressing at an incredible pace, practices which were common 2-3 years ago may not still be the status quo today. However; we must accept that engineers/practitioners should not perform quantitative decline curve analysis without 1.5-2 years of production history.

Our approach in this chapter is to demonstrate the application of decline curve analysis techniques to various vintages of production history specifically at 6 months, 1, 2, 3, 5, 10, and 30 years. In this study the simulated production history data from the Eagle Ford mechanistic model validation case produced at a constant bottomhole pressure was used. As a standard, the full 30 years of simulated data was used to perform the "precise" decline curve analysis. Next, decline curve analysis was performed at each of the stated points in the production history. As comment, if a particular decline curve analysis model has a terminal decline parameter, it was held constant to the value estimated during the 30-year producing time analysis.

6.1. Modified Hyperbolic

Fig. 6.1 contains the time-rate projections of the modified hyperbolic decline curve analysis model, along with the respective *D*- and *b*-parameters for the 7 different producing times. A constant D_{min} value of 5.0% / year was used throughout the study. It can be seen in **Fig. 6.1** that the numerically calculated *b*-parameter is decreasing with time, however during the hyperbolic section of the modified hyperbolic decline curve it assumes a constant *b*-parameter. Therefore, as the producing time used to perform the analysis became less, the *b*-parameter value that was determined for the model increased. This leads to the time-rate projection to increase during transient flow. It can be observed that the forecasted oil flowrate at the end of 30 years remains comparable between all producing times. It does not appear to be a large difference in **Fig. 6.1**, but this increased flowrate during the transitional flow greatly impacts the estimate for EUR. Using the full simulated time-rate data, the modified hyperbolic had a 4.7% error of the simulated EUR. However, with only using 6 months of producing time the modified hyperbolic had a 48.2% error in EUR.

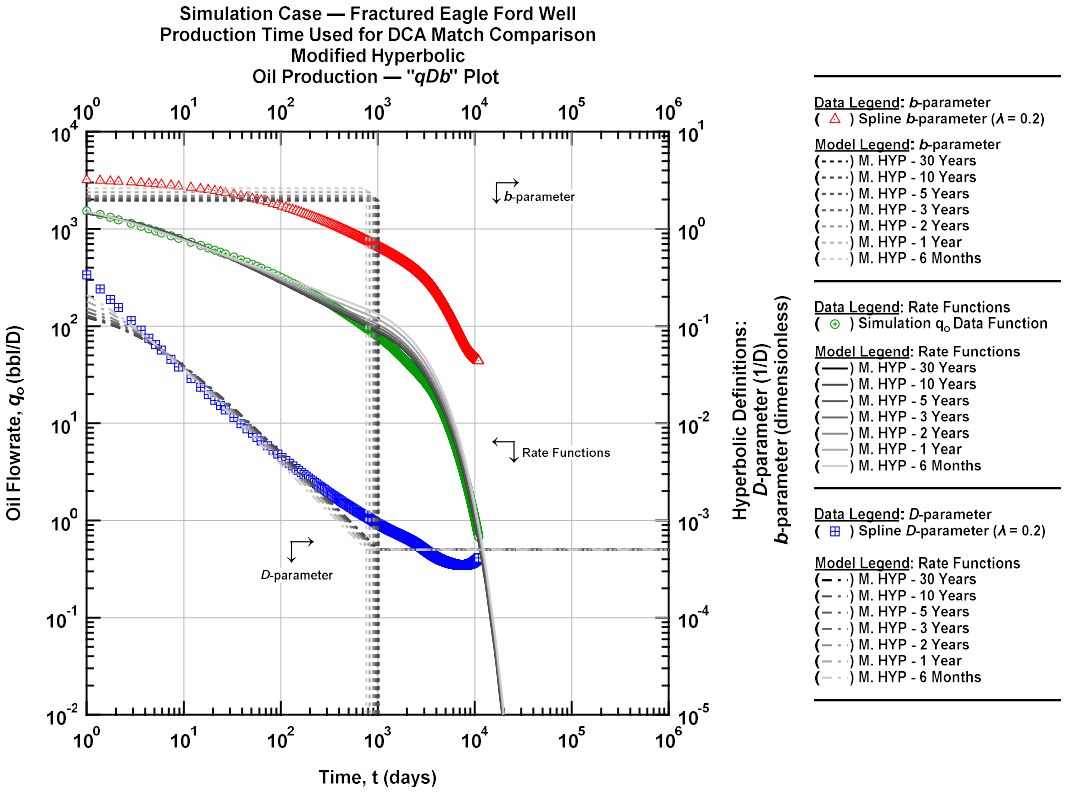

Figure 6.1 — (Log-log Plot) "*qDb*" plot – Eagle Ford shale simulation case. The effect of producing time used for DCA analysis on the modified hyperbolic model.

6.2. Power-Law Exponential

Fig. 6.2 contains the time-rate projections of the power-law exponential decline curve analysis model, along with the respective *D*- and *b*-parameters for the 7 different producing times. A constant D_∞ value of 2.3E-4 was used throughout the study. It can be observed that producing time used to perform the decline curve analysis had a much smaller impact on the time-rate projection of the power-law exponential as compared to the modified hyperbolic. However, having the quality estimate for the terminal decline parameter greatly assisted in this ability to obtain quality forecasts with little producing time. As mentioned before, if the time-rate data exhibits a transient flow initially the use of a non-zero D_∞-parameter greatly improves the power-law exponential's ability to accurately forecast production. The power-law exponential is based

on observed power-law in the *D*-parameter. This allows for accurate projections for EUR to be determined with fewer producing days, as long as that power-law trend continues. This study has shown that power-law is observed in the *D*-parameter for unconventional reservoirs, until terminal decline is experienced, in which the terminal decline parameter within the power-law exponential allows for. Using the entire 30 years of simulation history, the power-law exponential was able to calculate EUR within 1% of the simulated production. Using only 6 months of producing time, the EUR was still within 10% of the simulated value. It is imperative that a representative estimate for D_∞ be used in order to obtain this high-quality match.

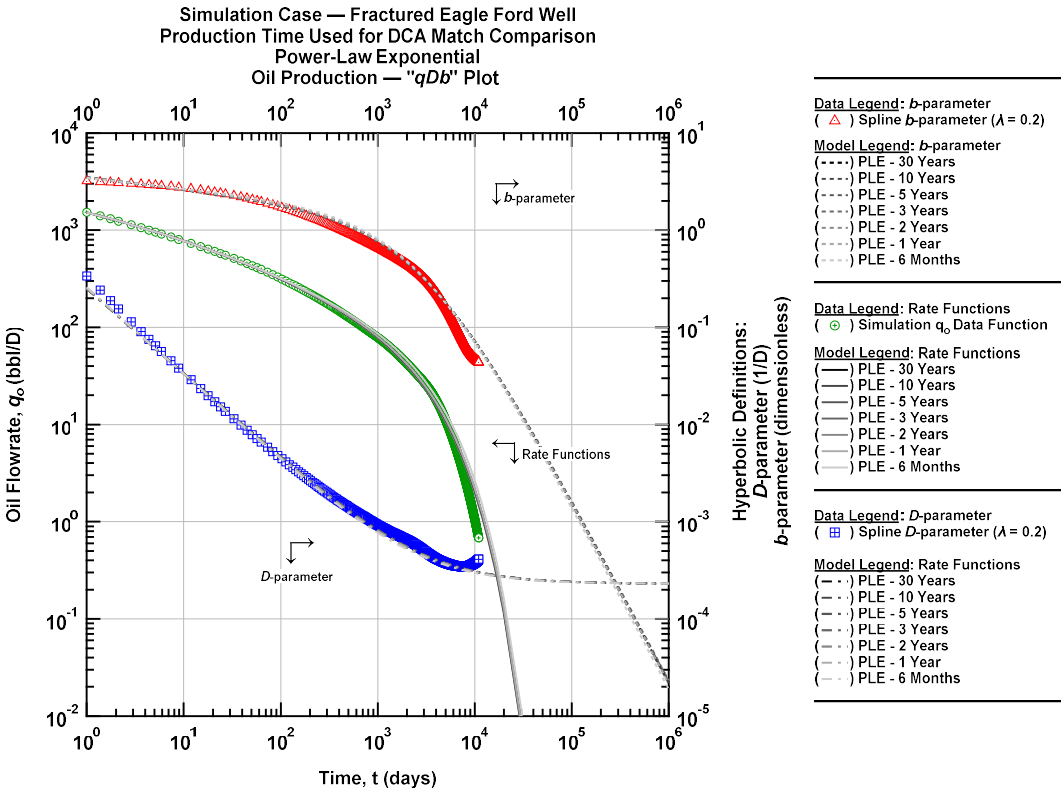

Figure 6.2 — (Log-log Plot) "*qDb*" plot – Eagle Ford shale simulation case. The effect of producing time used for DCA analysis on the power-law exponential model.

6.3. Stretched Exponential

Fig. 6.3 contains the time-rate projections of the stretched exponential decline curve analysis model, along with the respective *D*- and *b*-parameters for the 7 different producing times. As mentioned previously, the stretched exponential model is the same as the power-law exponential decline curve model, except it does not have a terminal decline parameter and the notation is different. In **Fig. 6.3** we observe that power-law behavior occurs in the *D*-parameter. Looking at all 7 model estimates for the *D*-parameter, these all appear to be valid and should be considered a valid approximation for the numerically calculated values from the time-rate data.

The weakness of the stretched exponential is not having a terminal decline parameter, which is highlighted in the *b*-parameter. As less time-rate data is used for the analysis the higher the *b*-parameter is projected to be during late-life production. The terminal decline parameter in other decline curve analysis models can assist with correcting this over-projection in late-life production. It has been mentioned throughout this thesis that Duong's method over-estimates EUR in almost every scenario. Overall, the stretched exponential is regarded as one of the more valid decline curve analysis models. However, in this producing time study it can be seen that the stretched exponential can provide overestimations for EUR that are similar to those provided by Duong's Method. When the full 30 years of the simulated production history is used for analysis the EUR estimate from the stretched exponential showed 4% error from the simulated EUR. When only 6 months of producing history was used, the stretched exponential obtained an estimate that was 78.5% over the simulated data EUR.

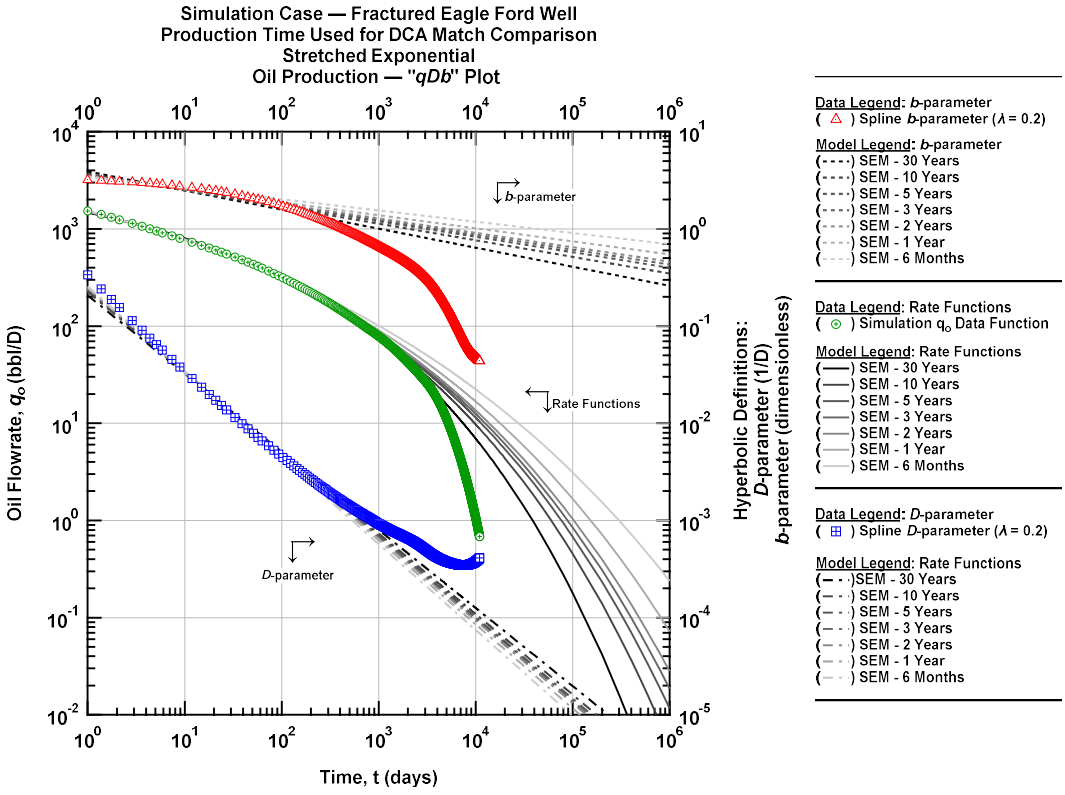

Figure 6.3 — (Log-log Plot) "*qDb*" plot – Eagle Ford shale simulation case. The effect of producing time used for DCA analysis on the stretched exponential model.

6.4. Duong's Method

Fig. 6.4 contains the time-rate projections of Duong's Method decline curve analysis model, along with the respective *D*- and *b*-parameters for the 7 different producing times. Outlined in Duong's original paper, a graph of $\log[q(t)/G_p(t)]$ verses $\log[t]$ is used to estimate the values for the *a*- and *m*-parameters. This plot should yield a straight-line trend in order for Duong's method to be valid. Initially, with the simulated data the straight-line trend is observed, however this model deviates from this trend in late-life production. In **Fig. 6.4** we observe that the amount of producing time used for analysis has less of an impact on the time-rate projection of Duong's Method, as compared to the stretched exponential. That is because the *a*- and *m*-parameters were determined from early time data. Although Duong's Method has less variability as other decline curve analysis models

with less producing time used for analysis the model itself still projects transient behaviors into late-late of the wells production. Using the full 30 years of simulated production from the mechanistic model, Duong's method over estimated EUR by 45.6%. The modified hyperbolic yielded a similar error when only 6 months of producing time was used for analysis. When only 6 months was used for analysis with Duong's Method it estimated a EUR nearly double the simulated amount.

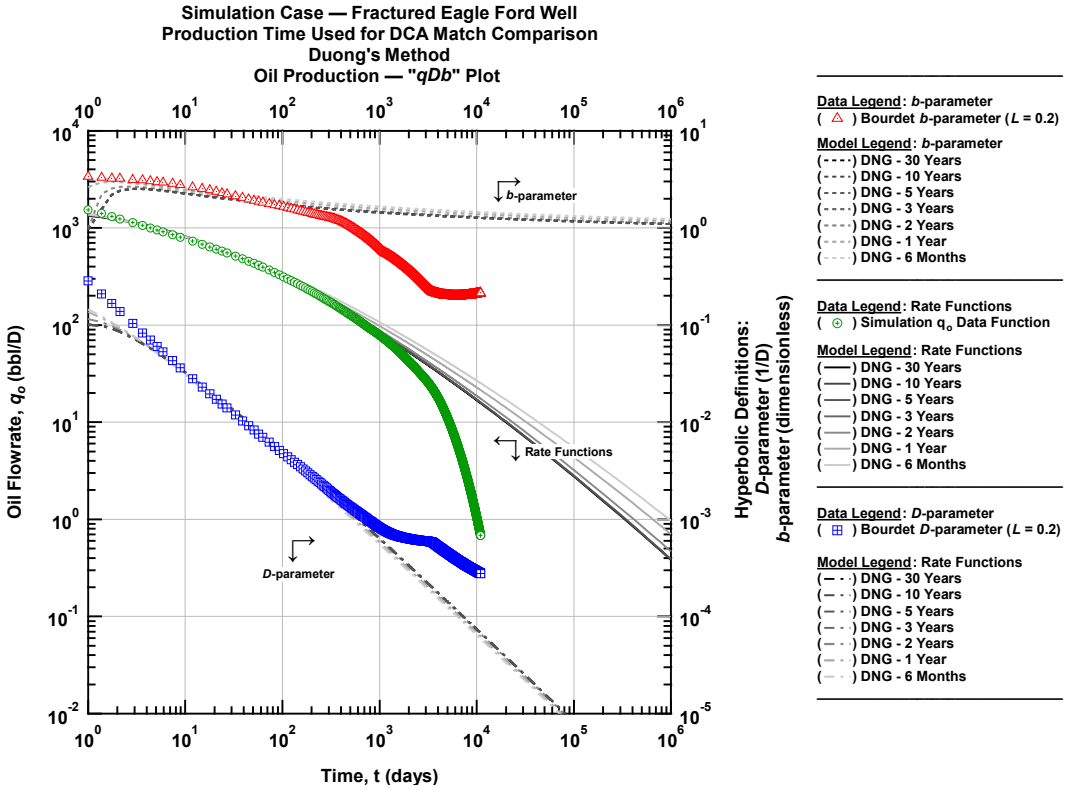

Figure 6.4 — (Log-log Plot) "*qDb*" plot – Eagle Ford shale simulation case. The effect of producing time used for DCA analysis on Duong's Method.

6.5. Logistical Growth Model

Fig. 6.5 contains the time-rate projections of the logistical growth decline curve analysis model, along with the respective *D*- and *b*-parameters for the 7 different producing times. The behavior

of the logistical growth model is quite interesting because for all of the producing times it did provide accurate estimates for EUR, comparable to those obtained by the power-law exponential. However, comparing **Fig. 6.5** to **Fig. 6.2**, the time-rate projection of the power-law exponential was much more representative of the simulated data. The logistical growth model does have a decreasing *b*-parameter, which has been observed throughout this research, but it does not have a terminal decline parameter. Overall, the logistical growth model can obtain EUR values with about the same amount of accuracy as other decline curve analysis methods, however the projection of the actual time-rate data may not be as representative as other models.

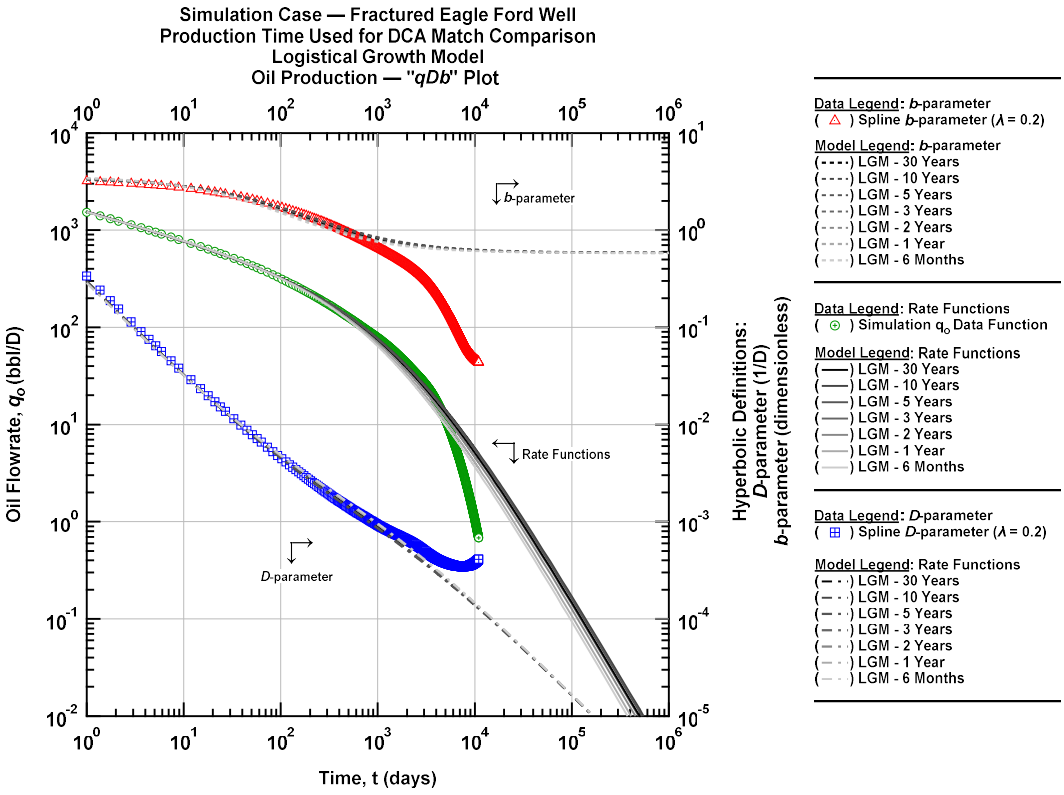

Figure 6.5 — (Log-log Plot) "*qDb*" plot – Eagle Ford shale simulation case. The effect of producing time used for DCA analysis on the logistical growth model.

6.6. Summary

In **Fig 6.6** we present a "bar chart" containing all of the EUR values determined using the different decline curve analysis models in this study at each of the 7 producing times. The modified hyperbolic yielded good values for EUR as long as at least 2 years of production data was used for calibration. After that the model overestimates EUR at an increasing rate. The power-law exponential yielded excellent estimates for EUR at all producing times. *However, it needs to be noted that this level of precision was due to a quality estimate for the terminal decline parameter*. The stretched exponential stood out in this study, due to it lacking a terminal decline parameter. Often it is stated that the power-law exponential and the stretched exponential are the same. However, the incorporation of the terminal decline parameter in the power-law exponential allowed it to be the best performing decline curve model, while the stretched exponential was the second worst performing. The stretched exponential likely could have similar results to the power-law exponential if the decline in the *b*-parameter is overestimated at the time of analysis. However, this behavior is strongly non-unique and it is preferred to use the power-law exponential model with a non-zero terminal decline exponent. We also recall that it was shown in the non-constant bottomhole pressure validation case that <u>not</u> using a terminal decline parameter can yield the best EUR estimates for the power-law exponential if transient flow is not observed in early time. This means that the stretched exponential would yield similar results in these particular cases. The logistical growth model did yield accurate estimates for EUR for all producing times. However, by looking at **Fig. 6.6** the logistical growth model yielded overestimates for EUR up to 3 year of producing time and then yielded under projections beyond that. As mentioned earlier, the logistical growth model does yield accurate estimates for EUR, but the time-rate projection is not as valid as other models.

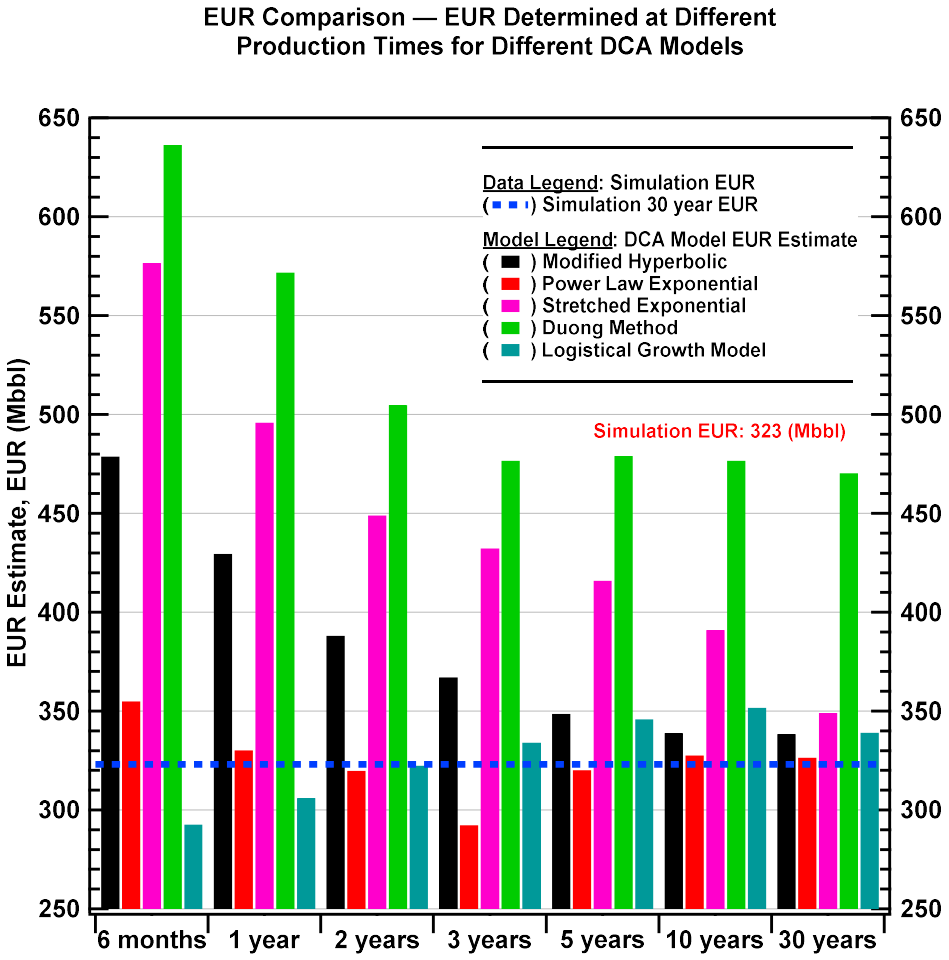

Figure 6.6 — (Bar-Chart) The effect of producing time used in decline curve analysis on the estimate EUR.

CHAPTER VII

IMPROVED DECLINE CURVE ANALYSIS TECHNIQUE

Although counterintuitive in 2020, one of the major issues facing the oil and gas industry today is data quality. The time-rate data from an unconventional well is quite often very sporadic (typically due to onsite and offsite operational activities), see **Fig. 7.1**. These operational conditions, combined with "lease-averaging" of data makes decline curve analysis quite difficult. This is particularly true when applying the "*qDb*" methodology proposed by Ilk (2008), which requires the instantaneous calculation of the $D(t)$ and $b(t)$ functions. The issue with this methodology is that in order to calculate the loss-ratio ($1/D(t)$) and the loss-ratio derivative ($b(t)$), a numerical differentiation method must be applied, most commonly the Bourdet (1989) algorithm typically used for pressure transient analysis (*i.e.*, the pressure derivative calculation).

This Bourdet method is a weight-averaged derivative formulation, but it is still quite susceptible to data noise (particularly at/near the endpoints). When a derivative is calculated for a dataset with any noise, the errors are magnified. As we see in **Fig. 7.1**, we can see how difficult (if not impossible) it would be to correctly diagnose the underlying model for these data using decline curve analysis — let alone trying to take a derivative. This data must be thoroughly edited (or some would say "cleaned") before <u>any</u> analysis can be performed — however data editing is a very non-unique process. How any individual edits a given dataset reflect their bias and their expectations, and in the case of decline curve analyses, such biases can and will drastically change the expectation of a given flow regime. A common approach is to take a "time" average, for example 1-week averaging, which is shown in **Fig. 7.2**.

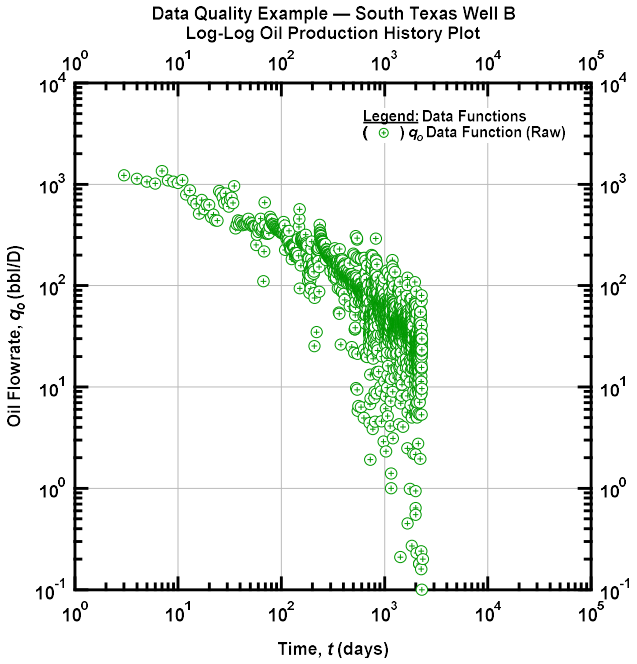

Figure 7.1 — (Log-log Plot) Oil flowrate (q_o) versus producing time (t). Production history plot – South Texas Well B. Presented to emphasize the issue with data quality and its impact on decline curve analysis.

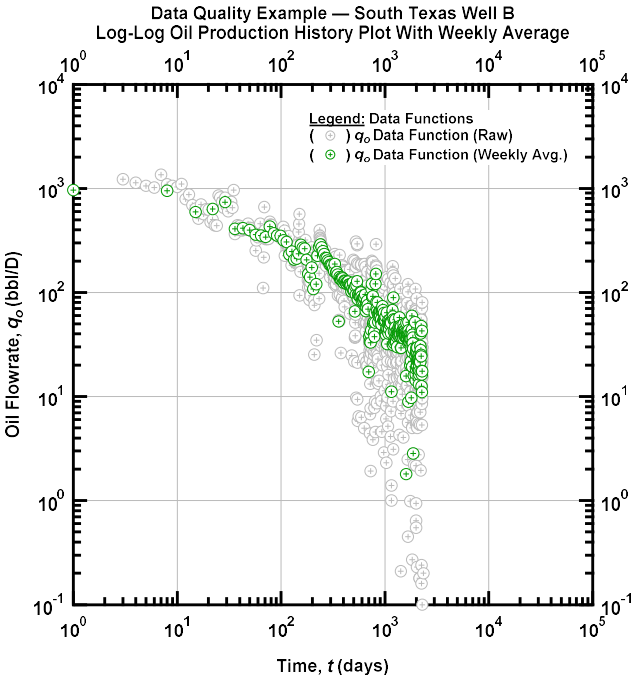

Figure 7.2 — (Log-log Plot) Weekly average oil flowrate (q_o) versus producing time (t). Production history plot – South Texas Well B. Presented to emphasize the non-uniqueness of cleaning data in order to perform decline curve analysis.

Using the weekly averaged data, the *D*- and *b*-parameters were calculated using the Bourdet (1989) pressure derivative algorithm, which can be seen in **Fig. 7.3**. There is only evidence of a trend in the reciprocal of the loss-ratio (*i.e.*, the $D(t)$ trend) and no trend can be seen (or inferred) in the loss-ratio derivative, therefore any attempt at a model match will be non-unique to say the least. Other researchers (such as Ilk (2008)) have attempted to create ways to deal with this data quality issue. Ilk used splines to represent the data, and then take the respective derivatives. The issue with this approach it is also subject to a smoothing parameter (as well as regularization criteria). In order to encourage the use of "*qDb*" models such as the power-law exponential and the stretched exponential, a reliable methodology must be presented to smooth the data.

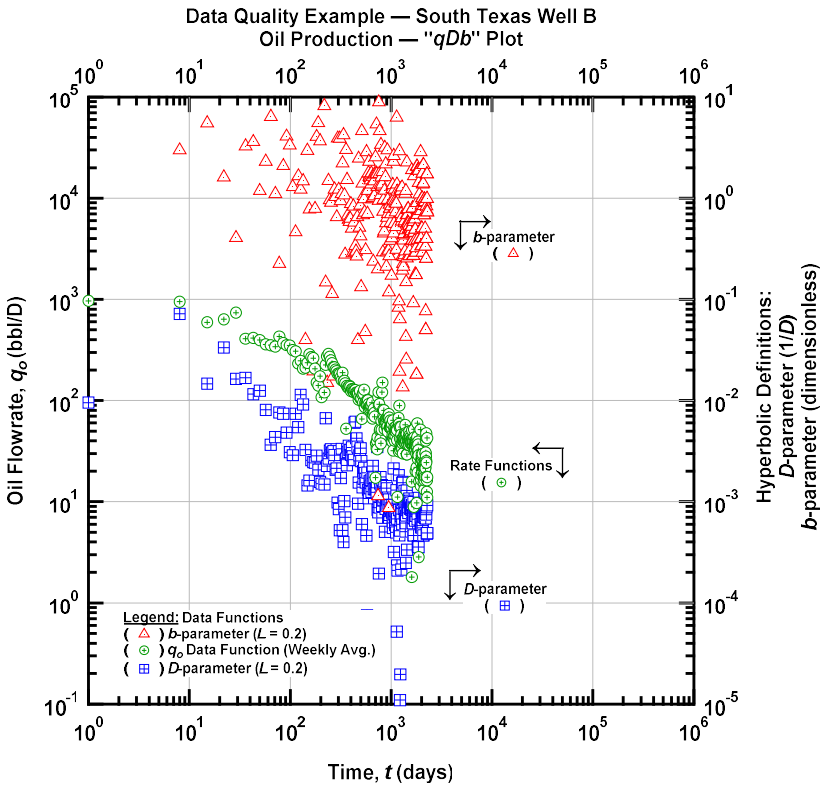

Figure 7.3 — (Log-log Plot) "*qDb*" plot – South Texas Well B. No clear trend can be identified on loss-ratio or loss-ratio derivative.

7.1. Proposed Methodology and Related Equations

This work proposes to use the rate-integral function (actually the time-averaged cumulative production) to assist with creating a more unique matching protocol for performing decline curve analysis. Once the rate-integral of the time-rate data is calculated, the specialized *D*- and *b*-parameters are then determined using the rate-integral data. Decline curve analysis is then performed using both the time-rate and time-rate-integral data, as well as their respective derivatives on an expanded version of the traditional "*qDb*" plot. It is recommended that both projections are used in the analysis because ultimately the time-rate projection is the plot of interest to engineers and the rate-integral is simply an auxiliary function used to assist with being able to create interpretable trends and to perform a more consistent interpretation and analysis.

The rationale for this work was the desire to create a methodology to better observe power-law behavior in the *D*-parameter. In our validation cases prepared for this thesis, the *b*-parameter most often provided the best insight into how well a particular decline curve model represented the simulated time-rate data. Since the *b*-parameter is a second derivative type of function, the calculation is strongly influenced (even corrupted) by the noise in the *D*-parameter. This methodology will also assist with being able to observe trends within the *b*-parameter derived from the rate-integral function. From the validation cases reviewed for this research, it was determined that the modified hyperbolic, the power-law exponential, and the stretched exponential are the most relevant decline curve analysis models for time-rate data obtained from wells in unconventional reservoirs — as such, we will focus on these relations in this chapter.

The rate-rate integral can be calculated using the following:

$$q_{\text{int}}(t) = \frac{\int_0^t q\ dt}{t} \quad \text{.....(7.1)}$$

7.1.1. Power-Law Exponential

By inspection of **Eq. 7.1**, an issue immediately arises for the power-law exponential. With a non-zero terminal decline parameter (*i.e.*, D_∞), there is no direct integration for the time-rate equation. Therefore, if a non-zero D_∞-parameter is used in the power-law exponential the rate-integral as well as the loss-ratio and the loss-ratio derivative of the rate-integral must be computed numerically — this is not a critical issue, it just must be noted. If we assume $D_\infty = 0$, the following equations can be analytically derived.

The time-rate form of the power-law exponential with no terminal decline: [Valko (2009)]

$$q(t) = \hat{q}_i \exp\left[-\hat{D}_i t^n\right] \quad \text{.....(7.2)}$$

The time-rate integral form of the power-law exponential with no terminal decline: [Valko (2009)]

$$q_{\text{int}}(t) = \frac{\hat{q}_i}{\hat{D}_i^{1/n} nt}\left\{\Gamma\left[\frac{1}{n}\right] - \Gamma\left[\frac{1}{n}, \hat{D}_i t^n\right]\right\} \quad \text{.....(7.3)}$$

Where Γ is the complete and incomplete Gamma function.

The loss-ratio of the rate-integral form of the power-law exponential with no terminal decline:

$$D_{\text{int}}(t) = \frac{1}{t} - \frac{\hat{D}_i^{1/n} n e^{-\hat{D}_i t^n}}{\Gamma\left[\frac{1}{n}\right] - \Gamma\left[\frac{1}{n}, \hat{D}_i t^n\right]} \quad \text{.....(7.4)}$$

The derivative of the loss-ratio of the rate-integral form of the power-law exponential with no terminal decline:

$$b_{\text{int}}(t) = -\frac{\dfrac{\hat{D}_i^{1+1/n} n^2 t^{n-1} e^{-\hat{D}_i t^n}}{\left\{\Gamma\left[\frac{1}{n}\right] - \Gamma\left[\frac{1}{n}, \hat{D}_i t^n\right]\right\}} + \dfrac{\hat{D}_i^{2/n} n^2 e^{-2\hat{D}_i t^n}}{\left\{\Gamma\left[\frac{1}{n}\right] - \Gamma\left[\frac{1}{n}, \hat{D}_i t^n\right]\right\}^2} - \dfrac{1}{t^2}}{\left\{\dfrac{1}{t} - \dfrac{\hat{D}_i^{1/n} n e^{-\hat{D}_i t^n}}{\Gamma\left[\frac{1}{n}\right] - \Gamma\left[\frac{1}{n}, \hat{D}_i t^n\right]}\right\}^2} \quad \text{.....(7.5)}$$

The full derivation of **Eq. 7.2 – 7.5** can be found in **Appendix F**.

To use **Eq. 7.2 – 7.5** in the nomenclature defined by the stretched exponential [Valko (2009)] rather than the power-law exponential [Ilk, 2008], the following equation can be used to relate the two decline curve analysis models:

$$\hat{D}_i = \left(\frac{1}{\tau}\right)^n \quad \text{.....(7.6)}$$

More information regarding this can be found in **Appendix G**.

7.1.2 Modified Hyperbolic

The modified hyperbolic is included for completeness since the is (by far) the most commonly applied decline curve in unconventional reservoirs.

The time-rate integral form of the modified hyperbolic decline curve model is defined as:

$$q_{\text{int}}(t) = \begin{Bmatrix} \dfrac{q_i}{D_i(1-b)t}\left[1-(1+bD_i t)^{1-1/b}\right] & (t < t^*) \\ \dfrac{q_i^* - q_i^* e^{-D_{\min}(t-t^*)}}{D_{\min}(t-t^*)} & (t > t^*) \end{Bmatrix} \quad \text{.....(7.7)}$$

The reciprocal loss-ratio for the time-rate integral form of the modified hyperbolic decline curve is defined as:

$$D_{\text{int}}(t)=\begin{Bmatrix}\left[t+\dfrac{(b-1)D_i t^2}{-(bD_i t+1)^{1/b}+D_i t+1}\right]^{-1} & (t<t^*)\\ \left[(t-t^*)+\dfrac{D_{\min}(t-t^*)^2}{e^{D_{\min}(t-t^*)}-D_{\min}(t-t^*)-1}\right]^{-1} & (t>t^*)\end{Bmatrix} \quad \text{.....(7.8)}$$

The derivative of the loss-ratio for the time-rate integral form of the modified hyperbolic decline curve is defined as:

$$b_{\text{int}}(t)=\begin{Bmatrix}1+\dfrac{2(b-1)D_i t}{[-(bD_i t+1)^{1/b}+D_i t+1]}-\dfrac{(b-1)D_i t^2[D_i-D_i(bD_i t+1)^{-1+1/b}]}{[-(bD_i t+1)^{1/b}+D_i t+1]^2} & (t<t^*)\\ 1+\dfrac{2D_{\min}(t-t^*)}{[e^{D_{\min}(t-t^*)}-D_{\min}(t-t^*)-1]^2}-\dfrac{D_{\min}(t-t^*)^2(D_{\min}e^{D_{\min}(t-t^*)}-D_{\min})}{(e^{D_{\min}(t-t^*)}-D_{\min}(t-t^*)-1)^2} & (t>t^*)\end{Bmatrix} \quad \text{.....(7.9)}$$

Where

$$t^*=\frac{\dfrac{D_i}{D_{\lim}}-1}{bD_i} \quad \text{.....(7.10)}$$

$$q_i^*=\frac{q_i-q_i e^{(-D_i t^*)}}{D_i t^*} \quad \text{.....(7.11)}$$

The full derivation of **Eq. 7.7 – 7.11** can be found in **Appendix H**.

7.2. Field Production Data Validation

To demonstrate the utility of this methodology, we will investigate the data from South Texas Well I. The data has been slightly edited, but we note in **Fig. 7.4** that the using the $D(t)$ and $b(t)$ data it is difficult to identify specific trends, leading to non-uniqueness when performing decline curve analysis. We note that **Fig 7.4** is the traditional format for a "*qDb*" plot for South Texas Well I.

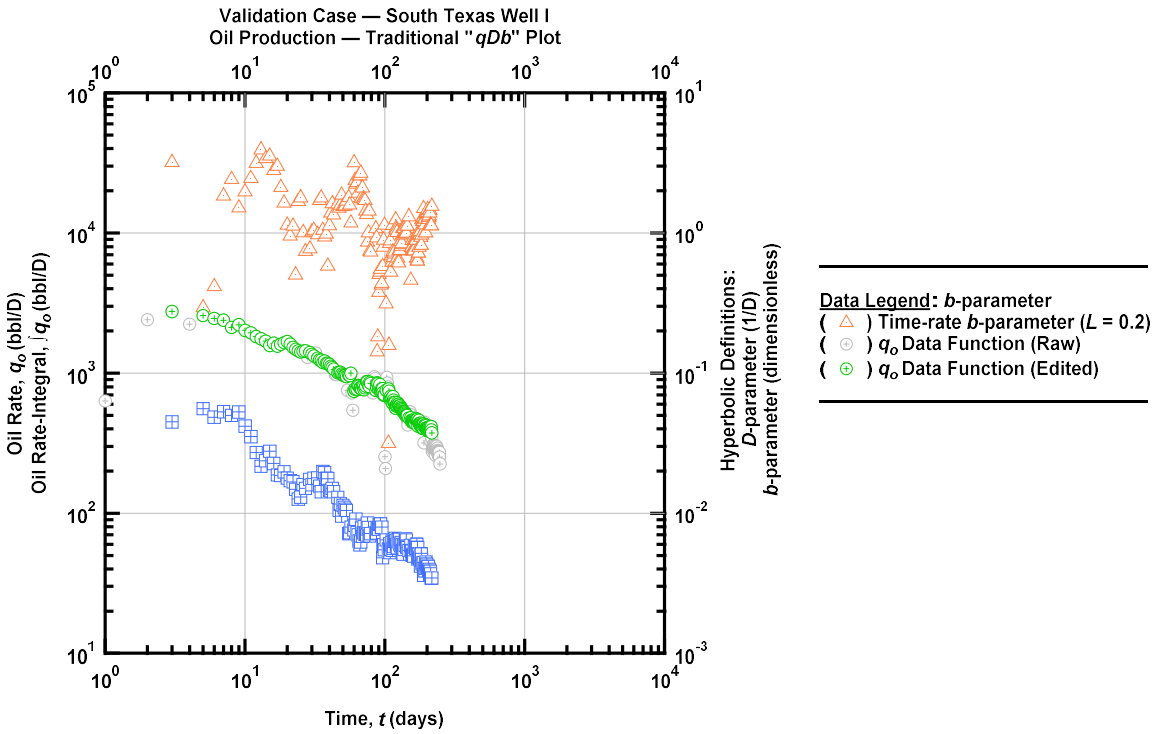

Figure 7.4 — (Log-log Plot) Traditional "*qDb*" plot – South Texas Well I.

Fig. 7.5 is the proposed "*modified qDb*" plot, which includes both the time-rate data as well as the time-rate integral data. We propose that both types of data should be displayed on the "*modified qDb*" plot, this is because ultimately the projection of the time-rate data is desired, the use of the rate-integral and its auxiliary functions are there to support the analysis/interpretation.

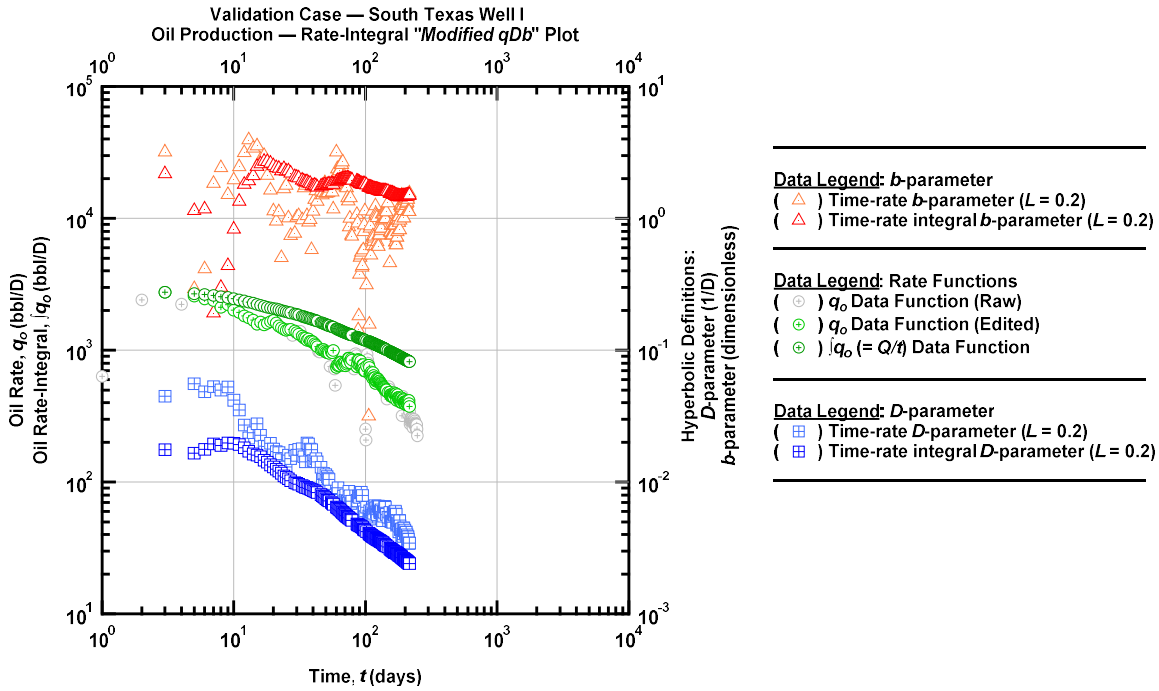

Figure 7.5 — (Log-log Plot) Rate-integral "*modified qDb*" plot – South Texas Well I. Note: both time-rate and time-integral data should be plotted, along with their respective analysis functions

Fig. 7.6 is the same "*modified qDb*" plot as **Fig. 7.5**, but now we include the power-law exponential decline curve model applied ($D_\infty = 0$ case). **Fig. 7.7** is the "*modified qDb*" plot for the stretched exponential model and is essentially identical to **Fig. 7.6**. We propose that using the time-rate-integral functions in **Figs. 7.7 – 7.8** provides this particular data set with a clear and distinct interpretation. We do not propose to evolve the time-rate-integral functions in to a separate path for decline curve analyses, merely to use these functions as part of a workflow for decline curve analysis, particularly for cases with noisy time-rate data. Conceptually, this should be thought of as an approach that provides more clarity of certain behavior, but it is by no means a panacea, data editing and the experience/aptitude of the analyst remains to be very important.

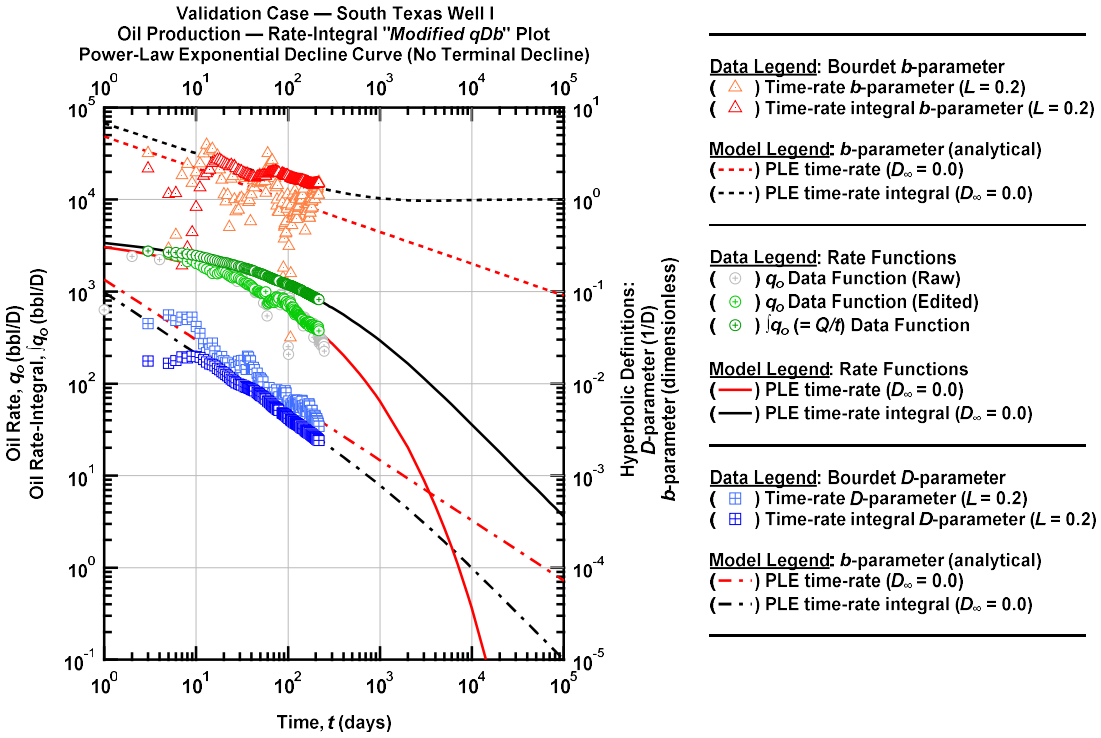

Figure 7.6 — (Log-log Plot) Rate-integral "*modified qDb*" plot – South Texas Well I. Power-law exponential decline curve model assuming a zero terminal decline parameter.

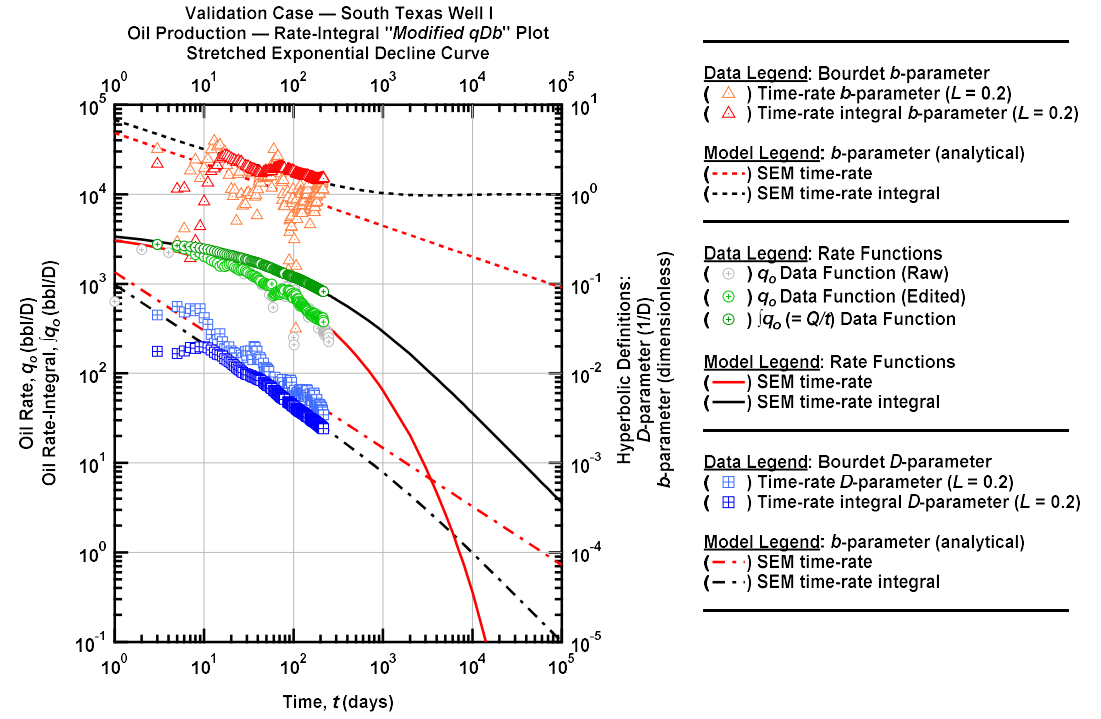

Figure 7.7 — (Log-log Plot) Rate-integral "*modified qDb*" plot – South Texas Well I. Stretched exponential decline curve model.

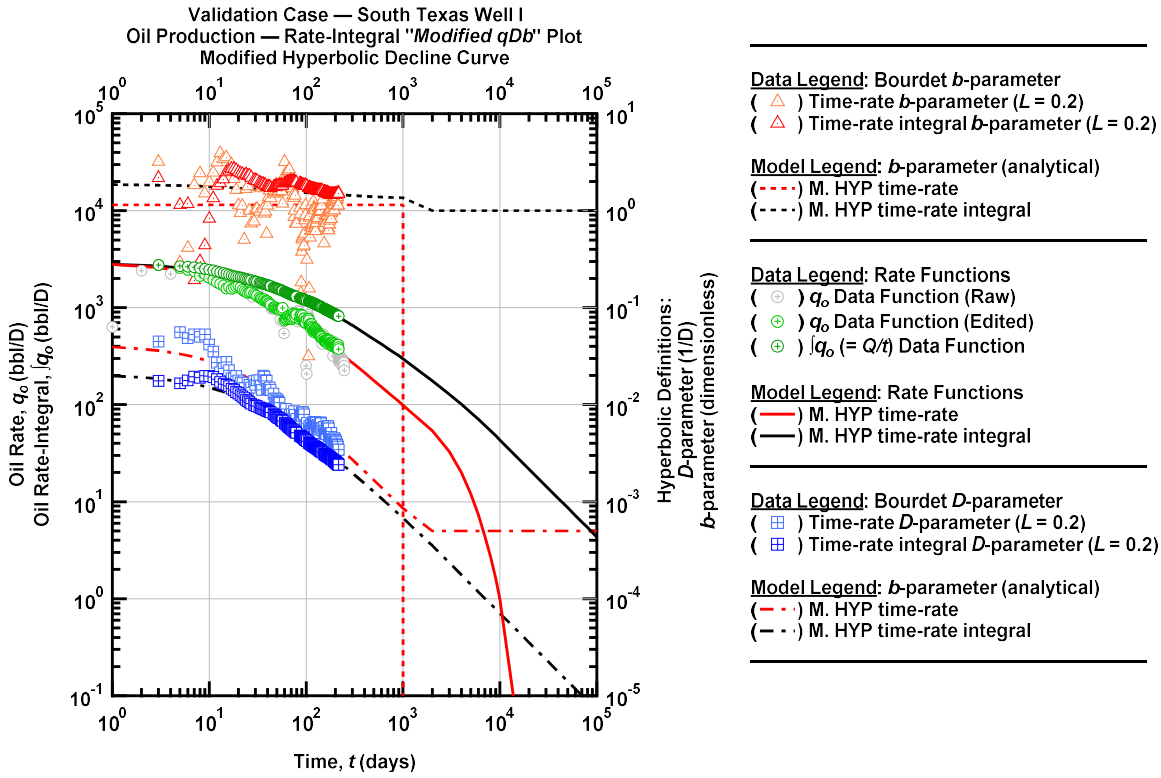

Figure 7.8 — (Log-log Plot) Rate-integral "*modified qDb*" plot – South Texas Well I. Modified hyperbolic decline curve model.

In **Fig. 7.8** we present the same data functions as **Figs. 7.6 and 7.7**, but now we impose the modified hyperbolic decline curve model on the data trends. Based on the observed trends, one could conclude that this data set is "not" hyperbolic, but is rather "power-law" (or "stretched") exponential as the modified hyperbolic is not a perfect match for the *b*-parameter (assumed constant in the modified hyperbolic time-rate formulation).

7.3. Mechanistic Model Validation

To validate the proposed methodology, the Eagle Ford mechanistic model validation case will be expanded to include the time-rate integral formulation. In **Fig. 7.9** we present the rate-integral "*modified qDb*" plot of the time-rate data generated using the mechanistic model Eagle Ford case. This is exactly the same data that was presented in **Section 5.2**. The reciprocal loss-ratio and loss-

ratio derivative functions for the time-rate and time-rate integral data were calculated numerically using a spline representation of the time-rate data (this is the same methodology as used in the mechanistic validation cases presented in **Chapter 5**). We note that this can also be done using the Bourdet (1989) pressure derivative algorithm, as presented in **Section 7.1**. In this case the spline approach was used for consistency with the mechanistic validation cases.

In **Fig. 7.10** we present the rate-integral "*modified qDb*" plot with the decline curve analysis being performed using the *stretched exponential model*, which does not have a terminal decline parameter and it cannot represent the "late-life" behavior of the time-rate data correctly. We chose this model for the simplicity of having a direct (analytical) integration solution for cumulative production.

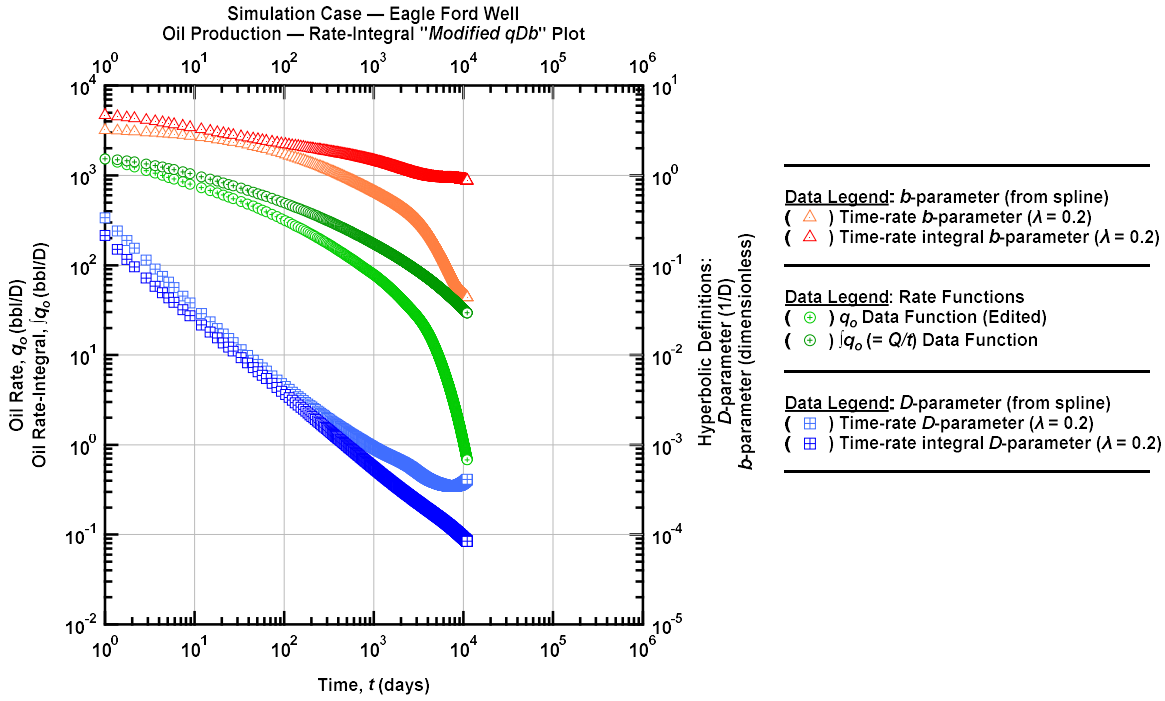

Figure 7.9 — (Log-log Plot) Rate-integral "*modified qDb*" plot – Eagle Ford shale validation case.

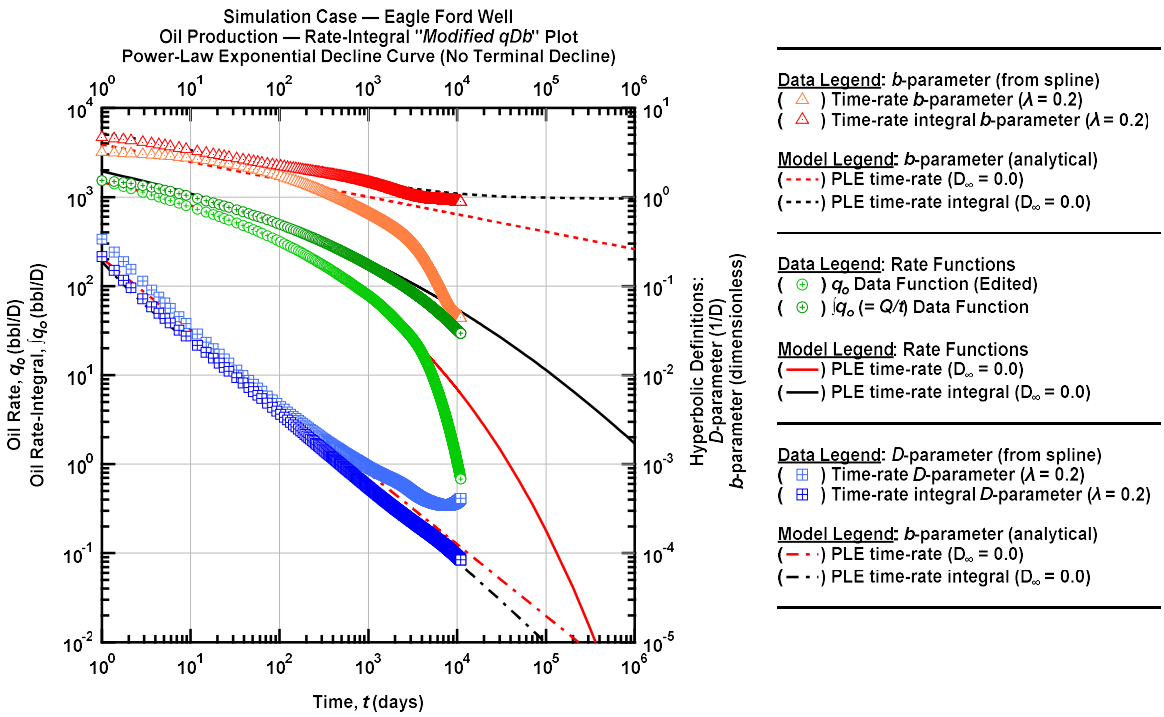

Figure 7.10 — (Log-log Plot) Rate-integral "*modified qDb*" plot – Eagle Ford shale validation case. Power-law exponential decline curve model with no terminal decline parameter.

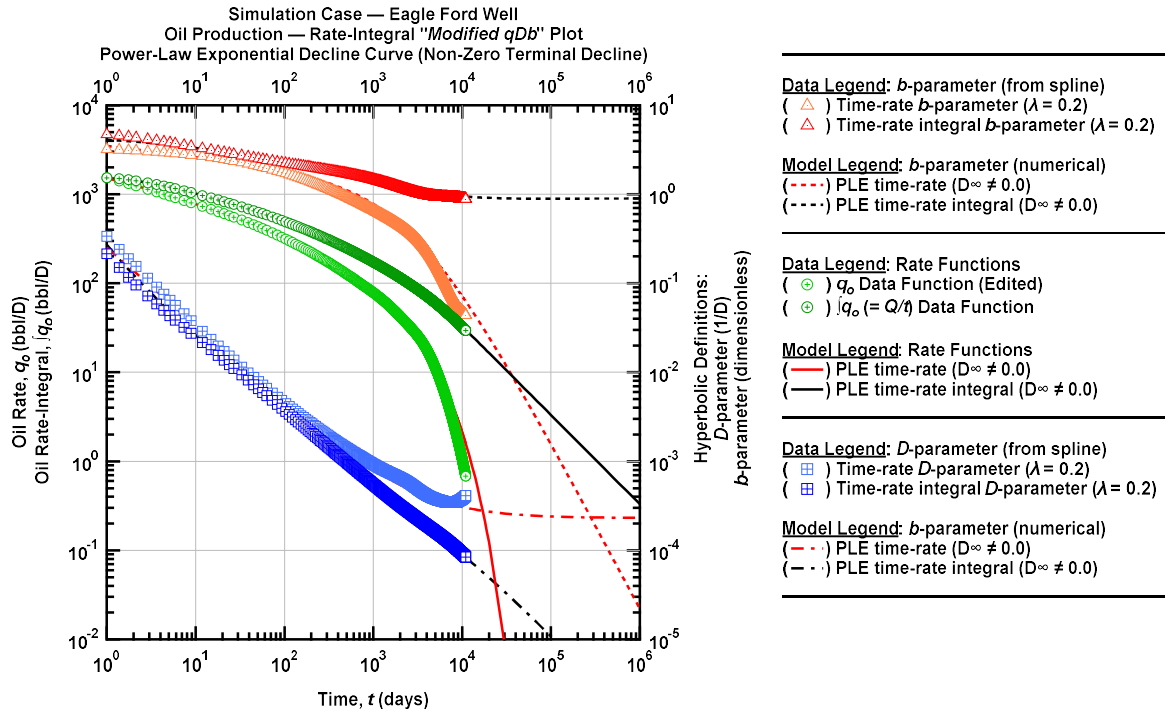

Figure 7.11 — (Log-log Plot) Rate-integral "*modified qDb*" plot – Eagle Ford shale validation case. Power-law exponential decline curve model with a non-zero terminal decline parameter.

In **Fig. 7.11** we present the rate-integral "*modified qDb*" plot for the power-law exponential model where in this case the ($D_\infty \neq 0$ case), hence we must compute the cumulative production function numerically (rather than analytically as in the case of the stretched exponential model). We note a very good to excellent match of the power-law exponential model against all data functions (*i.e.*, time-rate and time-rate-integral), indicating that this approach does have utility in adding the auxiliary time-rate-integral functions for better resolution and clarity of the data trends.

Lastly, we present the methodology applied to the modified hyperbolic model in **Fig. 7.12** and we immediately note an excellent match of the modified hyperbolic model to each data function. As comment, there are minor mismatches in the $D(t)$, $b(t)$, $D_{int}(t)$, and $b_{int}(t)$ functions after the constant D-parameter is imposed (*i.e.*, the terminal decline) — however; the time-rate and time-rate-integral matches are excellent despite these conditions.

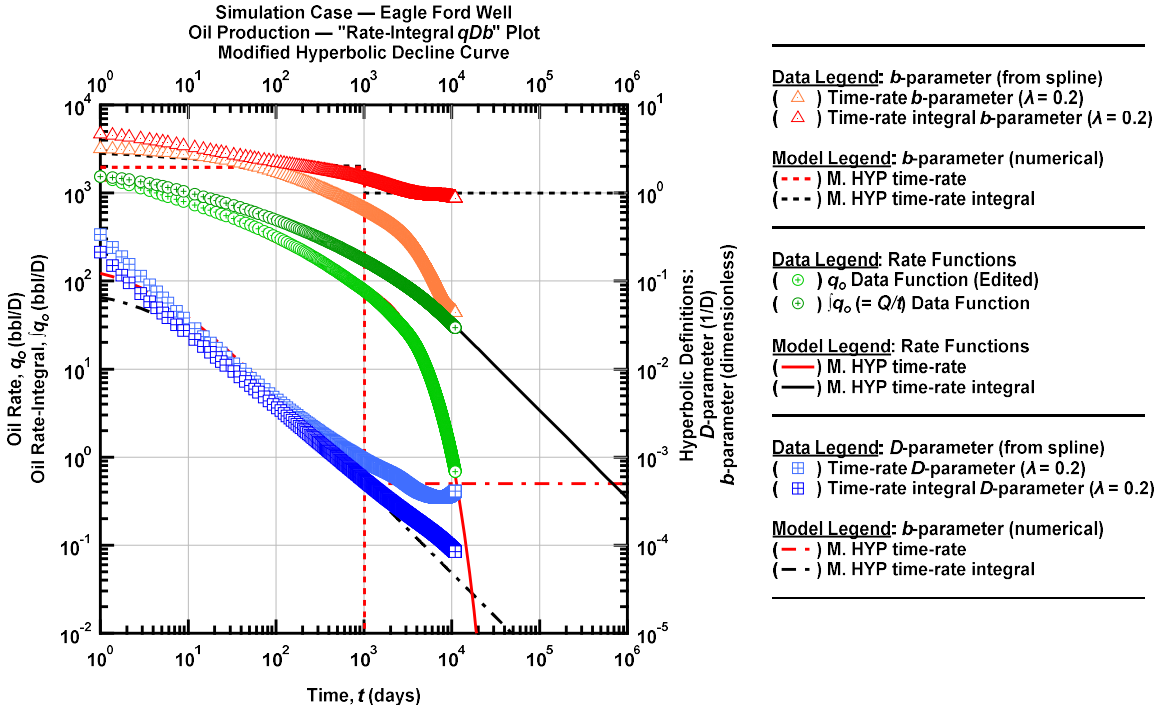

Figure 7.12 — (Log-log Plot) Rate-integral "*modified qDb*" plot – Eagle Ford shale validation case. Modified hyperbolic curve model.

It has been shown with this mechanistic model validation that the proposed methodology is a valid approach to performing decline curve analysis. The purpose of using the rate-integral is to allow for trends to be better observed within the data. It is not intended to replace typical time-rate decline curve analysis, but rather to be used as another form of validation when calibrating a decline curve model.

CHAPTER VIII

BEST PRACTICE GUIDELINES AND RANKING

One of the main objectives for this research was to develop best practice guidelines for decline curve analysis model presented for its ability to accurately represent data from unconventional reservoirs. In this section the learnings from the mechanistic model validation cases are summarized for each investigated decline curve analysis model. Overall guidelines for performing decline curve analysis will also be discussed. Finally, ranking of the decline curve models investigated in this research will be presented.

8.1 General Best Practices for DCA

The following are general best practices and guidelines that can assist with decline curve analysis:

- *Always use a "qDb" plot.*

  The use of a "*qDb*" plot allows for a more unique decline curve analysis to be performed and therefore more accurate predictions of future performance. The use of the reciprocal loss-ratio and the loss-ratio derivative allow for greater insight into how well the selected decline curve model is able to represent the time-rate data. It can be seen throughout the validation cases presented in this thesis that nearly all of the decline curve analysis models appeared to represent the time-rate data well, but it wasn't until further analysis was performed to see how well the model represented the time-rate data's associated derivatives that it was able to be determined if the selected decline curve model was valid or not for that particular case.

- *In situations where data quality is a concern, use the rate-integral "qDb" plot.*

  The methodology presented in **Chapter VII** allows for trends to be more clearly identified in the loss-ratio and loss-ratio derivative, enabling more unique decline curve analysis to be performed in instances of poor time-rate data quality. The advantage of the methodology presented in **Chapter VII** over other data interpretation techniques is that it is not subject to additional smoothing factors.

- *In most cases, DCA models with terminal decline parameters are less likely to lead to overestimates in EUR.*

  The DCA models with terminal decline parameters tend to better represent not only the transient/transitional behavior experienced in time-rate data, but also the terminal decline behavior. In all of the mechanistic model cases we considered the terminal decline behavior (flattening of the $D(t)$ profile) was observed in well performance results. In such cases when decline curve analysis is performed, the transient portion of the trend is "over-extrapolated" unless the terminal decline parameter for a given model are used. In cases where the DCA relation does not have a terminal decline parameter, or said parameter is not used, significant overestimates of forecasted rates and EUR values can and will occur.

- *Do not attempt to perform DCA until the well has produced at a near-constant bottomhole pressure for a period of time.*

  This recommendation references two of the primary assumptions Lee and Wattenbarger (1996) presented for the classical Arps' decline curve models; the well is being produced at a constant bottom hole pressure, and that previous production performance is representative of future performance. The current practice for EUR calculations is 30

years. For most of the well's productive life it will be produced at (or near) a constant bottomhole pressure.

As discussed in Section 5.4, the example cases from South Texas that we used for the non-constant bottomhole validation case reached a relatively constant bottomhole pressure after approximately140 days of producing time. Prior to this time, the simulated mechanistic model results produced at a near constant-rate solution. Performing decline curve analysis prior to (approximately) constant bottomhole pressure production leads to overestimates in forecasted flowrates and EUR.

- *Reservoir size greatly impacts late-life behavior.*

  This phenomenon is best expressed in the time it took for the mechanistic model simulated time-rate data to exhibit terminal decline behavior between the Eagle Ford and the Wolfcamp validation cases. The Wolfcamp validation case assumed that there was more reservoir volume for the hydraulic fractures to access, which lead to the terminal decline being less aggressive and much later in the well's producing life. This may be obvious for simulation purposes, but in terms of decline curve analysis in practice, it may be overlooked.

  When unconventional reservoirs were first being exploited through the use of horizontal drilling and hydraulic fracturing, the wells were spaced much farther apart and the well completions had much wider cluster spacing with less proppant being used. Now, well spacing has decreased (significantly) and the hydraulic fracturing treatments have become much larger. Newer wells may be able to repeat the initial production performance of the "vintage" wells though the advancements in hydraulic fracturing design, but the reservoir volume dedicated to each well has decreased, perhaps significantly. From the results of

our mechanistic model, it is suggested that newer, more tightly-spaced wells will experience terminal decline behavior earlier and may not produce the long-term transient performance exhibited by the older wells that have had access to a larger reservoir volume.

- *Do not only use techniques such as the method of least squares to determine decline parameters for decline curve analysis models.*

  It can be very tempting to only use techniques such as the method of least squares to determine the decline curve parameters associated with a particular decline curve model when performing an analysis. It is not unreasonable to believe that if the statistical error between the decline curve model and available production data is minimized, that such scenarios will yield the best forecasted future production. However, relying solely on this assumption can lead to significantly overestimating EUR and a poor representation of future performance.

  All of the decline curve analysis models used in this work are entirely empirical, meaning that none of these are a direct solution to the governing mass and flow equations. When only using statistical methods (*e.g.*, least squares), the worst model in terms of forecasting *may be* the very popular modified hyperbolic model. Unfortunately, modified hyperbolic DCA model is the most common model used for decline curve analysis in unconventional reservoirs and using the method of least squares is probably the most common way this model is applied. A better "application" is to use the computed $D(t)$ and $b(t)$ functions (from the given data), where we note specifically that the hyperbolic portion of the modified hyperbolic suggests a constant b-parameter during the "transient" portion of production behavior (which could last for years).

If the decline parameters for the modified hyperbolic are determined using the method of least squares it is likely that the estimated *b*-parameter will be the (approximate) average over the production interval. However, if more production data are available, the *b*-parameter (constant) will be consistently lower as more data are added. This is very apparent for the cases shown in **Fig. 6.1**. In short, it is highly recommended that the decline curve model calibration be fine-tuned by hand.

- *Perform lookback analysis on previous DCA models.*

  It is good practice to review previous decline curve analyses performed on a well once more production data becomes available. This will allow for insight — for example, in the validation cases, the *b*-parameter was shown to be decreasing with time, therefore it is expected that if a lookback on previous decline curve analysis is performed the current *b*-value of the time-rate data will be less than when the analysis was initially performed. This allows engineers to review if the previous assumptions for a given behavior of the *b*-parameters are valid or need revision.

8.2. DCA Model Specific Recommendations and Guidelines

The following are recommendations and guidelines that were determined by the lessons-learned from performing this research for each of decline curve analysis models investigated.

8.2.1. Modified Hyperbolic DCA Model

- When properly calibrated, the modified hyperbolic model provides a good estimate for EUR and is (relatively) simple to apply. The modified hyperbolic remains the most commonly applied model for wells in unconventional reservoirs.

- It is commonly recommended (based on company guidelines) that a D_{min}-parameter of 10% / year is a good (conservative) estimate for the D_{min}-parameter. From the validation cases generated using the mechanistic model for this research, a value of about 5.0% / year seems more appropriate for the D_{min}-parameter.
- Do not select a b-parameter > 2 — $b = 2$ is indicative of linear flow and it has been shown that linear flow is not observed for the entire production life of a well in an unconventional reservoir system. Some may be tempted to use $b = 4$ (bilinear flow), but this is clearly transient flow only and will yield a significant overestimation in the production forecast and EUR.
- The exponential tail is likely too aggressive in terms of production decline for the terminal decline behavior, but in a practical sense, the terminal exponential decline is both conservative and yields a very specific (read, predictable) trend.

8.2.2. Power-Law Exponential Model

- Overall, the power-law exponential is the most accurate decline curve analysis model investigated most in terms of observed diagnostic trends, production forecasts, and EUR estimates. This could be due to the relatively conservative nature of the mechanistic model process, and other researchers have also commented similarly that the power-law exponential was, on average, the best model for representing production performance.
- The "terminal decline" is modelled by the D_∞-parameter and using a non-zero estimate of D_∞ seems to be most appropriate when a strong decline trend is noted in the $D(t)$ and $b(t)$ data functions. Specifically, it may be most appropriate to use a non-zero estimate of D_∞ for cases of long-term transient production behavior.

- For cases where transient behavior is less apparent at early times, then the use of $D_\infty = 0$ (which actually reverts to the "Stretched Exponential" model) tends to provide a better estimate for EUR.

8.2.3. Stretched Exponential Model

- The Stretched Exponential is identical to the Power-Law Exponential for the case of $D_\infty = 0$. In practice, it is recommended to use the power-law exponential in lieu of the stretched exponential due to its ability to incorporate a terminal decline parameter (*i.e.*, $D_\infty \neq 0$).

8.2.4. Duong's Method

- Tends to significantly overestimate EUR and consistently provided the highest estimate for EUR in all validation cases conducted in this research.
- The Duong method is not recommended as a general approach to forecast unconventional time-rate data and should only be used in scenarios where *very* long-term transient behavior is expected for nearly the entire production life of the well.
- If an early-time straight-line trend is observed in a plot of $\log[q(t)/G_p(t)]$ versus $\log[t]$, then the Duong method may have "theoretical" validity. However, this is not indicative of future production and the straight-line trend is no longer valid in late-life time-rate data.

8.2.5. Logistical Growth Model

- The logistical growth model acts as a "hybrid" decline curve relation, where the b-parameter is constant initially, decreases during transient flow, and then is constant during late life-production.

- Due to the logistical growth model not including a terminal decline parameter it is not able to represent late-life behavior as well as the power-law exponential or the modified hyperbolic.
- Due to the nature of the equation, the *K*-parameter is the carrying capacity of the system, which Clark *et al*. (2011) suggested is the EUR for the well without economic constraints. In calibrating the logistical growth model using the simulated 30-year EUR as an estimate for the *K*-parameter did not improve the quality of the time-rate projection. The *K*-parameter needed to be much greater than the simulated 30-year EUR to obtain a higher quality calibration. Therefore, it is not recommended to use the *K*-parameter estimate as a substitute for the EUR of the well.

8.3. Ranking of Investigated DCA Models

Based on the observations/learnings derived from this research, we provide the following ranking of the decline curve analysis models that were investigated (best to worst):

1. Power-Law Exponential (best)
2. Modified Hyperbolic
3. Stretched Exponential
4. Logistical Growth Model
5. Duong Method (worst)

The power-law exponential model was determined to be the best overall decline curve analysis model for unconventional reservoirs due to its consistent ability to accurately predict future flowrates and EUR, correctly represent the reciprocal loss-ratio and the loss-ratio derivative,

provide accurate EUR estimates based on a short producing time, and its inclusion of a strong terminal decline parameter.

The modified hyperbolic was the second-best model investigated in this study largely due to its ability to provide accurate estimates for EUR and its incorporation of a terminal (exponential) decline parameter. Although it was shown that the *b*-parameter for wells in unconventional reservoirs consistently decrease with time, often the assumption of a constant *b*-parameter in the modified hyperbolic was a "good enough" approximation for this decline.

The stretched exponential was ranked behind the modified hyperbolic, ultimately due to its lack of a terminal decline parameter. In all validation cases a terminal decline was observed and without a parameter to capture the late-life production the stretched exponential can lead to overestimates in predicted flowrates and EUR (as discussed in the producing time study in **Chapter VI**).

The Logistical Growth Model has characteristics similar to the modified hyperbolic and power-law exponential models. As a "population" model the Logistical Growth Model does not have a terminal decline component and it is felt that the modified hyperbolic and power-law exponential models will produce more consistent results.

Lastly, the Duong model was generally the poorest performer and tended to over-extrapolate future flowrates and EUR. As an aside, there have been proposals to add a terminal decline component to the Duong model and while we acknowledge that the Duong model does have a theoretical / conceptual basis for early-time (power-law) rate behavior, without "dampening" (*i.e.,* a terminal decline) component, this approach will consistently and possibly significantly over-extrapolate.

CHAPTER IX

SUMMARY, CONCLUSIONS, AND RECOMMENDATIONS FOR FUTURE WORK

9.1. Summary

This work provides the validation and ranking of numerous decline curve analysis models. From the validation cases analyzed in this research, best practice guidelines for each of the decline curve analysis models are presented. In addition to the decline curve specific guidelines, general best practices were outlined for implementation when performing decline curve analysis. A built-for-purpose mechanistic (numerical simulation) model was developed and successfully used as a validation tool. The mechanistic model was able to accurately able to represent "non-mechanistic" behaviors experienced in unconventional reservoirs including:

- Early-time performance, production is dominated by a high water cut from the fractures.
- Transient performance, where linear or bi-linear flow regimes can be clearly identified.
- Transitional performance, where linear nor boundary regimes cannot be clearly identified.
- Late-time performance, where pressure-dependent properties and/or depletion effects hinder well performance.

The primary validation cases were analyzed using typical well performance data, reservoir, and completion properties from the Haynesville, Eagle Ford, and the Wolfcamp formations. All are prolific unconventional oil and gas reservoirs found onshore in the United States. All of these formations require the use of "multi-fractured horizontal wells" (MFHWs) in order to produce hydrocarbons economically.

Mechanistic model studies are typically conducted based on idealized production scenarios (*e.g.*, production at a constant bottomhole flowing pressure). However; in reality such scenarios are not valid. For this purpose, we used the field production data for validation of the decline curve analysis models.

We did perform a "validation" of decline curve analysis models using our mechanistic model in order to provide insight into each of the decline curve analysis methods. However, the overall purpose of performing decline curve analysis is to forecast future performance using the available time-rate data via a simple proxy model. In other words, we cannot necessarily "invert" our results obtained from proxy models applied to the performance data generated using our mechanistic models to yield the parameters input into the mechanistic model.

In addition, we propose a methodology to assist with the analysis and interpretation of poor-quality time-rate data obtained from wells in unconventional reservoirs. The respective equations for the power-law exponential, stretched exponential, and modified hyperbolic decline curve models were derived and presented as well as the associated modified "*qDb*" plot (referred to as the rate-integral "*modified qDb*" plot). Examples using field-derived time-rate data, as well as well performance results from our mechanistic model were conducted using the new proposed methodology.

9.2. Conclusions

- The power-law exponential relation was consistently the best decline curve analysis model investigated in terms of observed trends and statistical regressions.
- Power-law (straight-line) behavior is the most commonly observed behavior in terms of the reciprocal of the reciprocal loss-ratio (*i.e.,* the $D(t)$ function) for the unconventional reservoir cases considered in this work.

- The derivative of the loss-ratio (*i.e., b*(*t*) function) was observed to "continuously decrease" for the unconventional reservoir cases considered in this work.
- The "terminal decline" feature is observed in nearly all of the time-rate data from both the unconventional reservoir cases considered in this case and the well performance results obtained from our mechanistic model.

9.3 Recommendations for Future Work

- Develop a decline curve analysis model that accurately forecasts three phase (*i.e.,* oil, water, and gas) time-rate data simultaneously using relations that represent projections for water-oil-ratio (WOR) and gas-oil-ratio (GOR).
- Continue validation of decline curve analysis models with additional mechanistic models (these could be specific numerical, semi-analytical, and analytical models).
- Continue the validation and ranking of decline curve analysis models on their ability to accurately represent time-rate-pressure data from unconventional reservoirs.
- Continue to asses non-mechanistic behaviors experienced in unconventional reservoir systems.

REFERENCES

Arps, J.J. 1945. Analysis of Decline Curves. *Trans*. AIME **160**: 228-247.

Arps, J.J. 1956. Estimation of Primary Oil Reserves. *Trans*. AIME **207**: 182-191.

Blasingame, T.A., McCray, T.L., and Lee, W.J. 1991. Decline Curve Analysis for Variable Pressure Drop/Variable Flowrate Systems. Paper SPE 21513 presented at the SPE Gas Technology Symposium, Houston, TX, 23-24 January 1991.

Blumberg, A.A. 1968. Logistic Growth Rate Functions. *Journal of Theoretical Biology* **21**: 42-44.

Bourdet, D., Ayoub, J.A., and Pirard, Y.M. 1989. Use of Pressure Derivative in Well-Test Interpretation. *SPEFE* (June 1989) 293, *Trans.*, AIME, **287**.

Camacho-Velazquiez, R.G. and Raghavan, R. 1989. Boundary-Dominated Flow in Solution-Gas-Drive Reservoirs. *SPERE* **4** (4): 503-512.

Chung, T. H., Lee, L. L., & Starling, K. E. (1984). Applications of Kinetic Gas Theories and Multiparameter Correlation for Prediction of Dilute Gas Viscosity and Thermal Conductivity. *Industrial & Engineering Chemistry Fundamentals*, **23**(1), 8–13. doi: 10.1021/i100013a002.

Chung, T. H., Ajlan, M., Lee, L. L., & Starling, K. E. (1988). Generalized Multiparameter Correlation for Nonpolar and Polar Fluid Transport Properties. *Industrial & Engineering Chemistry Research*, **27**(4), 671–679. doi: 10.1021/ie00076a024

Clark, A.J., Lake, L.W., and Patzek, T.W. 2011. Production Forecasting with Logistic Growth Models. Paper SPE 144790 presented at the SPE Annual Technical Conference and Exhibition, Denver, CO, 30 October – 02 November 2011.

Collins, P 2016. Decline Curve Analysis for Unconventional Reservoir Systems – Variable Pressure Drop Case. M.S. Thesis. Texas A&M University, College Station, Texas.

Collins, P.W., Ilk, D., and Blasingame, T.A. 2014. Practical Considerations for Forecasting Production Data in Unconventional Reservoirs - Variable Pressure Drop Case. Paper SPE 170945 presented at the SPE Annual Technical Conference and Exhibition, Amsterdam, The Netherlands, 17-29 October 2014.

Cutler, W.W. 1924. Estimation of Underground Oil Reserves by Oil-Well Production Curves. *Bull*. USBM 228 (1).

Dietrich, J. K., & Bondor, P. L. (1976). Three-Phase Oil Relative Permeability Models. SPE Annual Fall Technical Conference and Exhibition. doi: 10.2118/6044-MS

Duong, A.N. 2011. Rate-Decline Analysis for Fracture-Dominated Shale Reservoirs. SPE *Reservoir Evaluation and Engineering* **14** (3): 337-387.

Egbogah, E.O., Ng, J.T. (1990). An Improved Temperature-Viscosity Correlation for Crude-Oil Systems. *J. Pet. Sci. Eng.* **4** (3): 197–200. doi:10.1016/0920-4105(90)900009-R

Hagedorn, A., Brown, K., 1965. Experimental Study of Pressure Gradients Occuring During Continuous Two-Phase Flow in Small-Diameter Vertical Conduits. *Journal of Petroleum Technology* **17** (4): SPE-940-PA. doi:10.2118/940-PA

Ilk, D. 2010. Well Performance Analysis for Low to Ultra-Low Permeability Reservoir Systems. PhD dissertation. Texas A&M University, College Station, Texas.

Ilk, D. and Blasingame, T.A. 2013. Decline Curve Analysis for Unconventional Reservoir Systems - Variable Pressure Drop Case. Paper SPE 167253 presented at the SPE Unconventional Resources Conference-Canada, Calgary, Alberta, Canada, 05-07 November 2013.

Ilk, D., Currie, S.M., Symmons, D., Rushing, J.A., and Blasingame, T.A. 2010. Hybrid Rate-Decline Models for the Analysis of Production Performance in Unconventional Reservoirs. Society of Petroleum Engineers. doi:10.2118/135616-MS.

Ilk, D., Rushing, J.A., and Blasingame, T.A. 2009. Decline Curve Analysis for HP/HT Gas Wells: Theory and Applications. Paper SPE 125031 presented at the SPE Annual Technical Conference and Exhibition, New Orleans, LA, 04–07 October 2009.

Ilk, D., Rushing, J.A., Perego, A.D., and Blasingame, T.A. (2008) Exponential vs. Hyperbolic Decline in Tight Gas Sands: Understanding the Origin and Implications for Reserve Estimates Using Arps' Decline Curves. Society of Petroleum Engineers. doi:10.2118/116731-MS.

Ilk, D., Perego, A.D., Rushing, J.A., and Blasingame, T.A. 2008. Exponential vs. Hyperbolic Decline in Tight Gas Sands – Understanding the Origin and Implications for Reserve Estimates Using Arps' Decline Curves. Paper SPE 116731 presented at the SPE Annual Technical Conference and Exhibition, Denver, CO, 21–24 September 2008.

International Association for the Properties of Water and Steam, IAPWS R6-95(2018), Revised Release on the IAPWS Formulation 1995 for the Thermodynamic Properties of Ordinary Water Substance for General and Scientific Use (2018).

Johnson, R.H. and Bollens, A.L. 1927. The Loss Ratio Method of Extrapolating Oil Well Decline Curves. *Trans*. AIME **77**: 771.

Kisslinger, C. 1993. The Stretched Exponential Function as an Alternative Model for Aftershock Decay Rate. *Journal of Geophysical Research* **98** (2): 1913-1921.

Lee, W.J. and Sidle, R.E. 2010. Gas Reserves Estimation in Resource Plays. Paper SPE 130102 presented at the 2010 SPE Unconventional Reservoirs Conference, Pittsburgh, PA, USA, 23-25 February 2010

Lee, J. and Wattenbarger, R.A. 1996. *Gas Reservoir* Engineering, Vol. 5, 215. Richardson, Texas. Textbook Series, SPE.

Lewis, J.O. and Beal, C.H. 1918. Some New Methods for Estimating the Future Production of Oil Wells. *Trans*. AIME **59**: 492-525.

Maley, S. 1985. The Use of Conventional Decline Curve Analysis in Tight Gas Well Applications. Paper SPE 13898 presented at the Low Permeability Gas Reservoirs Conference, Denver, CO, 19-22 May 1985.

Moridis, G. J., & Freeman, C. M. (2014). The RealGas and RealGasH2O options of the TOUGH+ code for the simulation of coupled fluid and heat flow in tight/shale gas systems. *Computers & Geosciences,* 65, 56–71. doi: 10.1016/j.cageo.2013.09.010

Muskat, M. 1934. The flow of compressible fluids through porous media and some problems in heat conduction. *Physics*, *5*(3), pp.71-94. https://doi.org/10.1063/1.1745233.

Okouma, V., Symmons, D., Hosseinpour-Zonoozi, N., Ilk, D., and Blasingame, T.A. 2012. Practical Considerations for Decline Curve Analysis in Unconventional Reservoirs-Application of Recently Deve0loped Time-Rate Relations. Paper SPE 162910 presented at the SPE Hydrocarbon, Economics, and Evaluation Symposium, Calgary, Alberta, Canada, 24-25 September 2012.

Peng, D. Y.; Robinson, D. B. (1976). "A New Two-Constant Equation of State". Industrial and Engineering Chemistry: Fundamentals. 15: 59–64. doi:10.1021/i160057a011

Poling, B. E., Prausnitz, J. M., & OConnell, J. P. (2007). *The Properties of Gases and Liquids* (5th ed.). Boston: McGraw-Hill.

Pruess, K., Oldenburg, C., & Moridis, G. (1999). TOUGH2 User's Guide, Version 2.0, Report LBNL-43134, Lawrence Berkeley National Laboratory, Berkeley, California. doi: 10.2172/751729

Robertson, S. 1988. Generalized Hyperbolic Equation. Paper SPE 18731 available from SPE, Richardson, Texas.

Rushing, J.A., Perego, A.D., Sullivan, R.B., and Blasingame, T.A. 2007. Estimating Reserves in Tight Gas Sands at HP/HT Reservoir Conditions: Use and Misuse of an Arps Decline Curve Methodology. Paper SPE 109625 presented at the SPE Annual Technical Conference and Exhibition, Anaheim, CA, 11-14 November 2007.

Spencer, R.P. and Coulombe M. J. 1966. Quantitation of Hepatic Growth and Regeneration. *Growth, Development and Aging* **30** (3): 277-284.

Standing, M.B. 1947. A Pressure-Volume-Temperature Correlation for Mixures of California Oils and Gases. Drilling and Production Practice, New York, NY, 1 January. API-47-275/

Stehfest, H. (1970). Algorithm 368: Numerical Inversion of Laplace Transforms [D5]. *Communications of the ACM*, 13(1), 47–49. doi: 10.1145/361953.361969

Stone, H.L. (1973). Estimation of Three-Phase Relative Permeability and Residual Oil Data. *Journal of Canadian Petroleum Technology*, 12(04). doi: 10.2118/73-04-06

Tsonopoulos, C., & Wilson, G. M. (1983). High-Temperature Mutual Solubilities of Hydrocarbons and Water. Part I: Benzene, Cyclohexane and n-Hexane. *AIChE Journal*, 29(6), 990–999. doi: 10.1002/aic.690290618

Tsonopoulos, C. (1999). Thermodynamic Analysis of The Mutual Solubilities of Normal Alkanes and Water. *Fluid Phase Equilibria*, 156(1-2), 21–33. doi: 10.1016/s0378-3812(99)00021-7

Valkó, P.P. 2009. Assigning Value to Stimulation in the Barnett Shale: A Simultaneous Analysis of 7000 Plus Production Histories and Well Completion Records. Paper SPE 119369 presented at the SPE Hydraulic Fracturing Technology Conference, College Station, TX, 19-21 January 2009.

Van Everdingen, A.F., and Hurst, W. (1949, December 1). The Application of the Laplace Transformation to Flow Problems in Reservoirs. Society of Petroleum Engineers. https://doi.org/10.2118/949305-G.

Vazquez, M., & Beggs, H. D. (1977). Correlations for Fluid Physical Property Prediction. Society of Petroleum Engineers. doi:10.2118/6719-MS

Wiewiorowski, N.E. 2016. Characterization of Early-Time Performance of a Well with a Vertical Fracture Producing at a Constant Pressure. MS Thesis, Texas A&M University, College Station, TX (August 2016).

APPENDIX A

ARPS' AND MODIFIED HYPERBOLIC DECLINE CURVE RELATIONS

In this section, the Arps' (1945) decline curve relations for exponential and hyperbolic decline. The modified hyperbolic relation that was proposed by Roberson (1988) is also presented. The loss-ratio and loss-ratio derivative equations for all relations is included. A "*qDb* plot" is included in this section as well for orientation. Before applying any decline curve model, the limitations of the equations themselves needs to be understood. Arps' hyperbolic decline is based on observed behavior, and therefore is entirely empirical. Arps' originally developed the exponential relationship empirically, however later it was shown that it can be derived using pseudo-steady state production of a slightly compressible fluid produced at a constant pressure [Camacho and Raghavan, 1989]. For all of Arps' decline curve models we must make the following assumptions:

- Historical production adequately represents future production trends.
- Current operating conditions will not change dramatically change in the future and therefore will not affect the extrapolation curve (i.e. time-rate model) in the future.
- The well is producing from a finite drainage area and therefore will experience boundary dominated flow.
- The well is producing at a constant bottomhole pressure, rather than a constant rate.

All Arp's decline curves consider the nominal decline rate (D), which is defined as

$$D(t) = -\frac{(\Delta q/q)}{\Delta t} = -\frac{1}{q(t)}\frac{dq(t)}{dt} \quad \text{.....(A.1)}$$

Rewriting Eq. A.1 so that the decline rate (D) is based on rate (q) and a constant decline component (b):

$$D(t) = kq^b \quad \text{(A.2)}$$

A.1 Arps' Exponential Decline Curve Relation

The definition of exponential decline is that $b = 0$. Plugging this into Eq. A.1:

$$D(t) = kq^0 \quad \text{(A.3)}$$

Solving for k at initial conditions:

$$k = \frac{D_i}{q_i^b} = \frac{D_i}{q_i^0} = D_i = D(t) \quad \text{(A.4)}$$

Where k is a constant. We can see here that the decline rate remains constant. Integrating Eq. A.4 for decline rate:

$$D_i = kq^b = -\frac{1}{q}\frac{dq}{dt}$$

$$\int_0^t D_i \, dt = \int_{q_i}^{q} -\frac{dq}{q}$$

$$-D_i t = \ln\frac{q}{q_i}$$

$$q(t) = q_i \exp[-D_i t] \quad \text{(A.5)}$$

Eq. A.5 is the equation used for rate-time data analysis for Arp's exponential decline curve method. On a logarithmic axis, a plot of flow rate vs. time results in a straight line.

Cumulative production is defined as:

$$Q(t) = \int_0^t q \, dt \quad \text{.....(A.6)}$$

Plugging in Eq. A.5 into Eq. A.6 and solving the integral:

$$Q(t) = \int_0^t q_i e^{(-D_i t)} \, dt$$

$$Q(t) = \frac{q_i - q_i e^{(-D_i t)}}{D_i}$$

$$Q(t) = \frac{q_i - q}{D_i} \quad \text{.....(A.7)}$$

Therefore, a plot of flow rate vs. cumulative production yields a straight line.

For analysis purposes, the *D*- and *b*-parameter equations are needed. These are the basis of the "*qDb*" plots that are showing throughout this text. They can also be referred to as the reciprocal loss-ratio and loss-ratio derivative which were originally proposed by Johnson and Bollens (1927). Recalling the definition of loss-ratio:

$$\frac{1}{D(t)} = -\frac{q(t)}{dq(t)/dt} \quad \text{.....(A.8)}$$

Plugging in Eq. A.5 into Eq. A.8:

$$D(t) = -\frac{1}{q_i \exp[-D_i t]} \frac{d}{dt} \{q_i \exp[-D_i t]\} \quad \text{.....(A.9)}$$

Completing the derivative with respect to time:

$$D(t) = -\frac{D_i q_i \exp[-D_i t]}{q_i \exp[-D_i t]} \quad \text{.....(A.10)}$$

Simplifying Eq. A.10:

$$D(t) = D_i \quad \text{.....(A.11)}$$

Eq. A.11 is the reciprocal loss-ratio for exponential decline. Recalling the definition of the loss-ratio derivative:

$$b(t) = \frac{d}{dt}\left[\frac{1}{D(t)}\right] \quad \text{.....(A.12)}$$

Plugging Eq. A.11 into Eq. A.12:

$$b(t) = \frac{d}{dt}\left[\frac{1}{D_i}\right] \quad \text{.....(A.13)}$$

Completing the derivative in Eq. A.13 yields the loss-ratio derivative for the exponential relationship.

$$b(t) = 0 \quad \text{.....(A.14)}$$

A.2 Arps' Hyperbolic Decline Curve Relation

Hyperbolic decline is defined as when *b* is between 0 and 1. Recalling the decline rate equation:

$$D(t) = kq^b \quad \text{.....(A.2)}$$

Therefore:

$$D(t) \propto q^b \quad \text{.....(A.15)}$$

Solving for k at initial conditions:

$$k = \frac{D_i}{{q_i}^b} \quad \text{.....(A.16)}$$

Where k is a constant. Plugging Eq. A.16 into Eq. A.1 and integrating:

$$D(t) = \frac{D_i}{{q_i}^b} q^b = -\frac{1}{q}\frac{dq}{dt}$$

$$\int_0^t \frac{D_i}{{q_i}^b} dt = \int_{q_i}^{q} -\frac{dq}{q^{(b+1)}}$$

$$\frac{D_i}{{q_i}^b} t = \frac{1}{b}\left(q^{-b} - {q_i}^{-b}\right)$$

$$q(t) = \frac{q_i}{\left(1 + bD_i t\right)^{1/b}} \quad \text{.....(A.17)}$$

Eq. A.17 is the equation used for rate-time data analysis for Arp's hyperbolic decline curve method.

Recalling the definition of cumulative production:

$$Q(t) = \int_0^t q \, dt \quad \text{.....(A.6)}$$

Plugging in Eq. A.1 into Eq. A.6 and solving the integral:

$$Q(t) = \int_0^t \frac{q_i}{\left(1 + ba_i t\right)^{1/b}} dt$$

$$Q(t) = \frac{q_i}{D_i(1-b)}\left[1-\left(1+bD_it\right)^{1-\frac{1}{b}}\right] \quad \text{.....(A.18)}$$

Defining a substitution variable:

$$\left(\frac{q_i}{q}\right)^b = 1+bD_it \quad \text{.....(A.19)}$$

Substituting Eq. A.12 into Eq. A.11:

$$Q(t) = \frac{q_i}{D_i(1-b)}\left[1-\left(\frac{q_i}{q}\right)^{b-1}\right]$$

$$Q(t) = \frac{q_i}{D_i(1-b)}\left(q_i^{1-b}-q^{1-b}\right) \quad \text{.....(A.20)}$$

Eq. A.13 is the cumulative production equation for Arp's hyperbolic decline. A plot of either flow rate vs time or flow rate vs cumulative production results in a linear relationship, regardless if it is plotted on either a logarithmic or cartesian axis.

Once again, we will determine the reciprocal loss-ratio and loss-ratio derivative for the hyperbolic relation. Plugging Eq. A.17 into Eq. A.8:

$$D(t) = -\frac{(1+bD_it)^{1/b}}{q_i}\frac{d}{dt}\left[\frac{q_i}{(1+bD_it)^{1/b}}\right] \quad \text{.....(A.21)}$$

Using the derivation technique referred to as u-substitution, we define *u* and its derivative as:

$$u = 1+bD_it \quad \text{.....(A.22)}$$

$$\frac{du}{dt} = bD_i \quad \text{.....(A.23)}$$

Substituting Eq. A.22 and A.23 into Eq. A.21:

$$D(t) = -u^{1/b} \frac{d}{dt}(u^{-1/b}) \quad \text{.....(A.24)}$$

Applying chain rule to Eq. A.24:

$$D(t) = -u^{1/b} \frac{d(z^{-1/b})}{dz} \frac{dz}{dt} \quad \text{.....(A.25)}$$

Applying Eq. A.23 to Eq. A.25:

$$D(t) = -bD_i u^{1/b} \frac{d(z^{-1/b})}{dz} \quad \text{.....(A.26)}$$

Completing the differentiation and simplifying:

$$D(t) = \frac{bD_i}{b} u^{1/b} u^{-(1/b)-1}$$

$$D(t) = D_i u^{1/b} u^{-1/b} u^{-1}$$

$$D(t) = \frac{D_i}{u} \quad \text{.....(A.27)}$$

Substituting Eq. A.22 back into Eq. A.27 to obtain the reciprocal loss-ratio for the hyperbolic relationship:

$$D(t) = \frac{D_i}{1 + bD_i t} \quad \text{.....(A.28)}$$

Now, we will solve for the loss-ratio derivative for the hyperbolic relationship. Plugging Eq. A.28 into Eq. A.12:

$$b(t) = \frac{d}{dt}\left[\frac{1 + bD_i t}{D_i}\right]$$

……...(A.29)

Separating and completing the differentiation:

$$b(t) = \frac{d}{dt}\left[\frac{1}{D_i}\right] + \frac{d}{dt}\left[\frac{bD_i t}{D_i}\right]$$

$$b(t) = b$$ ……...(A.30)

Eq. A.30 is the loss-ratio derivative for the hyperbolic relation and as expected it is equal to a constant.

A.3 Modified Hyperbolic Decline Curve Relation

The modified hyperbolic decline curve analysis method was initially proposed by Robertson (1988). This method was created because when the Arp's hyperbolic decline with a *b*-parameter greater than one is extrapolated over a long period of time it tends to overestimate reserves. Therefore, Roberson proposed that at some point in the wells production the hyperbolic decline needs to be switched to exponential decline. This point in time is specified by a limiting effective decline rate, D_{min}.

When the decline rate is greater than the limited decline rate, we use Arp's equation for hyperbolic decline:

$$q(t) = \frac{q_i}{(1 + bD_i t)^{\frac{1}{b}}} \quad \text{.....(A.17)}$$

When the decline rate is less than or equal to the limited decline rate, we use Arp's equation for exponential decline:

$$q(t) = q_i \exp[-D_i t] \quad \text{.....(A.5)}$$

However, we cannot use the same rate and nominal decline rate as before, therefore we must change Eq. A.5 into limited variables.

$$q(t) = q_i^* \exp[-D_{\min}(t - t^*)]$$

.....(A.31)

Where:

$$q_i^* = q_i \left(\frac{D_{\lim}}{D_i} \right)^{1/b} \quad \text{.....(A.32)}$$

$$t^* = \frac{\left(\frac{q_i}{q_i^*} \right)^b - 1}{bD_i} \quad \text{.....(A.33)}$$

Therefore, the full time-rate relationship for the modified hyperbolic is defined as:

$$q(t) = \begin{Bmatrix} \frac{q_i}{(1 + bD_i t)^{1/b}} & (t < t^*) \\ q_i^* \exp[-D_{\min}(t - t^*)] & (t > t^*) \end{Bmatrix} \quad \text{.....(A.34)}$$

Recalling the derivation of reciprocal loss-ratio for the hyperbolic and exponential relationship, the reciprocal loss-ratio for the modified hyperbolic is defined as (using correct variables):

$$D(t)=\left\{\begin{array}{ll}\dfrac{D_i}{(1+bD_it)} & (t<t^*)\\ D_{\min} & (t>t^*)\end{array}\right\} \quad \text{.....(A.35)}$$

Recalling the derivation of loss-ratio derivative for the hyperbolic and exponential relationship, the loss-ratio derivative for the modified hyperbolic is defined as (using correct variables):

$$b(t)=\left\{\begin{array}{ll}b & (t<t^*)\\ 0 & (t>t^*)\end{array}\right\} \quad \text{.....(A.36)}$$

Fig. A.1 is a schematic of the diagnostic behavior for Arps' hyperbolic and the modified hyperbolic relations, also referred to as a "*qDb*" plot.

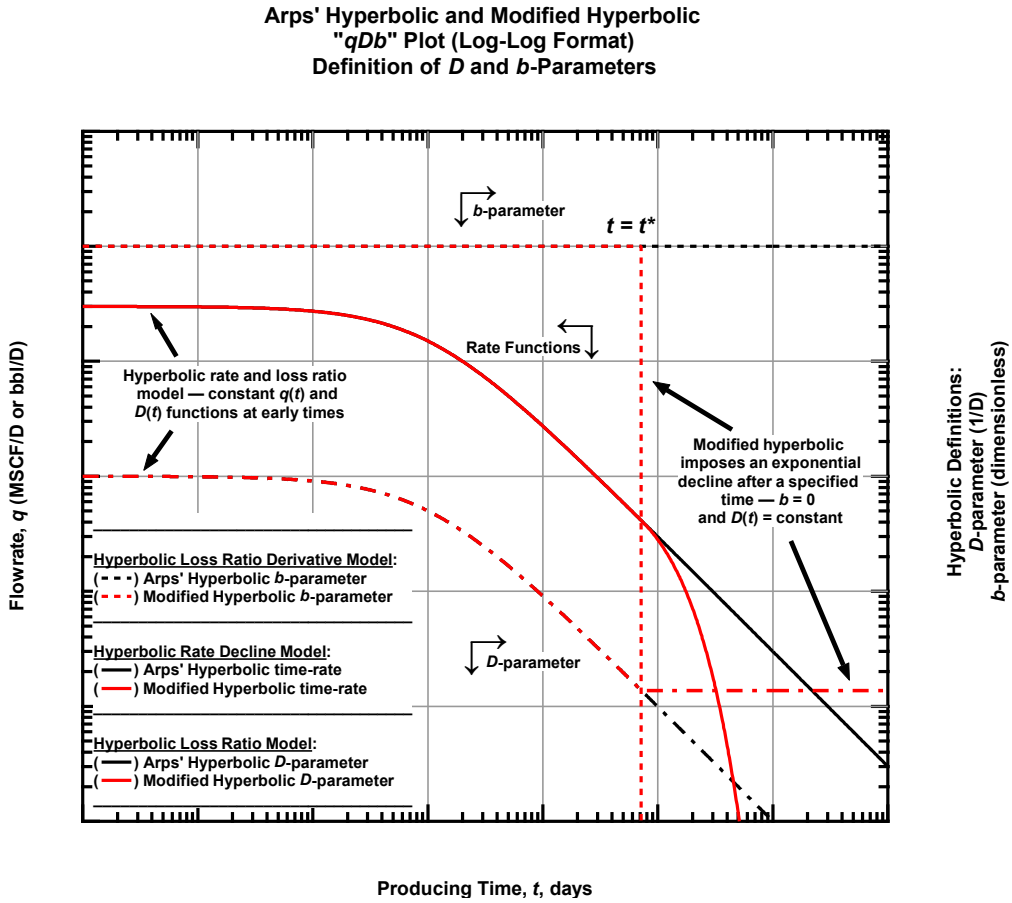

Figure A.1 — (Log-log Plot) Schematic type plot of "*qDb*" behavior for Arps' hyperbolic and modified hyperbolic decline curve relations.

APPENDIX B

POWER-LAW EXPONENTIAL DECLINE CURVE RELATION

The purpose of this section of to derive the power-law exponential decline curve relation that was first presented by Ilk *et al*. (2008). The reciprocal loss-ratio and loss-ratio derivative supplementary functions are derived and a sample "*qDb*" plot is provided for orientation. The power-law exponential model is based on the idea off observation of power-law behavior in the *D*-parameter. This relation was derived from analyzing the limitations of Arps' hyperbolic relation for fractured low-permeability tight gas wells. As with the Arps' relations it needs to be remembered that this relation is entirely empirical. Johnson and Bollens (1927) initially proposed loss-ratio and the derivative of the loss-ratio equations. The original equation for loss-ratio is defined as:

$$r = \frac{y}{\Delta y} \quad \text{.....(B.1)}$$

Where *r* is the loss-ration and *y* is oil production. Putting Eq. B.1 into more "modern" variables to be used with decline curve models:

$$\frac{1}{D} = -\frac{q}{dq/dt} \quad \text{.....(B.2)}$$

Eq. B.2 is the definition of the loss-ratio. Taking a derivative of the loss-ratio yields:

$$b = \frac{d}{dt}\left[\frac{1}{D}\right] = -\frac{d}{dt}\left[\frac{q}{dq/dt}\right] \quad \text{.....(B.3)}$$

In Arps (1945) original equations, it was suggested that the *b*-exponent needs to be between 0 and 1.0, however often in practice values above one can be observed. The purpose of using a loss-ratio

is to make the *b*-exponent a function of time. Ilk, *et al* [2008] proposed the following equation, which used a different form of the *D*-parameter:

$$D(t) = D_\infty + D_1 t^{n-1} \quad \text{.....(B.4)}$$

Eq. B.4 is a decaying power law function that considers the decline constant at one day (D_1) and the decline constant at "infinite time" (D_∞). Plugging Eq. B.4 into Eq. B.2:

$$\frac{1}{q}\frac{dq}{dt} = -D_\infty - D_1 t^{n-1} \quad \text{.....(B.5)}$$

Separating the variables and completing the integral:

$$\frac{dq}{q} = -D_\infty dt - D_1 t^{n-1} dt$$

$$\int_{\hat{q}_i}^{q(t)} \frac{dq}{q} = -D_\infty \int_0^t dt - D_1 \int_0^t t^{n-1} dt$$

$$\ln[q(t)] - \ln[\hat{q}_i] = -D_\infty t - \frac{D_1}{n} t^n \quad \text{.....(B.6)}$$

Rewriting Eq. B.6 into a more useful form:

$$q(t) = \hat{q}_i \exp\left[-D_\infty t - \frac{D_1}{n} t^n \right] \quad \text{.....(B.7)}$$

The final published time-rate form of the power-law exponential uses the following substitution:

$$\hat{D}_i = \frac{D_1}{n} \quad \text{.....(B.8)}$$

Plugging Eq. B.8 into Eq. B.7:

$$q(t) = \hat{q}_i \exp\left[-\hat{D}_i t^n - D_\infty t\right] \quad \text{.....(B.9)}$$

Eq. B.9 is the final time-rate form of the power-law exponential. It is important to note that $\hat{D}_i$ is not congruent with the D_i-parameter in Arps' decline curve models.

For analysis purposes the *D*- and *b*-parameters are wanted to assist with the calibration of the model parameters. Ilk (2008) discussed the value of using these analysis variables in order to obtain a proper match with the decline curve models on the historical time-rate data. The basis of the power-law exponential is the *D*-parameter itself, which has already been defined as:

$$D(t) = D_\infty + D_1 t^{n-1} \quad \text{.....(B.4)}$$

To keep the same variables in the equations we will substitute Eq. B.8 into Eq. B.4:

$$D(t) = D_\infty + \hat{D}_i n t^{n-1} \quad \text{.....(B.10)}$$

Eq. B.10 is the equation that should be used for the reciprocal loss-ratio, since it is in the same variables as the time-rate equation. Plugging in Eq. B.10 into Eq. B.3 to solve for loss-ratio derivative:

$$b(t) = \frac{d}{dt}\left[\frac{1}{D_\infty + \hat{D}_i n t^{-(1-n)}}\right] \quad \text{.....(B.11)}$$

Taking the derivative of Eq. B.10:

$$\frac{dD(t)}{dt} = (n-1)\hat{D}_i t^{n-2} \quad \text{.....(B.12)}$$

Applying the chain rule to Eq. B.11 and substituting in Eq. B.12:

$$b(t) = -\frac{(n-1)nt^{n-2}\hat{D}_i}{(D_\infty t + \hat{D}_i nt^{n-1})^2} \quad \text{.....(B.13)}$$

To simplify Eq. B.13 we will first expand the numerator and the denominator:

$$b(t) = \frac{n^2 t^{n-2}\hat{D}_i - nt^{n-2}\hat{D}_i}{n^2 t^{2n-2}\hat{D}_i^2 + 2nt^{n-1}\hat{D}_i D_\infty + D_\infty^2} \quad \text{.....(B.14)}$$

Continuing to simplify:

$$b(t) = \frac{n^2 \frac{t^n}{t^2}\hat{D}_i - n\frac{t^n}{t^2}\hat{D}_i}{n^2 \frac{t^{2n}}{t^2}\hat{D}_i^2 + 2n\frac{t^n}{t}\hat{D}_i D_\infty + D_\infty^2} \quad \text{.....(B.15)}$$

Multiplying by $1/t^2$:

$$b(t) = \frac{\frac{n^2 t^n \hat{D}_i - nt^n \hat{D}_i}{t^4}}{\frac{n^2 t^{2n}\hat{D}_i^2 + 2nt^{n+1}\hat{D}_i D_\infty + t^2 D_\infty^2}{t^4}} \quad \text{.....(B.16)}$$

Cancelling terms and simplifying Eq. B.16 yields the final form of the *b*-parameter for the power-law exponential model:

$$b(t) = \frac{\hat{D}_i(1-n)nt^n}{(D_\infty t + \hat{D}_i nt^n)^2} \quad \text{.....(B.17)}$$

Ilk et al. (2008) outlined the following procedure for calibrating the power-law exponential decline curve relation:

1. Compute the *D*- and *b*-parameters as a function of time.
2. Observe "power-law" behavior in the *D*-parameter. (i.e., a straight line on a log-log axis)
3. Calibrate the model to the straight-line behavior observed in the *D*-parameter by adjusting the n and $\hat{D}_i$ parameters only.
4. Calibrate the model to the time-rate data by adjusting the $\hat{q}_i$ parameter only.
5. Forecast future production

Fig. B.1 is a schematic of the diagnostic behavior for the power-law exponential, also referred to as a "*qDb*" plot. Presented is an example that includes the terminal decline parameter (D_∞) and one that does not.

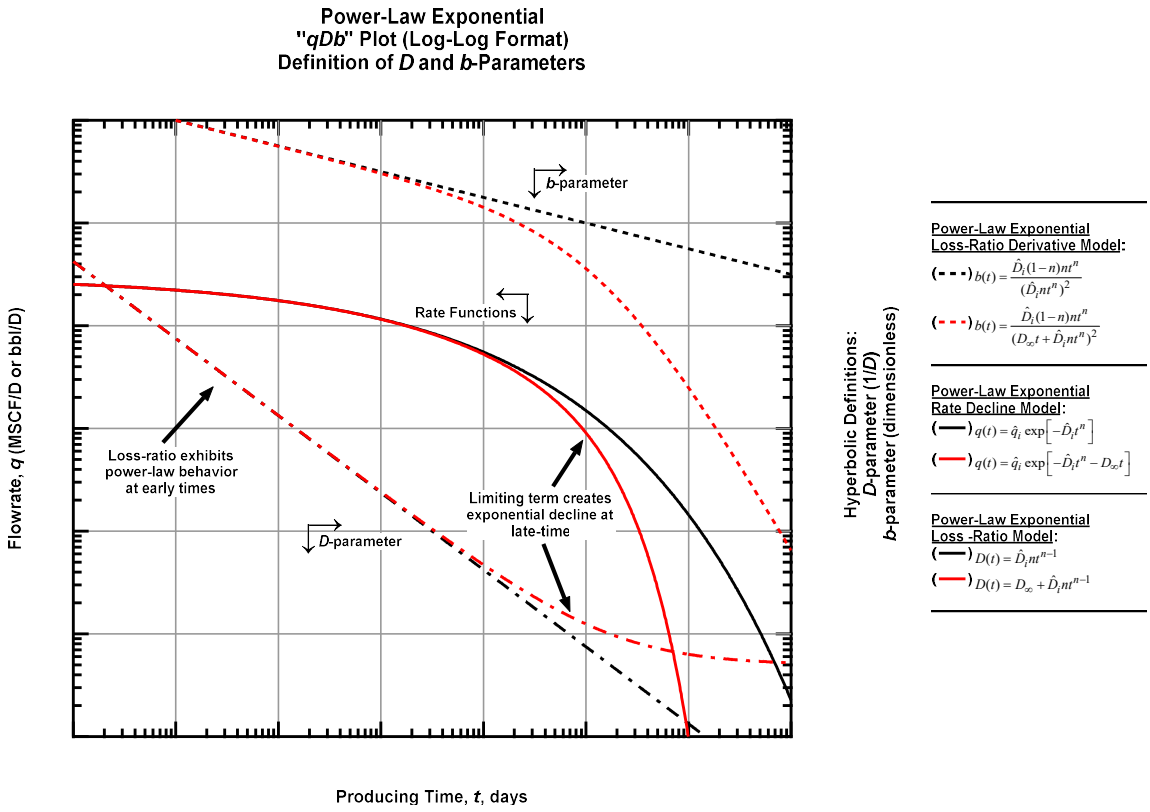

Figure B.1 — (Log-log Plot) Schematic type plot of "*qDb*" behavior for the power-law exponential decline curve relations.

APPENDIX C

STRETCHED EXPONENTIAL DECLINE CURVE RELATION

The purpose of this this section is to derive the stretched exponential decline curve relation. The reciprocal loss-ratio and loss-ratio derivative supplementary functions are derived and a sample "*qDb*" plot is provided for orientation. Stretched exponential functions were first introduced by Kohlrausch (1854), in which he used it to describe the discharge rate from a capacitor. The stretched exponential decline model was proposed by Valkó (2009) from a study of production from the Barnet Shale. This relation, like the others presented throughout this work is entirely empirical at this time. The differential equation that is the basis of the stretched exponential decline curve relation is as follows:

$$\frac{dq}{dt} = -n\left(\frac{t}{\tau}\right)^n \frac{q}{t} \quad \text{.....(C.1)}$$

In Eq. C.1 the τ parameter is a model parameter that describes the "characteristic number of periods", which is related to half-life parameters that are presented in other related works. To solve Eq. C.1 for the time-rate relation of the stretched exponential we must first separate the variables:

$$\frac{dq}{q} = -n\left(\frac{t}{\tau}\right)^n \frac{dt}{t} \quad \text{.....(C.2)}$$

Integrating both sides of Eq. C.2:

$$\int_{\hat{q}_i}^{q(t)} \frac{dq}{q} = -n\tau^{-1} \int_0^t t^{n-1} dt$$

$$\ln(q)\Big|_{\hat{q}_i}^{q(t)} = -n\tau^{-1}\left(\frac{t^n}{n}\right)\Big|_0^t$$

$$\ln\left(\frac{q(t)}{\hat{q}_i}\right) = -\left(\frac{t}{\tau}\right)^n \quad \text{.....(C.3)}$$

Simplifying Eq. C.3 by taking the exponential of each side and solving for $q(t)$:

$$q(t) = \hat{q}_i \exp\left[-\left(\frac{t}{\tau}\right)^n\right] \quad \text{.....(C.4)}$$

Eq. C.4 is the time-rate relation for the stretched exponential. Valkó (2009) outlined the following procedure for calibrating the stretched exponential model to time-rate data:

1. Prepare the data series q_D and Q.
2. Assume an n-parameter and calculate recover potential (rp).
3. Plot rp vs Q on a cartesian axis. A straight-line trend should be observed. EUR is the x-intercept of the straight line.
4. The y-intercept of the straight-line should be one. If it is not, the n-parameter needs to be adjusted until it is.
5. Once the EUR is determined from the x-intercept, the τ parameter is adjusted to obtain the time-rate profile.

In order to follow the procedure outlined by Valkó (2009), the time-rate cumulative relation must be known, which is the integral of Eq. C.4 and is defined as:

$$Q(t) = \frac{\hat{q}_i\tau}{n}\left\{\Gamma\left[\frac{1}{n}\right] - \Gamma\left[\frac{1}{n}, \left(\frac{t}{\tau}\right)^n\right]\right\} \quad \text{.....(C.5)}$$

Therefore, the EUR of the well in terms of model parameters is defined as:

$$EUR = \frac{\hat{q}_i \tau}{n} \Gamma\left[\frac{1}{n}\right] \quad \text{.....(C.6)}$$

Recovery potential is defined as:

$$rp = 1 - \frac{Q(t)}{EUR} \quad \text{.....(C.7)}$$

Plugging in Eq. C.5 and C.6 into Eq. C.7:

$$rp = 1 - \frac{Q(t)}{EUR} = \frac{1}{\Gamma\left[\frac{1}{n}\right]} \Gamma\left[\frac{1}{n}, -\ln\left(\frac{q}{\hat{q}_i}\right)\right] \quad \text{.....(C.8)}$$

Dimensionless flowrate must also be calculated using the following equation:

$$q_D(t) = \frac{q(t)}{\hat{q}_i} \quad \text{.....(C.9)}$$

For this research we are also interested in calculating the loss-ratio and loss-ratio derivative for each decline curve relation, recalling their definitions:

$$\frac{1}{D} = -\frac{q}{dq/dt} \quad \text{.....(C.10)}$$

$$b = \frac{d}{dt}\left[\frac{1}{D}\right] = -\frac{d}{dt}\left[\frac{q}{dq/dt}\right] \quad \text{.....(C.11)}$$

To solve for the loss-ratio we must first calculate the derivative of Eq. C.4 with respect to time:

$$\frac{dq(t)}{dt} = \hat{q}_i \frac{d}{dt}\left\{\exp\left[-\left(\frac{t}{\tau}\right)^n\right]\right\} \quad \text{.....(C.12)}$$

Using *u*-substitution to complete the derivative, where:

$$u = -\left(\frac{t}{\tau}\right)^n \quad \text{.....(C.14)}$$

$$\frac{du}{dt} = -\frac{nt^{n-1}}{\tau^n} \quad \text{.....(C.15)}$$

Plugging in Eq. C.14 and C.15 into Eq. C.13:

$$\frac{dq(t)}{dt} = \hat{q}_i \frac{d}{dt}\{\exp[u]\} \quad \text{.....(C.16)}$$

Completing the derivative in Eq. C.16:

$$\frac{dq(t)}{dt} = \hat{q}_i \exp[u]\frac{du}{dt} \quad \text{.....(C.17)}$$

Plugging in Eq. C.14 and C.15 into Eq. C.17:

$$\frac{dq(t)}{dt} = -\hat{q}_i \exp\left[-\left(\frac{t}{\tau}\right)^n\right]\frac{nt^{n-1}}{\tau^n} \quad \text{.....(C.18)}$$

Plugging in Eq. C.4 and C.18 into Eq. C.10

$$D(t) = \frac{\hat{q}_i \exp\left[-\left(\frac{t}{\tau}\right)^n\right]}{\hat{q}_i \exp\left[-\left(\frac{t}{\tau}\right)^n\right]}\frac{nt^{n-1}}{\tau^n}$$

$$D(t) = \frac{nt^{n-1}}{\tau^n} \quad \text{.....(C.20)}$$

Eq. C. 20 is the reciprocal loss-ratio of the stretched exponential.

To solve for the derivative of the loss ratio for we must substitute Eq. C.20 into Eq. C.10:

$$b(t) = \frac{d}{dt}\left[\frac{1}{D(t)}\right] = \frac{d}{dt}\left(\frac{\tau^n}{nt^{n-1}}\right) \quad \text{.....(C.21)}$$

Completing the derivative in Eq. C.21:

$$b(t) = \frac{1-n}{nt^n}\tau^n \quad \text{.....(C.22)}$$

Eq. C.22 is the derivative of the loss-ratio for the stretched exponential decline curve relation.

Fig. C.1 is a schematic of the diagnostic behavior for the stretched exponential, also referred to as a "*qDb*" plot.

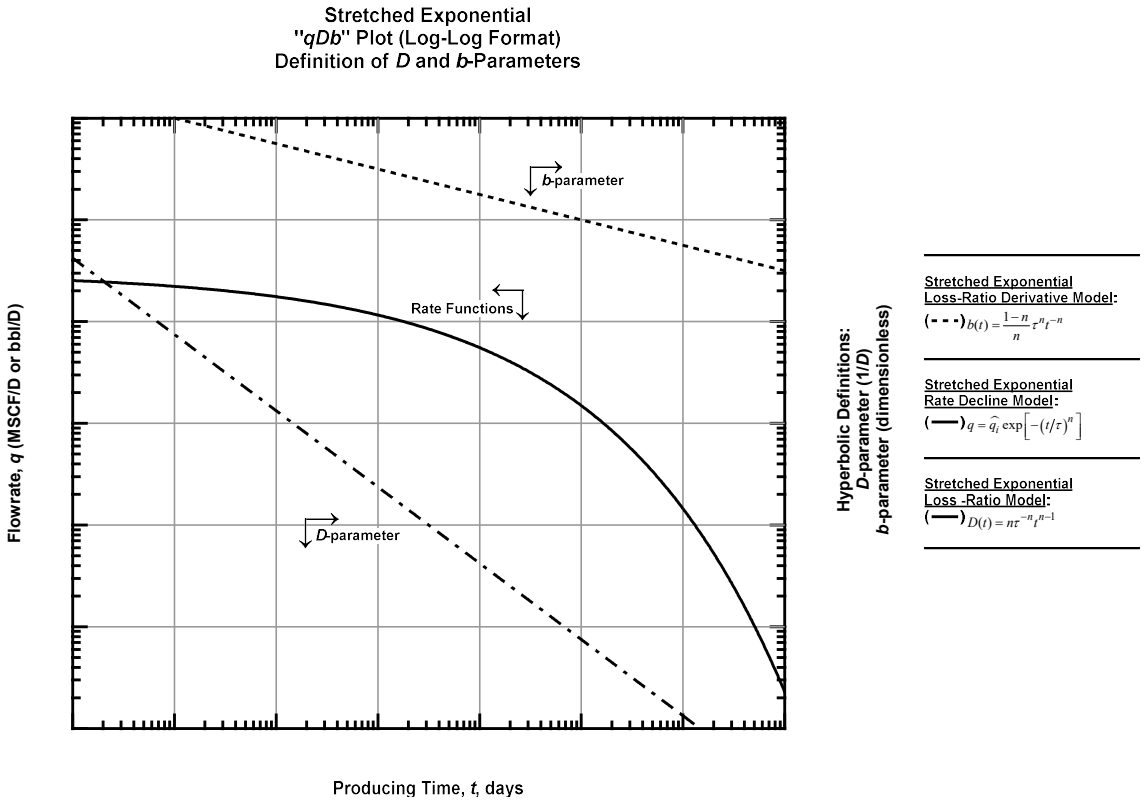

Figure C.1 — (Log-log Plot) Schematic type plot of "*qDb*" behavior for the stretched exponential decline curve relation.

APPENDIX D

DUONG'S METHOD DECLINE CURVE RELATION

The purpose of this this section is to derive Duong's Method (2011) decline curve relation. The reciprocal loss-ratio and loss-ratio derivative supplementary functions are derived and a sample "*qDb*" plot is provided for orientation. This decline curve relation, like the others presented for this research is entirely empirical. Duong developed this model specifically for very low permeability unconventional reservoirs. The basis for this relation is the power-law behavior observed on a log-log plot of rate divided by cumulative production versus time. Duong defined decline rate as:

$$\varepsilon(t) = \frac{q(t)}{Q(t)} \quad \text{.....(D.1)}$$

Solving Eq. D.1 for cumulative production:

$$Q(t) = \frac{q(t)}{\varepsilon(t)} \quad \text{.....(D.2)}$$

Taking the derivative of Eq. D.2 with respect to time yields:

$$\frac{d}{dt}Q(t) = \frac{d}{dt}\left[\frac{q(t)}{\varepsilon(t)}\right]$$

$$q(t) = \frac{dq(t)}{dt}\frac{1}{\varepsilon(t)} - q(t)\frac{d\varepsilon(t)}{dt}\frac{1}{\varepsilon^2(t)}$$

$$\frac{dq(t)}{q} = \frac{d\varepsilon(t)}{\varepsilon(t)} + \varepsilon(t)dt \quad \text{.....(D.3)}$$

Integrating Eq. D.3 from $t = 1$ to t:

$$\ln\left[\frac{q(t)}{q_1}\right] = \ln\left[\frac{\varepsilon(t)}{\varepsilon(1)}\right] + \int_1^t e(t)\,dt$$

$$q = q_1 \frac{\varepsilon(t)}{\varepsilon(1)} \exp\left[\int_1^t e(t)\,dt\right] \quad \text{.....(D.4)}$$

Assuming the following:

$$\frac{q(t)}{Q(t)} = at^{-m} \quad \text{.....(D.5)}$$

Eq. D.5 is the defining foundational relationship Duong's Method.

Plugging in Eq. D.1 into Eq. D.5:

$$\varepsilon(t) = at^{-m} \quad \text{.....(D.6)}$$

Plugging in Eq. D.6 into Eq. D.4 and completing the integral:

$$q(t) = q_1 \frac{at^{-m}}{a(1)^{-m}} \exp\left[\int_1^t at^{-m}\,dt\right]$$

$$q(t) = q_1 t^{-m} \exp\left[\frac{a}{1-m}\left(t^{1-m} - 1\right)\right] \quad \text{.....(D.7)}$$

Eq. D.7 is the final time-rate equation for Duong's Method.

Duong outlined the following procedure for calibrating his decline curve relation:

1. Plot log[q(t)/Q(t)] versus log [t] to estimate the a- and m-parameters.

2. Plot q(t) versus $t^{-m}\exp\left[\frac{a}{1-m}\left(t^{1-m}-1\right)\right]$ using the previously determined a- and m-parameters to calibrate the q_1 parameter.
3. Forecast production

A straight-line trend must be observed in the plot of log[q(t)/Q(t)] versus log [t] or Duong's Method is not valid for that particular data set. This plot is able to obtain estimates for the a- and m-parameters because the equation for a straight-line on a log-log plot is defined as:

$$y = ax^k \quad \text{(D.8)}$$

Where a is the slope of the of the line and k is the intercept on the log(y)-axis (i.e., x = 1). Comparing Eq. D.8 to Eq. D.6 it can be seen that Duong's a-parameter is the slope of the line (a) and m is the intercept (k). This is why power-law behavior must be observed in this plot or Duong's Method does not apply.

For this research we are also interested in calculating the loss-ratio and loss-ratio derivative for each decline curve relation, recalling their definitions:

$$\frac{1}{D} = -\frac{q}{dq/dt} \quad \text{(D.9)}$$

$$b = \frac{d}{dt}\left[\frac{1}{D}\right] = -\frac{d}{dt}\left[\frac{q}{dq/dt}\right] \quad \text{(D.10)}$$

To solve for the reciprocal loss-ratio of Duong's method we must take the derivative of Eq. D.7:

$$\frac{dq(t)}{dt} = q_1 \frac{d}{dt}\left\{t^{-m}\exp\left[\frac{a}{1-m}\left(t^{1-m}-1\right)\right]\right\} \quad \text{(D.11)}$$

Recalling the product rule:

$$\frac{\partial}{\partial t}(uv) = v\frac{\partial u}{\partial t} + u\frac{\partial v}{\partial t} \quad \text{.....(D.12)}$$

Where in this case:

$$u = t^{-m} \quad \text{.....(D.13)}$$

$$v = \exp\left[\frac{a}{1-m}\left(t^{1-m} - 1\right)\right] \quad \text{.....(D.14)}$$

Taking the derivatives of Eq. D.13 and D.14:

$$\frac{\delta u}{\delta t} = -mt^{-m-1} \quad \text{.....(D.15)}$$

$$\frac{\delta v}{\delta t} = at^{-m}\exp\left[\frac{a}{1-m}\left(t^{1-m} - 1\right)\right] \quad \text{.....(D.16)}$$

Plugging in Eq. D.12 – D.16 into Eq. D.11:

$$\frac{dq(t)}{dt} = q_1\left\{-mt^{-m-1}\exp\left[\frac{a}{1-m}\left(t^{1-m} - 1\right)\right] + t^{-m}at^{-m}\exp\left[\frac{a}{1-m}\left(t^{1-m} - 1\right)\right]\right\} \quad \text{.....(D.18)}$$

Simplifying Eq. D.18:

$$\frac{dq(t)}{dt} = q_1 t^{-m}\exp\left[\frac{a}{1-m}\left(t^{1-m} - 1\right)\right](-mt^{-1} + at^{-m}) \quad \text{.....(D.19)}$$

Plugging in Eq. D.19 and D.7 into Eq. D.9:

$$D(t) = -\frac{q_1 t^{-m} \exp\left[\frac{a}{1-m}\left(t^{1-m}-1\right)\right]}{q_1 t^{-m} \exp\left[\frac{a}{1-m}\left(t^{1-m}-1\right)\right]}(-mt^{-1}+at^{-m})$$

$$D(t) = mt^{-1} - at^{-m} \quad \text{.....(D.20)}$$

Eq. D.20 is the reciprocal loss-ratio of Duong's Method. To calculate the derivative of the loss ratio we must plug Eq. D.20 into Eq. D.10:

$$b(t) = \frac{d}{dt}\left[\frac{1}{D}\right] = \frac{d}{dt}\left[\frac{1}{mt^{-1}-at^{-m}}\right] \quad \text{.....(D.21)}$$

Recalling the quotient rule:

$$\frac{\partial}{\partial t}\left(\frac{u}{v}\right) = \frac{v\frac{\partial u}{\partial t} - u\frac{\partial v}{\partial t}}{v^2} \quad \text{.....(D.22)}$$

Where in this case:

$$u = 1 \quad \text{.....(D.23)}$$

$$v = mt^{-1} - at^{-m} \quad \text{.....(D.24)}$$

Taking the derivatives of Eq. D.23 and D.24

$$\frac{\delta u}{\delta t} = 0 \quad \text{.....(D.25)}$$

$$\frac{\delta v}{\delta t} = -mt^{-2} + mat^{-m-1} \quad \text{.....(D.26)}$$

Plugging in Eq. D.22 – D.26 into Eq. D.21.

$$b(t) = \frac{mt^{-2} - mat^{-m-1}}{(mt^{-1} - at^{-m})^2} \quad \text{.....(D.27)}$$

Expanding the denominator in Eq. D.27 and simplifying

$$b(t) = \frac{mt^{-2} - mat^{-m-1}}{m^2t^{-2} - 2mat^{-m-1} + a^2t^{-2m}}$$

$$b(t) = \frac{mt^{-2-m}(t^m - at)}{mt^{-2-2m}(a^2t^2 - 2amt^{1+m} + m^2t^{2m})}$$

$$b(t) = \frac{mt^m(t^m - at)}{(at - mt^m)^2} \quad \text{.....(D.28)}$$

Eq. D.28 is the derivative of the loss-ratio for Duong's Method.

Fig. D.1 is a schematic of the diagnostic behavior for the Duong's Method, also referred to as a "*qDb*" plot.

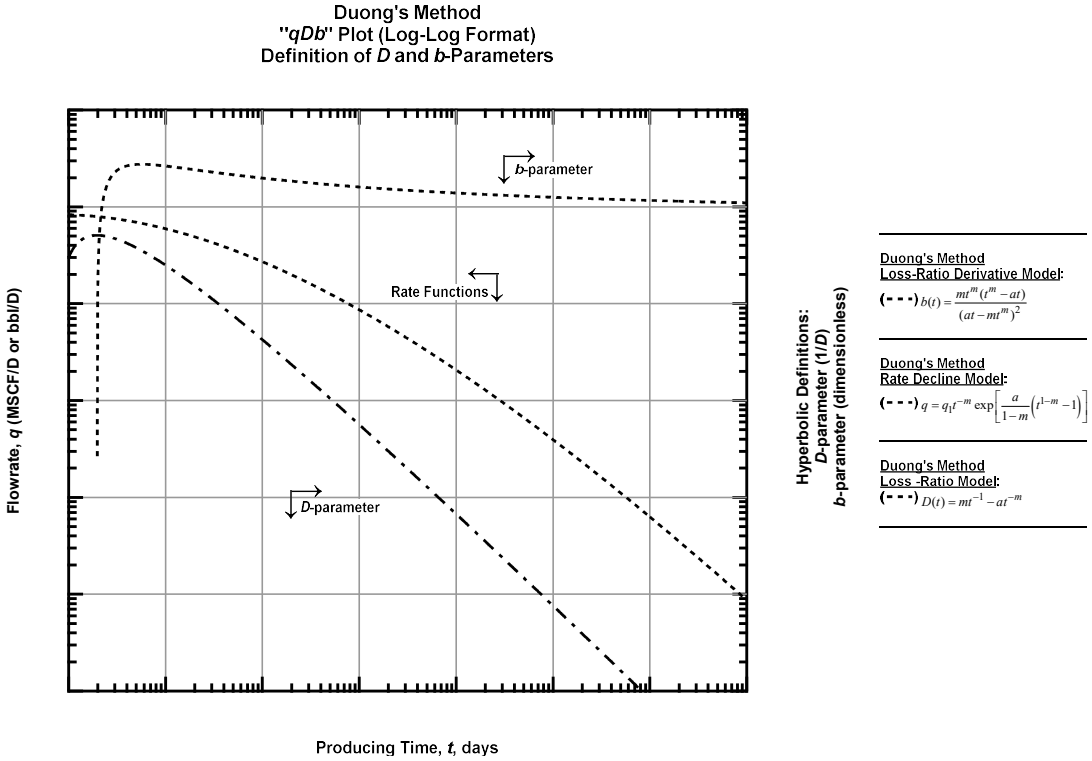

Figure D.1 — (Log-log Plot) Schematic type plot of "*qDb*" behavior for Duong's Method decline curve relation.

APPENDIX E

LOGISTICAL GROWTH MODEL DECLINE CURVE RELATION

The purpose of this this section is derive the logistical growth model decline curve relation. The reciprocal loss-ratio and loss-ratio derivative supplementary functions are derived and a sample "*qDb*" plot is provided for orientation. This decline curve relation, like the others presented for this research is entirely empirical. Clark *et al.* (2011) developed the logistical growth model from a hyperlogistic growth function. Since it is a growth function, rather than a decay function, the original equation is for cumulative production and then it was differentiated to obtain the time-rate equation. The cumulative form of the logistical growth model is defined as:

$$Q(t) = \frac{Kt^n}{a + t^n} \quad \text{.....(E.1)}$$

To solve for the time-rate form of the logistical growth model decline curve relation we must take a derivative of Eq. E.1:

$$q(t) = \frac{dQ(t)}{dt} = K \frac{d}{dt}\left(\frac{t^n}{a + t^n} \right) \quad \text{.....(E.2)}$$

Recalling the quotient rule:

$$\frac{\partial}{\partial t}\left(\frac{u}{v} \right) = \frac{v\frac{\partial u}{\partial t} - u\frac{\partial v}{\partial t}}{v^2} \quad \text{.....(E.3)}$$

Where in this case:

$$u = t^n \quad \text{.....(E.4)}$$

$$v = a + t^n \quad \text{.....(E.5)}$$

$$\frac{\delta u}{\delta t} = nt^{n-1} \quad \text{.....(E.6)}$$

$$\frac{\delta v}{\delta t} = nt^{n-1} \quad \text{.....(E.7)}$$

Plugging in Eq. E.3 – E.7 into Eq. E.2:

$$q(t) = K\left[\frac{(a+t^n)(nt^{n-1}) - (t^n)(nt^{n-1})}{(a+t^n)^2}\right] \quad \text{.....(E.8)}$$

Expanding the numerator in Eq. E.8 and simplifying:

$$q(t) = K\left[\frac{ant^{n-1} + nt^{2n-1} - nt^{2n-1}}{(a+t^n)^2}\right]$$

$$q(t) = \frac{Knat^{n-1}}{(a+t^n)^2} \quad \text{.....(E.9)}$$

Eq. E.9 is the time-rate form of the logistical growth model decline curve relation.

For this research we are also interested in calculating the loss-ratio and loss-ratio derivative for each decline curve relation, recalling their definitions:

$$\frac{1}{D} = -\frac{q}{dq/dt} \quad \text{.....(E.10)}$$

$$b = \frac{d}{dt}\left[\frac{1}{D}\right] = -\frac{d}{dt}\left[\frac{q}{dq/dt}\right] \quad \text{.....(E.11)}$$

To solve for the reciprocal loss-ratio of the logistical growth model we need to take the derivative of Eq. E.9:

$$\frac{q(t)}{dt} = Kna\frac{d}{dt}\left[\frac{t^{n-1}}{(a+t^n)^2}\right] \quad \text{(E.9)}$$

Recalling the quotient rule:

$$\frac{\partial}{\partial t}\left(\frac{u}{v}\right) = \frac{v\frac{\partial u}{\partial t} - u\frac{\partial v}{\partial t}}{v^2} \quad \text{(E.3)}$$

Where in this case:

$$u = t^{n-1} \quad \text{(E.10)}$$

$$v = (a+t^n)^2 \quad \text{(E.11)}$$

$$\frac{\delta u}{\delta t} = (n-1)t^{n-2} \quad \text{(E.12)}$$

$$\frac{\delta v}{\delta t} = 2nt^{n-1}(a+t^n) \quad \text{(E.13)}$$

Plugging in Eq. E.3 and Eq. E.11 – E.13 into Eq. E.9:

$$\frac{q(t)}{dt} = Kna\left\{\frac{(a+t^n)^2(n-1)t^{n-2} - t^{n-1}2nt^{n-1}(a+t^n)}{[(a+t^n)^2]^2}\right\} \quad \text{(E.14)}$$

Plugging in Eq. E.14 and Eq. E.9 into Eq. E.10

$$D(t) = \frac{Kna(a+t^n)^2}{Knat^{n-1}}\left\{\frac{(a+t^n)^2(n-1)t^{n-2} - t^{n-1}2nt^{n-1}(a+t^n)}{[(a+t^n)^2]^2}\right\} \quad \text{(E.14)}$$

Simplifying Eq. E.14.

$$D(t) = \frac{a(1-n)+(n+1)t^n}{t(a+t^n)} \quad \text{.....(E.15)}$$

Eq. E.14 is the loss-ratio of the logistical growth model decline curve relation.

To solve for the derivative of the loss ratio we must plug Eq. E.14 into Eq. E.11.

$$b(t) = \frac{d}{dt}\left[\frac{1}{D}\right] = \frac{d}{dt}\left[\frac{t(a+t^n)}{a(1-n)+(n+1)t^n}\right] \quad \text{.....(E.16)}$$

Recalling the quotient rule.

$$\frac{\partial}{\partial t}\left(\frac{u}{v}\right) = \frac{v\frac{\partial u}{\partial t} - u\frac{\partial v}{\partial t}}{v^2} \quad \text{.....(E.3)}$$

Where in this case:

$$u = t(a+t^n) \quad \text{.....(E.17)}$$

$$v = a(1-n)+(n+1)t^n \quad \text{.....(E.18)}$$

$$\frac{\delta u}{\delta t} = a + t^n + nt^n \quad \text{.....(E.19)}$$

$$\frac{\delta v}{\delta t} = n(1+1)t^{n-1} \quad \text{.....(E.20)}$$

Plugging in Eq. E.3 and Eq. E.17 – E.20 into Eq. E.16:

$$b(t) = \frac{[a(1-n)+(n+1)t^n](a+t^n+nt^n) - t(a+t^n)n(1+1)t^{n-1}}{[a(1-n)+(n+1)t^n]^2} \quad \text{.....(E.21)}$$

Simplifying Eq. E.21:

$$b(t) = \frac{a^2(1-n) - 2a(n^2-1)t^n + (n+1)t^{2n}}{[a(1-n) + (n+1)t^n]^2} \quad \text{.....(E.22)}$$

Eq. E.21 is the derivative of the loss-ratio for the logistical growth model decline curve relation.

Fig. E.1 is a schematic of the diagnostic behavior for the Logistical Growth Model, also referred to as a "*qDb*" plot.

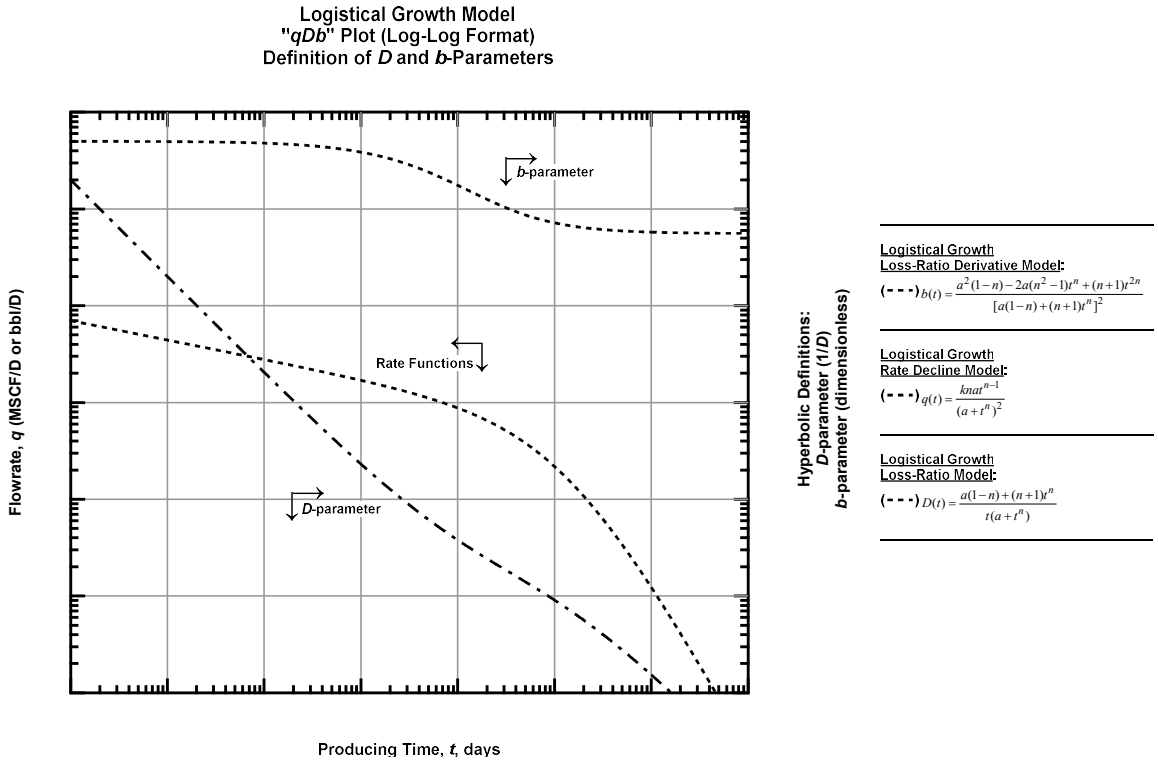

Figure E.1 — (Log-log Plot) Schematic type plot of "*qDb*" behavior for the Logistical Growth Model decline curve relation.

APPENDIX F

RATE-INTEGRAL FORM OF POWER LAW-EXPONENTIAL

In this appendix the rate-integral, reciprocal loss-ratio of the rate-integral, and the loss-ratio derivative of the rate-integral for the power-law exponential are derived. In order to use the "*modified qDb*" plot the rate-integral form of the power-law exponential and the associated loss-ratio and loss-ratio derivatives need to be derived. This is only possible if there is no terminal decline parameter (*i.e.*, $D_\infty = 0.0$), because with it the integration of the time-rate relation is not possible algebraically. Therefore, if a D_∞ parameter is used, the associated time-rate integral, reciprocal loss-ratio, and loss-ratio derivatives must be determined numerically. Assuming that there is no-terminal decline parameter we can derive the associated equations as follows. We begin with the rate integral, which is defined as:

$$q_{\text{int}}(t) = \frac{\int_0^t q(t)\,dt}{t} \quad \text{.....(F.1)}$$

Where q is flowrate and t is time. The stretched exponential time-rate equation is defined as [Valko, 2009]:

$$q(t) = \widehat{q_i} \exp\left[-(t/\tau)^n\right] \quad \text{.....(F.2)}$$

Where $\widehat{q_i}$ is the initial rate parameter, n is the time exponent, and τ is the time parameter. The power-law exponential is defined as:

$$q(t) = \hat{q}_i \exp\left[-\hat{D}_i t^n - D_\infty t\right] \quad \text{.....(F.3)}$$

Where $\widehat{q_i}$ is the initial rate parameter, $\hat{D}_i$ is the initial decline parameter, n is the time exponent and D_∞ is a terminal decline parameter. In order to calculate the rate-integral we need the time-cumulative form of Eq. F.2 and Eq. F.3. For the stretched exponential (Eq. F.2) cumulative production is defined as:

$$Q(t) = \int_0^t q(t)\, dt = \frac{\hat{q}_i \tau}{n}\left\{\Gamma\left[\frac{1}{n}\right] - \Gamma\left[\frac{1}{n}, \left(\frac{t}{\tau}\right)^n\right]\right\} \quad \text{.....(F.4)}$$

Where Γ is the complete Gamma function and the upper incomplete Gamma function. The complete Gamma function in Euler's integral form is defined as:

$$\Gamma[x] = \int_0^\infty t^{x-1} e^{-t} dt \quad \text{.....(F.5)}$$

The upper incomplete gamma function, also referred to as the "second" incomplete Gamma function, in Euler's integral form is defined as:

$$\Gamma[a, x] = \int_x^\infty e^{-t} t^{a-1} dt \quad \text{.....(F.6)}$$

Eq. F.5 and F.6 can be related using the lower limit Gamma function, also referred to as the "first" incomplete Gamma function. This is defined as:

$$\gamma[a, x] = \int_0^x e^{-t} t^{a-1} dt \quad \text{.....(F.7)}$$

Eq. F.5 – F.7 can be related using the following equation

$$\Gamma[a, x] = \Gamma[x] - \gamma[a, x] \quad \text{.....(F.8)}$$

There is no direct integration for cumulative production for the power-law exponential due to the D_∞ term. However, if this is assumed to be zero, we can relate the power-law exponential with the stretched exponential using the following equation:

$$\hat{D}_i = \left(\frac{1}{\tau}\right)^n \quad \text{.....(F.9)}$$

Plugging Eq. F.6 into Eq. F.5:

$$Q(t) = \int_0^t q(t)\, dt = \frac{\hat{q}_i}{\hat{D}_i^{1/n} n}\left\{\Gamma\left[\frac{1}{n}\right] - \Gamma\left[\frac{1}{n}, \hat{D}_i t^n\right]\right\} \quad \text{.....(F.10)}$$

Plugging in Eq. F.10 into Eq. F.1:

$$q_{\text{int}}(t) = \frac{\hat{q}_i}{\hat{D}_i^{1/n} nt}\left\{\Gamma\left[\frac{1}{n}\right] - \Gamma\left[\frac{1}{n}, \hat{D}_i t^n\right]\right\} \quad \text{.....(F.11)}$$

Eq. F.11 is the time-rate integral form of the power-law exponential equation. For analysis purposes, we are interested in calculating the loss-ratio and the loss-ratio derivative, which is defined as:

$$\frac{1}{D} \equiv -\frac{q(t)}{dq(t)/dt} \quad \text{(Definition of the loss-ratio) .....(F.12)}$$

$$b \equiv \frac{d}{dt}\left[\frac{1}{D}\right] \equiv \frac{d}{dt}\left[\frac{q(t)}{dq(t)/dt}\right] \quad \text{(Derivative of the loss-ratio) .....(F.13)}$$

To calculate the reciprocal loss-ratio, we must first differentiate Eq. F.11 with respect to time. First, we factor the constants within the integration, which yields:

$$\frac{dq_{\text{int}}(t)}{dt} = \frac{\hat{q}_i}{\hat{D}_i^{1/n} n} \frac{\partial}{\partial t} \left\{ \frac{\Gamma\left[\frac{1}{n}\right] - \Gamma\left[\frac{1}{n}, \hat{D}_i t^n\right]}{t} \right\} \quad \text{.....(F.14)}$$

Recalling the quotient rule:

$$\frac{\partial}{\partial t}\left(\frac{u}{v}\right) = \frac{v\frac{\partial u}{\partial t} - u\frac{\partial v}{\partial t}}{v^2} \quad \text{.....(F.15)}$$

Where:

$$u = \Gamma\left[\frac{1}{n}\right] - \Gamma\left[\frac{1}{n}, \hat{D}_i t^n\right] \quad \text{.....(F.16)}$$

$$v = t \quad \text{.....(F.17)}$$

Plugging in Eq. F.15 – F.17 into Eq. F.14:

$$\frac{dq_{\text{int}}(t)}{dt} = \frac{\hat{q}_i}{\hat{D}_i^{1/n} n} \frac{t\frac{\partial}{\partial t}\left\{\Gamma\left[\frac{1}{n}\right] - \Gamma\left[\frac{1}{n}, \hat{D}_i t^n\right]\right\} - \left\{\Gamma\left[\frac{1}{n}\right] - \Gamma\left[\frac{1}{n}, \hat{D}_i t^n\right]\right\}\frac{\partial}{\partial t}(t)}{t^2} \quad \text{.....(F.18)}$$

Simplifying Eq. F.18:

$$\frac{dq_{\text{int}}(t)}{dt} = \frac{\hat{q}_i}{\hat{D}_i^{1/n} n} \frac{\Gamma\left[\frac{1}{n}, \hat{D}_i t^n\right] - \Gamma\left[\frac{1}{n}\right] + t\frac{\partial}{\partial t}\left\{\Gamma\left[\frac{1}{n}\right] - \Gamma\left[\frac{1}{n}, \hat{D}_i t^n\right]\right\}}{t^2} \quad \text{.....(F.19)}$$

Distributing the partial derivative over the summation term:

$$\frac{dq_{\text{int}}(t)}{dt} = \frac{\hat{q}_i}{\hat{D}_i^{1/n} n} \frac{\Gamma\left[\frac{1}{n}, \hat{D}_i t^n\right] - \Gamma\left[\frac{1}{n}\right] + t\left\{\frac{\partial}{\partial t}\Gamma\left[\frac{1}{n}\right] - \frac{\partial}{\partial t}\Gamma\left[\frac{1}{n}, \hat{D}_i t^n\right]\right\}}{t^2} \quad \text{(F.20)}$$

Since the $\Gamma\left[\frac{1}{n}\right]$ term is not a function of time, it can be said that:

$$\frac{\partial}{\partial t}\Gamma\left[\frac{1}{n}\right] = 0 \quad \text{(F.21)}$$

Plugging Eq. F.18 into Eq. F.17:

$$\frac{dq_{\text{int}}(t)}{dt} = \frac{\hat{q}_i}{\hat{D}_i^{1/n} n} \frac{\Gamma\left[\frac{1}{n}, \hat{D}_i t^n\right] - \Gamma\left[\frac{1}{n}\right] - t\frac{\partial}{\partial t}\Gamma\left[\frac{1}{n}, \hat{D}_i t^n\right]}{t^2} \quad \text{(F.22)}$$

To complete the last partial derivative, we will use the chain rule and *u*-substitution. In this case, the chain rule is defined as:

$$\frac{\partial}{\partial t}\left\{\Gamma\left[\frac{1}{n}, \hat{D}_i t^n\right]\right\} = \frac{\partial}{\partial t}\Gamma\left[\frac{1}{n}, u\right]\frac{\partial u}{\partial t} \quad \text{(F.23)}$$

Where:

$$u = \hat{D}_i t^n \quad \text{(F.24)}$$

$$\frac{\partial}{\partial t}\Gamma\left[\frac{1}{n}, u\right] = -e^{-u}u^{-1+1/n} \quad \text{(F.25)}$$

Plugging Eq. F.23 – F.25 into Eq. F.22:

$$\frac{dq_{\text{int}}(t)}{dt} = \frac{\hat{q}_i}{\hat{D}_i^{1/n} n} \frac{\Gamma\left[\frac{1}{n}, \hat{D}_i t^n\right] - \Gamma\left[\frac{1}{n}\right] - t\left[-e^{-\hat{D}_i t^n} (\hat{D}_i t^n)^{-1+1/n} \frac{\partial}{\partial t}(\hat{D}_i t^n)\right]}{t^2} \quad \text{.....(F.26)}$$

Simplifying Eq. F.26 and pulling out constants:

$$\frac{dq_{\text{int}}(t)}{dt} = \frac{\hat{q}_i}{\hat{D}_i^{1/n} n} \frac{\Gamma\left[\frac{1}{n}, \hat{D}_i t^n\right] - \Gamma\left[\frac{1}{n}\right] + e^{-\hat{D}_i t^n} t(\hat{D}_i t^n)^{-1+1/n} \hat{D}_i \frac{\partial}{\partial t}(t^n)}{t^2} \quad \text{.....(F.27)}$$

Completing the final partial derivative using the power rule:

$$\frac{dq_{\text{int}}(t)}{dt} = \frac{\hat{q}_i}{\hat{D}_i^{1/n} n} \frac{\Gamma\left[\frac{1}{n}, \hat{D}_i t^n\right] - \Gamma\left[\frac{1}{n}\right] + e^{-\hat{D}_i t^n} t(\hat{D}_i t^n)^{-1+1/n} \hat{D}_i n^{n-1}}{t^2} \quad \text{.....(F.28)}$$

Simplifying Eq. F.28:

$$\frac{dq_{\text{int}}(t)}{dt} = \frac{\hat{q}_i e^{-\hat{D}_i t^n} t(\hat{D}_i t^n)^{-1+1/n} \hat{D}_i n t^{n-1}}{\hat{D}_i^{1/n} n t^2} - \frac{\hat{q}_i \left\{\Gamma\left[\frac{1}{n}\right] - \Gamma\left[\frac{1}{n}, \hat{D}_i t^n\right]\right\}}{\hat{D}_i^{1/n} n t^2}$$

$$\frac{dq_{\text{int}}(t)}{dt} = \hat{q}_i e^{-\hat{D}_i t^n} t^{n-2} \hat{D}_i^{1-1/n} (\hat{D}_i t^n)^{-1+1/n} - \frac{\hat{q}_i \left\{\Gamma\left[\frac{1}{n}\right] - \Gamma\left[\frac{1}{n}, \hat{D}_i t^n\right]\right\}}{\hat{D}_i^{1/n} n t^2} \quad \text{.....(F.29)}$$

If we assume that $\hat{D}_i$, q, n, and t are positive, we can further simplify Eq. F.29:

$$\frac{dq_{\text{int}}(t)}{dt} = \hat{q}_i e^{-\hat{D}_i t^n} t^{n-2} \hat{D}_i^{1-1/n} \hat{D}_i^{-1+1/n} t^{n(-1+1/n)} - \frac{\hat{q}_i \left\{\Gamma\left[\frac{1}{n}\right] - \Gamma\left[\frac{1}{n}, \hat{D}_i t^n\right]\right\}}{\hat{D}_i^{1/n} n t^2}$$

$$\frac{dq_{\text{int}}(t)}{dt} = \hat{q}_i t^{n(-1+1/n)+n-2} e^{-\hat{D}_i t^n} - \frac{\hat{q}_i \left\{ \Gamma\left[\frac{1}{n}\right] - \Gamma\left[\frac{1}{n}, \hat{D}_i t^n\right] \right\}}{\hat{D}_i^{1/n} n t^2} \quad \text{.....(F.30)}$$

Simplifying the exponent on the time variable:

$$\frac{dq_{\text{int}}(t)}{dt} = \hat{q}_i e^{-\hat{D}_i t^n} t^{-n+1+n-2} - \frac{\hat{q}_i \left\{ \Gamma\left[\frac{1}{n}\right] - \Gamma\left[\frac{1}{n}, \hat{D}_i t^n\right] \right\}}{\hat{D}_i^{1/n} n t^2}$$

$$\frac{dq_{\text{int}}(t)}{dt} = \frac{\hat{q}_i e^{-\hat{D}_i t^n}}{t} - \frac{\hat{q}_i \left\{ \Gamma\left[\frac{1}{n}\right] - \Gamma\left[\frac{1}{n}, \hat{D}_i t^n\right] \right\}}{\hat{D}_i^{1/n} n t^2} \quad \text{.....(F.31)}$$

Eq. F.31 is the derivative of the rate-integral form of the power-law exponential. Plugging in Eq. F.31 and Eq. F.11 into Eq. F.12 to solve for the loss-ratio:

$$\frac{1}{D} \equiv -\frac{q(t)}{dq(t)/dt} = -\frac{\frac{\hat{q}_i}{\hat{D}_i^{1/n} n t} \left\{ \Gamma\left[\frac{1}{n}\right] - \Gamma\left[\frac{1}{n}, \hat{D}_i t^n\right] \right\}}{\frac{\hat{q}_i e^{-\hat{D}_i t^n}}{t} - \frac{\hat{q}_i \left\{ \Gamma\left[\frac{1}{n}\right] - \Gamma\left[\frac{1}{n}, \hat{D}_i t^n\right] \right\}}{\hat{D}_i^{1/n} n t^2}} \quad \text{..... (F.32)}$$

For our purpose, we are more interested in the reciprocal of Eq. F.32.

$$D_{\text{int}}(t) = -\frac{\frac{\hat{q}_i e^{-\hat{D}_i t^n}}{t} - \frac{\hat{q}_i \left\{ \Gamma\left[\frac{1}{n}\right] - \Gamma\left[\frac{1}{n}, \hat{D}_i t^n\right] \right\}}{\hat{D}_i^{1/n} n t^2}}{\frac{\hat{q}_i}{\hat{D}_i^{1/n} n t} \left\{ \Gamma\left[\frac{1}{n}\right] - \Gamma\left[\frac{1}{n}, \hat{D}_i t^n\right] \right\}} \quad \text{.....(F.33)}$$

Expanding the common denominator:

$$D_{\text{int}}(t) = -\frac{\dfrac{\hat{q}_i e^{-\hat{D}_i t^n}}{t}}{\dfrac{\hat{q}_i}{\hat{D}_i^{1/n} nt}\left\{\Gamma\left[\frac{1}{n}\right] - \Gamma\left[\frac{1}{n}, \hat{D}_i t^n\right]\right\}} + \frac{\dfrac{\hat{q}_i\left\{\Gamma\left[\frac{1}{n}\right] - \Gamma\left[\frac{1}{n}, \hat{D}_i t^n\right]\right\}}{\hat{D}_i^{1/n} nt^2}}{\dfrac{\hat{q}_i}{\hat{D}_i^{1/n} nt}\left\{\Gamma\left[\frac{1}{n}\right] - \Gamma\left[\frac{1}{n}, \hat{D}_i t^n\right]\right\}} \quad \text{.....(F.34)}$$

Cancelling like terms:

$$D_{\text{int}}(t) = -\frac{e^{-\hat{D}_i t^n}}{\dfrac{1}{\hat{D}_i^{1/n} n}\left\{\Gamma\left[\frac{1}{n}\right] - \Gamma\left[\frac{1}{n}, \hat{D}_i t^n\right]\right\}} + \frac{1}{t} \quad \text{.....(F.35)}$$

Rearranging Eq. F.35:

$$D_{\text{int}}(t) = \frac{1}{t} - \frac{\hat{D}_i^{1/n} n e^{-\hat{D}_i t^n}}{\Gamma\left[\frac{1}{n}\right] - \Gamma\left[\frac{1}{n}, \hat{D}_i t^n\right]} \quad \text{.....(F.36)}$$

Eq. F.37 is the reciprocal loss-ratio for the rate-integral of the power-law exponential. Now, to calculate the loss-ratio derivative the reciprocal of Eq. F.36 is needed, which is defined as:

$$\frac{1}{D} = \frac{1}{\dfrac{1}{t} - \dfrac{\hat{D}_i^{1/n} n e^{-\hat{D}_i t^n}}{\Gamma\left[\frac{1}{n}\right] - \Gamma\left[\frac{1}{n}, \hat{D}_i t^n\right]}} \quad \text{.....(F.37)}$$

Plugging in Eq. F.37 into Eq. F.13

$$b_{\text{int}}(t) = \frac{d}{dt}\left[\frac{1}{D}\right] = \frac{\partial}{\partial t}\left\{\frac{1}{\frac{1}{t} - \frac{\hat{D}_i^{1/n} n e^{-\hat{D}_i t^n}}{\Gamma\left[\frac{1}{n}\right] - \Gamma\left[\frac{1}{n}, \hat{D}_i t^n\right]}}\right\} \quad \text{(F.38)}$$

Using the chain rule, which for this problem is defined as:

$$\frac{\partial}{\partial t}\left\{\frac{1}{\frac{1}{t} - \frac{\hat{D}_i^{1/n} n e^{-\hat{D}_i t^n}}{\Gamma\left[\frac{1}{n}\right] - \Gamma\left[\frac{1}{n}, \hat{D}_i t^n\right]}}\right\} = \frac{\partial}{\partial u}\left(\frac{1}{u}\right)\frac{\partial u}{\partial t} \quad \text{(F.39)}$$

Where:

$$u = \frac{1}{t} - \frac{\hat{D}_i^{1/n} n e^{-\hat{D}_i t^n}}{\left\{\Gamma\left[\frac{1}{n}\right] - \Gamma\left[\frac{1}{n}, \hat{D}_i t^n\right]\right\}} \quad \text{(F.40)}$$

$$\frac{\partial}{\partial u}\left(\frac{1}{u}\right) = -\frac{1}{u^2} \quad \text{(F.41)}$$

Plugging in Eq. F.39 – F.41 into Eq. F.38:

$$b_{\text{int}}(t) = -\frac{\frac{\partial}{\partial t}\left\{\frac{1}{t} - \frac{\hat{D}_i^{1/n} n e^{-\hat{D}_i t^n}}{\Gamma\left[\frac{1}{n}\right] - \Gamma\left[\frac{1}{n}, \hat{D}_i t^n\right]}\right\}}{\left\{\frac{1}{t} - \frac{\hat{D}_i^{1/n} n e^{-\hat{D}_i t^n}}{\Gamma\left[\frac{1}{n}\right] - \Gamma\left[\frac{1}{n}, \hat{D}_i t^n\right]}\right\}^2} \quad \text{(F.42)}$$

Distributing the partial derivative across the summation and pulling out constants:

$$b_{\text{int}}(t) = -\frac{\frac{\partial}{\partial t}\left(\frac{1}{t}\right) - \hat{D}_i^{1/n} n \frac{\partial}{\partial t}\left\{\frac{e^{-\hat{D}_i t^n}}{\Gamma\left[\frac{1}{n}\right] - \Gamma\left[\frac{1}{n}, \hat{D}_i t^n\right]}\right\}}{\left\{\frac{1}{t} - \frac{\hat{D}_i^{1/n} n e^{-\hat{D}_i t^n}}{\Gamma\left[\frac{1}{n}\right] - \Gamma\left[\frac{1}{n}, \hat{D}_i t^n\right]}\right\}^2} \quad \text{.....(F.43)}$$

Completing the first partial derivative:

$$b_{\text{int}}(t) = -\frac{-\frac{1}{t^2} - \hat{D}_i^{1/n} n \frac{\partial}{\partial t}\left\{\frac{e^{-\hat{D}_i t^n}}{\Gamma\left[\frac{1}{n}\right] - \Gamma\left[\frac{1}{n}, \hat{D}_i t^n\right]}\right\}}{\left\{\frac{1}{t} - \frac{\hat{D}_i^{1/n} n e^{-\hat{D}_i t^n}}{\Gamma\left[\frac{1}{n}\right] - \Gamma\left[\frac{1}{n}, \hat{D}_i t^n\right]}\right\}^2} \quad \text{.....(F.44)}$$

Recalling the quotient rule:

$$\frac{\partial}{\partial t}\left(\frac{u}{v}\right) = \frac{v\frac{\partial u}{\partial t} - u\frac{\partial v}{\partial t}}{v^2} \quad \text{.....(F.15)}$$

Where in this case:

$$u = e^{-\hat{D}_i t^n} \quad \text{.....(F.45)}$$

$$v = \Gamma\left[\frac{1}{n}\right] - \Gamma\left[\frac{1}{n}, \hat{D}_i t^n\right] \quad \text{.....(F.46)}$$

Plugging Eq. F.15, F.45 and F.46 into Eq. F.44:

$$b_{\text{int}}(t) = -\frac{-\frac{1}{t^2} - \hat{D}_i^{1/n} n \frac{\left\{\Gamma\left[\frac{1}{n}\right] - \Gamma\left[\frac{1}{n}, \hat{D}_i t^n\right]\right\} \frac{\partial}{\partial t}\left(e^{-\hat{D}_i t^n}\right) - e^{-\hat{D}_i t^n} \frac{\partial}{\partial t}\left\{\Gamma\left[\frac{1}{n}\right] - \Gamma\left[\frac{1}{n}, \hat{D}_i t^n\right]\right\}}{\left\{\Gamma\left[\frac{1}{n}\right] - \Gamma\left[\frac{1}{n}, \hat{D}_i t^n\right]\right\}^2}}{\left\{\frac{1}{t} - \frac{\hat{D}_i^{1/n} n e^{-\hat{D}_i t^n}}{\Gamma\left[\frac{1}{n}\right] - \Gamma\left[\frac{1}{n}, \hat{D}_i t^n\right]}\right\}^2} \quad \text{.....(F.47)}$$

Applying the chain rule, which for this case is defined as:

$$\frac{\partial}{\partial t}\left(e^{-Dt^n}\right) = \frac{\partial}{\partial t}\left(e^u\right)\frac{\partial u}{\partial t} \quad \text{.....(F.48)}$$

Where:

$$u = \hat{D}_i t^n \quad \text{.....(F.49)}$$

$$\frac{\partial}{\partial t}\left(e^u\right) = e^u \quad \text{.....(F.50)}$$

Plugging Eq. F.48 – F.50 into Eq. F.47:

$$b_{\text{int}}(t) = -\frac{-\frac{1}{t^2} - \hat{D}_i^{1/n} n \frac{\left\{\Gamma\left[\frac{1}{n}\right] - \Gamma\left[\frac{1}{n}, \hat{D}_i t^n\right]\right\} e^{-\hat{D}_i t^n} \frac{\partial}{\partial t}\left(-\hat{D}_i t^n\right) - e^{-\hat{D}_i t^n} \frac{\partial}{\partial t}\left\{\Gamma\left[\frac{1}{n}\right] - \Gamma\left[\frac{1}{n}, \hat{D}_i t^n\right]\right\}}{\left\{\Gamma\left[\frac{1}{n}\right] - \Gamma\left[\frac{1}{n}, \hat{D}_i t^n\right]\right\}^2}}{\left\{\frac{1}{t} - \frac{\hat{D}_i^{1/n} n e^{-\hat{D}_i t^n}}{\Gamma\left[\frac{1}{n}\right] - \Gamma\left[\frac{1}{n}, \hat{D}_i t^n\right]}\right\}^2} \quad \text{.....(F.51)}$$

Factoring out the constants and completing the partial differentiation using the power rule:

$$b_{\text{int}}(t) = -\frac{-\frac{1}{t^2} - \hat{D}_i^{1/n} n \dfrac{-\left\{\Gamma\left[\frac{1}{n}\right] - \Gamma\left[\frac{1}{n}, \hat{D}_i t^n\right]\right\} e^{-\hat{D}_i t^n} \hat{D}_i n t^{n-1} - e^{-\hat{D}_i t^n} \dfrac{\partial}{\partial t}\left\{\Gamma\left[\frac{1}{n}\right] - \Gamma\left[\frac{1}{n}, \hat{D}_i t^n\right]\right\}}{\left\{\Gamma\left[\frac{1}{n}\right] - \Gamma\left[\frac{1}{n}, \hat{D}_i t^n\right]\right\}^2}}{\left\{\dfrac{1}{t} - \dfrac{\hat{D}_i^{1/n} n e^{-\hat{D}_i t^n}}{\Gamma\left[\frac{1}{n}\right] - \Gamma\left[\frac{1}{n}, \hat{D}_i t^n\right]}\right\}^2} \quad \text{.....(F.52)}$$

Distributing the partial derivative across the summation with the Gamma functions:

$$b_{\text{int}}(t) = -\frac{-\frac{1}{t^2} - \hat{D}_i^{1/n} n \dfrac{-\left\{\Gamma\left[\frac{1}{n}\right] - \Gamma\left[\frac{1}{n}, \hat{D}_i t^n\right]\right\} e^{-\hat{D}_i t^n} \hat{D}_i n t^{n-1} - e^{-\hat{D}_i t^n} \left\{\dfrac{\partial}{\partial t}\Gamma\left[\frac{1}{n}\right] - \dfrac{\partial}{\partial t}\Gamma\left[\frac{1}{n}, \hat{D}_i t^n\right]\right\}}{\left\{\Gamma\left[\frac{1}{n}\right] - \Gamma\left[\frac{1}{n}, \hat{D}_i t^n\right]\right\}^2}}{\left\{\dfrac{1}{t} - \dfrac{\hat{D}_i^{1/n} n e^{-\hat{D}_i t^n}}{\Gamma\left[\frac{1}{n}\right] - \Gamma\left[\frac{1}{n}, \hat{D}_i t^n\right]}\right\}^2}$$

$$b_{\text{int}}(t) = -\frac{-\frac{1}{t^2} - \hat{D}_i^{1/n} n \dfrac{-\left\{\Gamma\left[\frac{1}{n}\right] - \Gamma\left[\frac{1}{n}, \hat{D}_i t^n\right]\right\} e^{-\hat{D}_i t^n} \hat{D}_i n t^{n-1} + e^{-\hat{D}_i t^n} \dfrac{\partial}{\partial t}\left\{\Gamma\left[\frac{1}{n}\right] - \Gamma\left[\frac{1}{n}, \hat{D}_i t^n\right]\right\}}{\left\{\Gamma\left[\frac{1}{n}\right] - \Gamma\left[\frac{1}{n}, \hat{D}_i t^n\right]\right\}^2}}{\left\{\dfrac{1}{t} - \dfrac{\hat{D}_i^{1/n} n e^{-\hat{D}_i t^n}}{\Gamma\left[\frac{1}{n}\right] - \Gamma\left[\frac{1}{n}, \hat{D}_i t^n\right]}\right\}^2} \quad \text{.....(F.53)}$$

Applying the chain rule to Eq. F.53, which is defined as:

$$\frac{\partial}{\partial t}\left\{\Gamma\left[\frac{1}{n}, \hat{D}_i t^n\right]\right\} = \frac{\partial}{\partial t}\Gamma\left[\frac{1}{n}, u\right]\frac{\partial u}{\partial t} \quad \text{.....(F.23)}$$

Where:

$$u = \hat{D}_i t^n \quad \text{.....(F.24)}$$

$$\frac{\partial}{\partial t}\Gamma\left[\frac{1}{n}, u\right] = -e^{-u}u^{-1+1/n} \quad \text{.....(F.25)}$$

Plugging in Eq. F.23 – F.25 into Eq. F.53:

$$b_{\text{int}}(t) = -\frac{-\frac{1}{t^2} - \hat{D}_i^{1/n} n \dfrac{-\left\{\Gamma\left[\frac{1}{n}\right] - \Gamma\left[\frac{1}{n}, \hat{D}_i t^n\right]\right\} e^{-\hat{D}_i t^n} \hat{D}_i n t^{n-1} - e^{-\hat{D}_i t^n} e^{-\hat{D}_i t^n} \left(\hat{D}_i t^n\right)^{-1+1/n} \dfrac{\partial}{\partial t}\left(\hat{D}_i t^n\right)}{\left\{\Gamma\left[\frac{1}{n}\right] - \Gamma\left[\frac{1}{n}, \hat{D}_i t^n\right]\right\}^2}}{\left\{\frac{1}{t} - \dfrac{\hat{D}_i^{1/n} n e^{-\hat{D}_i t^n}}{\Gamma\left[\frac{1}{n}\right] - \Gamma\left[\frac{1}{n}, \hat{D}_i t^n\right]}\right\}^2} \quad \text{.....(F.54)}$$

Simplifying and factoring out constants

$$b_{\text{int}}(t) = -\frac{-\frac{1}{t^2} - \hat{D}_i^{1/n} n \dfrac{-\left\{\Gamma\left[\frac{1}{n}\right] - \Gamma\left[\frac{1}{n}, \hat{D}_i t^n\right]\right\} e^{-\hat{D}_i t^n} \hat{D}_i n t^{n-1} - e^{-2\hat{D}_i t^n} \hat{D}_i \left(\hat{D}_i t^n\right)^{-1+1/n} \dfrac{\partial}{\partial t}\left(t^n\right)}{\left\{\Gamma\left[\frac{1}{n}\right] - \Gamma\left[\frac{1}{n}, \hat{D}_i t^n\right]\right\}^2}}{\left\{\frac{1}{t} - \dfrac{\hat{D}_i^{1/n} n e^{-\hat{D}_i t^n}}{\Gamma\left[\frac{1}{n}\right] - \Gamma\left[\frac{1}{n}, \hat{D}_i t^n\right]}\right\}^2} \quad \text{.....(F.55)}$$

Completing the last partial derivative using the power rule.

$$b_{\text{int}}(t) = -\frac{-\frac{1}{t^2} - \hat{D}_i^{1/n} n \frac{-\left\{\Gamma\left[\frac{1}{n}\right] - \Gamma\left[\frac{1}{n}, \hat{D}_i t^n\right]\right\} e^{-\hat{D}_i t^n} \hat{D}_i n t^{n-1} - n t^{n-1} e^{-2\hat{D}_i t^n} \hat{D}_i \left(\hat{D}_i t^n\right)^{-1+1/n}}{\left\{\Gamma\left[\frac{1}{n}\right] - \Gamma\left[\frac{1}{n}, \hat{D}_i t^n\right]\right\}^2}}{\left\{\frac{1}{t} - \frac{\hat{D}_i^{1/n} n e^{-\hat{D}_i t^n}}{\Gamma\left[\frac{1}{n}\right] - \Gamma\left[\frac{1}{n}, \hat{D}_i t^n\right]}\right\}^2} \quad \text{.....(F.56)}$$

Simplifying

$$b_{\text{int}}(t) = -\frac{-\frac{1}{t^2} + \frac{\hat{D}_i^{1/n} n \left\{\Gamma\left[\frac{1}{n}\right] - \Gamma\left[\frac{1}{n}, \hat{D}_i t^n\right]\right\} e^{-\hat{D}_i t^n} \hat{D}_i n t^{n-1} + \hat{D}_i^{1/n} n n t^{n-1} e^{-2\hat{D}_i t^n} \hat{D}_i \left(\hat{D}_i t^n\right)^{-1+1/n}}{\left\{\Gamma\left[\frac{1}{n}\right] - \Gamma\left[\frac{1}{n}, \hat{D}_i t^n\right]\right\}^2}}{\left\{\frac{1}{t} - \frac{\hat{D}_i^{1/n} n e^{-\hat{D}_i t^n}}{\Gamma\left[\frac{1}{n}\right] - \Gamma\left[\frac{1}{n}, \hat{D}_i t^n\right]}\right\}^2}$$

$$b_{\text{int}}(t) = -\frac{-\frac{1}{t^2} + \frac{\hat{D}_i^{1+1/n} n^2 t^{n-1} e^{-\hat{D}_i t^n} \left\{\Gamma\left[\frac{1}{n}\right] - \Gamma\left[\frac{1}{n}, \hat{D}_i t^n\right]\right\} + \hat{D}_i^{1+1/n} n^2 t^{n-1} e^{-2\hat{D}_i t^n} \left(\hat{D}_i t^n\right)^{-1+1/n}}{\left\{\Gamma\left[\frac{1}{n}\right] - \Gamma\left[\frac{1}{n}, \hat{D}_i t^n\right]\right\}^2}}{\left\{\frac{1}{t} - \frac{\hat{D}_i^{1/n} n e^{-\hat{D}_i t^n}}{\Gamma\left[\frac{1}{n}\right] - \Gamma\left[\frac{1}{n}, \hat{D}_i t^n\right]}\right\}^2}$$

$$b_{\text{int}}(t) = -\frac{\dfrac{\hat{D}_i^{1+1/n} n^2 t^{n-1} e^{-\hat{D}_i t^n}}{\left\{\Gamma\left[\frac{1}{n}\right] - \Gamma\left[\frac{1}{n}, \hat{D}_i t^n\right]\right\}} + \dfrac{\hat{D}_i^{1+1/n} n^2 t^{n-1} e^{-2\hat{D}_i t^n} \left(\hat{D}_i t^n\right)^{-1+1/n}}{\left\{\Gamma\left[\frac{1}{n}\right] - \Gamma\left[\frac{1}{n}, \hat{D}_i t^n\right]\right\}^2} - \frac{1}{t^2}}{\left\{\frac{1}{t} - \dfrac{\hat{D}_i^{1/n} n e^{-\hat{D}_i t^n}}{\Gamma\left[\frac{1}{n}\right] - \Gamma\left[\frac{1}{n}, \hat{D}_i t^n\right]}\right\}^2} \quad \text{.....(F.57)}$$

If we assume that $\hat{D}_i$, q, n, and t are positive, we can further simplify Eq. F.57:

$$b_{\text{int}}(t) = -\frac{\dfrac{\hat{D}_i^{1+1/n} n^2 t^{n-1} e^{-\hat{D}_i t^n}}{\left\{\Gamma\left[\frac{1}{n}\right] - \Gamma\left[\frac{1}{n}, \hat{D}_i t^n\right]\right\}} + \dfrac{\hat{D}_i^{1+1/n} \hat{D}_i^{-1+1/n} n^2 t^{n-1} t^{n(-1+1/n)} e^{-2\hat{D}_i t^n}}{\left\{\Gamma\left[\frac{1}{n}\right] - \Gamma\left[\frac{1}{n}, \hat{D}_i t^n\right]\right\}^2} - \frac{1}{t^2}}{\left\{\frac{1}{t} - \dfrac{\hat{D}_i^{1/n} n e^{-\hat{D}_i t^n}}{\Gamma\left[\frac{1}{n}\right] - \Gamma\left[\frac{1}{n}, \hat{D}_i t^n\right]}\right\}^2}$$

$$b_{\text{int}}(t) = -\frac{\dfrac{\hat{D}_i^{1+1/n} n^2 t^{n-1} e^{-\hat{D}_i t^n}}{\left\{\Gamma\left[\frac{1}{n}\right] - \Gamma\left[\frac{1}{n}, \hat{D}_i t^n\right]\right\}} + \dfrac{\hat{D}_i^{2/n} n^2 e^{-2\hat{D}_i t^n}}{\left\{\Gamma\left[\frac{1}{n}\right] - \Gamma\left[\frac{1}{n}, \hat{D}_i t^n\right]\right\}^2} - \frac{1}{t^2}}{\left\{\frac{1}{t} - \dfrac{\hat{D}_i^{1/n} n e^{-\hat{D}_i t^n}}{\Gamma\left[\frac{1}{n}\right] - \Gamma\left[\frac{1}{n}, \hat{D}_i t^n\right]}\right\}^2} \quad \text{.....(F.58)}$$

Eq. F.58 is the loss-ratio derivative of the rate-integral form of the power-law exponential. It needs to be remembered that D_∞ had to be assumed to be zero in order to integrate the power-law exponential equation. As stated before if a D_∞ parameter is used, then the rate-integral, loss-ratio, and loss ratio derivative must me computed numerically.

APPENDIX G

RATE-INTEGRAL FORM OF STRETCHED EXPONENTIAL

In this appendix the rate-integral, loss-ratio of the rate-integral, and the loss-ratio derivative of the loss ratio for the stretched exponential are derived. The stretched exponential is equivalent to the power-law exponential with no terminal decline parameter and with different variables. In Appendix F, it was shown that for the power-law exponential the rate-integral is defined as:

$$Q(t) = \int_0^t q(t)\, dt = \frac{\hat{q}_i}{\hat{D}_i^{1/n} n}\left\{\Gamma\left[\frac{1}{n}\right] - \Gamma\left[\frac{1}{n}, \hat{D}_i t^n\right]\right\} \quad \text{.....(F.10)}$$

The reciprocal loss-ratio for rate-integral form of the power-law exponential is defined as:

$$D_{\text{int}}(t) = \frac{1}{t} - \frac{\hat{D}_i^{1/n} n e^{-\hat{D}_i t^n}}{\Gamma\left[\frac{1}{n}\right] - \Gamma\left[\frac{1}{n}, \hat{D}_i t^n\right]} \quad \text{.....(F.36)}$$

The loss-ratio derivative for the rate-integral form of the power-law exponential is defined as:

$$b_{\text{int}}(t) = -\frac{\dfrac{\hat{D}_i^{1+1/n} n^2 t^{n-1} e^{-\hat{D}_i t^n}}{\left\{\Gamma\left[\frac{1}{n}\right] - \Gamma\left[\frac{1}{n}, \hat{D}_i t^n\right]\right\}} + \dfrac{\hat{D}_i^{2/n} n^2 e^{-2\hat{D}_i t^n}}{\left\{\Gamma\left[\frac{1}{n}\right] - \Gamma\left[\frac{1}{n}, \hat{D}_i t^n\right]\right\}^2} - \dfrac{1}{t^2}}{\left\{\dfrac{1}{t} - \dfrac{\hat{D}_i^{1/n} n e^{-\hat{D}_i t^n}}{\Gamma\left[\frac{1}{n}\right] - \Gamma\left[\frac{1}{n}, \hat{D}_i t^n\right]}\right\}^2} \quad \text{.....(F.58)}$$

The power-law exponential and the stretched exponential can be related by using the following equation:

$$\hat{D}_i = \left(\frac{1}{\tau}\right)^n \quad \text{.....(G.1)}$$

Plugging in Eq. G.1 into Eq. F.10

$$q_{\text{int}}(t) = \int_0^t q(t)\, dt = \frac{\hat{q}_i \tau}{n}\left\{\Gamma\left[\frac{1}{n}\right] - \Gamma\left[\frac{1}{n}, \left(\frac{t}{\tau}\right)^n\right]\right\} \quad \text{.....(G.2)}$$

Eq. G.2 is the rate-integral for the stretched exponential.

Plugging in Eq. G.1 into Eq. F.37:

$$D_{\text{int}}(t) = \frac{1}{t} - \frac{1}{\tau}\frac{n e^{-\left(\frac{t}{\tau}\right)^n}}{\Gamma\left[\frac{1}{n}\right] - \Gamma\left[\frac{1}{n}, \left(\frac{t}{\tau}\right)^n\right]} \quad \text{.....(G.3)}$$

Eq. G.3 is the reciprocal loss-ratio of the rate-integral for the stretched exponential.

Plugging in Eq. G.1 into Eq. F.58:

$$b_{\text{int}}(t) = -\frac{\left(\frac{1}{\tau}\right)^{1+n}\frac{n^2 t^{n-1} e^{-\left(\frac{t}{\tau}\right)^n}}{\left\{\Gamma\left[\frac{1}{n}\right] - \Gamma\left[\frac{1}{n}, \left(\frac{t}{\tau}\right)^n\right]\right\}} + \frac{1}{\tau^2}\frac{n^2 e^{-2\left(\frac{t}{\tau}\right)^n}}{\left\{\Gamma\left[\frac{1}{n}\right] - \Gamma\left[\frac{1}{n}, \left(\frac{t}{\tau}\right)^n\right]\right\}^2} - \frac{1}{t^2}}{\left\{\frac{1}{t} - \frac{1}{\tau}\frac{n e^{-\left(\frac{t}{\tau}\right)^n}}{\Gamma\left[\frac{1}{n}\right] - \Gamma\left[\frac{1}{n}, \left(\frac{t}{\tau}\right)^n\right]}\right\}^2} \quad \text{.....(G.4)}$$

Eq. G.4 is the loss-ratio derivative of the rate-integral for the stretched exponential decline curve model.

APPENDIX H

RATE-INTEGRAL FORM OF MODIFIED HYPERBOLIC

In this appendix the rate-integral, reciprocal loss-ratio of the of the rate-integral, and the loss-ratio derivative of the rate-integral for the modified hyperbolic relation are derived. The modified hyperbolic decline curve is still the most commonly applied model for unconventional wells. We begin with the rate integral, which is defined as:

$$q_{\text{int}}(t) = \frac{\int_0^t q(t)\, dt}{t} \quad \text{.....(H.1)}$$

Since the modified hyperbolic consists of Arps' hyperbolic decline initially with the Arps' exponential decline in late-time, we will derive the associated equations for each section of the decline separately. Beginning with the hyperbolic decline portion of the modified hyperbolic, the time-rate equation is defined as:

$$q(t) = \frac{q_i}{(1+bD_i t)^{1/b}} \quad \text{.....(H.2)}$$

Plugging in Eq. H.2 into Eq. H.1:

$$q_{\text{int}}(t) = \frac{\int_0^t \frac{q_i}{(1+bD_i t)^{1/b}}\, dt}{t} \quad \text{.....(H.3)}$$

Factoring out the constants in Eq. H.3 and using *u*-substitution to complete the integral in Eq. H.3.

Defining variables:

$$u = bD_i t + 1 \quad \text{.....(H.4)}$$

$$du = bD_i\ dt \quad \text{.....(H.5)}$$

Plugging in Eq. H.4 and H.5 into Eq. H.3:

$$q_{\text{int}}(t) = \frac{\frac{q_i}{bD_i}\int_0^t \frac{1}{u^{1/b}}\ du}{t} \quad \text{.....(H.6)}$$

Completing the integral, plugging back in Eq. H.4 and H.3, and simplifying:

$$q_{\text{int}}(t) = \frac{\frac{q_i u^{1-1/b}}{bD_i(1-1/b)}}{t}$$

$$q_{\text{int}}(t) = \frac{\left.\frac{q_i(bD_i t+1)^{1-1/b}}{(b-1)D_i}\right|_0^t}{t}$$

$$q_{\text{int}}(t) = \frac{\frac{q_i(bD_i t+1)^{1-1/b}}{(b-1)D_i} - \frac{q_i(bD_i(0)+1)^{1-1/b}}{(b-1)D_i}}{t}$$

$$q_{\text{int}}(t) = \frac{q_i}{D_i(1-b)t}\left[1-(1+bD_i t)^{1-1/b}\right] \quad \text{.....(H.7)}$$

Eq. H.7 is the rate-integral of the hyperbolic portion of the modified hyperbolic equation.

Recalling the definitions of loss-ratio and the loss-ratio derivative:

$$\frac{1}{D} \equiv -\frac{q(t)}{dq(t)/dt} \qquad \text{(Definition of the loss-ratio) .....(H.8)}$$

$$b \equiv \frac{d}{dt}\left[\frac{1}{D}\right] \equiv \frac{d}{dt}\left[\frac{q(t)}{dq(t)/dt}\right] \qquad \text{(Derivative of the loss-ratio) .....(H.9)}$$

Therefore, in order to calculate the reciprocal loss-ratio we need to determine the derivative of Eq. H.7. Setting this up:

$$\frac{dq_{\text{int}}(t)}{dt} = \frac{q_i}{D_i(1-b)} \frac{\delta}{\delta t}\left[\frac{1-(1+bD_it)^{1-1/b}}{t}\right] \quad \text{(H.10)}$$

Recalling the quotient rule:

$$\frac{\partial}{\partial t}\left(\frac{u}{v}\right) = \frac{v\frac{\partial u}{\partial t} - u\frac{\partial v}{\partial t}}{v^2} \quad \text{(H.11)}$$

Where:

$$u = 1-(bD_it+1)^{1-1/b} \quad \text{(H.12)}$$

$$v = t \quad \text{(H.13)}$$

Plugging in Eq. H.12 and H.13 into Eq. H.10:

$$\frac{dq_{\text{int}}(t)}{dt} = \frac{q_i}{D_i(1-b)} \frac{t\frac{\partial}{\partial t}[1-(bD_it+1)^{1-1/b}] - [1-(bD_it+1)^{1-1/b}]\frac{\partial}{\partial t}(t)}{t^2} \quad \text{(H.14)}$$

Simplifying Eq. H.14:

$$\frac{dq_{\text{int}}(t)}{dt} = \frac{q_i}{D_i(1-b)} \frac{t\frac{\partial}{\partial t}[1-(bD_it+1)^{1-1/b}] - [1-(bD_it+1)^{1-1/b}]}{t^2}$$

$$\frac{dq_{\text{int}}(t)}{dt} = \frac{q_i}{D_i(1-b)} \frac{-1+(bD_it+1)^{1-1/b} + t\frac{\partial}{\partial t}[1-(bD_it+1)^{1-1/b}]}{t^2} \quad \text{(H.15)}$$

Completing the partial derivative of the summation term in the numerator by factoring out the constants:

$$\frac{dq_{\text{int}}(t)}{dt} = \frac{q_i}{D_i(1-b)} \frac{-1 + (bD_i t + 1)^{1-1/b} + \frac{\partial}{\partial t}(1) - t\frac{\partial}{\partial t}(bD_i t + 1)^{1-1/b}}{t^2}$$

$$\frac{dq_{\text{int}}(t)}{dt} = \frac{q_i}{D_i(1-b)} \frac{-1 + (bD_i t + 1)^{1-1/b} - t\frac{\partial}{\partial t}(bD_i t + 1)^{1-1/b}}{t^2} \quad \text{.....(H.16)}$$

To complete the last partial derivative, we will use the chain rule and *u*-substitution. In this case, the chain rule is defined as:

$$\frac{\partial}{\partial t}\left\{(bD_i t + 1)^{1-1/b}\right\} = \frac{\partial u^{1-1/b}}{\partial u}\frac{\partial u}{\partial t} \quad \text{.....(H.17)}$$

Where:

$$u = bD_i t + 1 \quad \text{.....(H.18)}$$

$$\frac{\partial}{\partial t}(u^{1-1/b}) = (1-1/b)u^{-1/b} \quad \text{.....(H.19)}$$

Plugging in Eq. H.17 though H.19 into Eq. H.16:

$$\frac{dq_{\text{int}}(t)}{dt} = \frac{q_i}{D_i(1-b)} \frac{-1 + (bD_i t + 1)^{1-1/b} - \frac{\partial}{\partial t}(1) + bD_i\frac{\partial}{\partial t}(t)(1-1/b)t(bD_i t + 1)^{-1/b}}{t^2} \quad \text{.....(H.16)}$$

Simplifying Eq. H.16:

$$\frac{dq_{\text{int}}(t)}{dt} = \frac{q_i}{D_i(1-b)} \frac{-1 + (bD_i t + 1)^{1-1/b} - (1-1/b)bD_i t(bD_i t + 1)^{-1/b}\frac{\partial}{\partial t}(t)}{t^2}$$

$$\frac{dq_{\text{int}}(t)}{dt} = \frac{q_i}{D_i(1-b)} \frac{-1+(bD_it+1)^{1-1/b} - (1-1/b)bD_it(bD_it+1)^{-1/b}}{t^2}$$

$$\frac{dq_{\text{int}}(t)}{dt} = \frac{q_i}{D_i(b-1)t^2}(bD_it+1)^{-1/b}[(bD_it+1)^{1/b} - D_it - 1] \quad \text{.....(H.17)}$$

Eq. H.17 is the derivative of the rate-integral for the hyperbolic section of the modified hyperbolic decline curve with respect to time. Plugging in Eq. H.17 and H.7 into Eq. H.8:

$$\frac{1}{D} \equiv -\frac{\frac{q_i}{D_i(1-b)t}\left[1-(1+bD_it)^{1-1/b}\right]}{\frac{q_i}{D_i(b-1)t^2}(bD_it+1)^{-1/b}[(bD_it+1)^{1/b} - D_it - 1]} \quad \text{.....(H.18)}$$

Simplifying Eq. H.18:

$$\frac{1}{D} \equiv -\frac{q_i[1-(1+bD_it)^{1-1/b}]}{D_i(1-b)t} \frac{D_i(b-1)t^2}{q_i(bD_it+1)^{-1/b}[(bD_it+1)^{1/b} - D_it - 1]}$$

$$\frac{1}{D} \equiv -\frac{(b-1)t[1-(1+bD_it)^{1-1/b}]}{(1-b)(bD_it+1)^{-1/b}[(bD_it+1)^{1/b} - D_it - 1]} \quad \text{.....(H.19)}$$

Assuming that b, D_i, and t are real:

$$\frac{1}{D} \equiv \frac{(b-1)D_it^2}{-(bD_it+1)^{1/b} + D_it + 1} + t \quad \text{.....(H.20)}$$

Eq. H.20 is the loss-ratio of the rate integral for the hyperbolic section of the modified hyperbolic decline curve. To solve for the D-parameter we take the reciprocal of Eq. H.20

$$D_{\text{int}}(t) \equiv \left[\frac{(b-1)D_it^2}{-(bD_it+1)^{1/b} + D_it + 1} + t\right]^{-1} \quad \text{.....(H.21)}$$

Plugging in Eq. H.20 into Eq. H.9 and solving for the loss-ratio derivative:

$$b_{\text{int}}(t) \equiv \frac{d}{dt}\left[\frac{1}{D}\right] \equiv \frac{d}{dt}\left[\frac{(b-1)D_i t^2}{-(bD_i t+1)^{1/b} + D_i t + 1} + t\right] \quad \text{.....(H.22)}$$

Expanding pulling constants out of the differentiation:

$$b_{\text{int}}(t) \equiv \frac{d}{dt}(t) + (b-1)D_i \frac{d}{dt}\left[\frac{t^2}{-(bD_i t+1)^{1/b} + D_i t + 1}\right]$$

$$b_{\text{int}}(t) \equiv 1 + (b-1)D_i \frac{d}{dt}\left[\frac{t^2}{-(bD_i t+1)^{1/b} + D_i t + 1}\right] \quad \text{.....(H.23)}$$

Recalling the quotient rule:

$$\frac{\partial}{\partial t}\left(\frac{u}{v}\right) = \frac{v\frac{\partial u}{\partial t} - u\frac{\partial v}{\partial t}}{v^2} \quad \text{.....(H.11)}$$

Where:

$$u = t^2 \quad \text{.....(H.24)}$$

$$v = -(bD_i t+1)^{1/b} + D_i t + 1 \quad \text{.....(H.25)}$$

Applying Eq. H.11, H.24 and H.25 to Eq. H.23:

$$b_{\text{int}}(t) \equiv 1 + (b-1)D_i \frac{[-(bD_i t+1)^{1/b} + D_i t + 1]\frac{\partial}{\partial t}(t^2) - t^2\frac{\partial}{\partial t}[-(bD_i t+1)^{1/b} + D_i t + 1]}{[-(bD_i t+1)^{1/b} + D_i t + 1]^2}$$

$$b_{\text{int}}(t) \equiv 1 + (b-1)D_i \frac{2t[-(bD_i t+1)^{1/b} + D_i t + 1] - t^2\frac{\partial}{\partial t}[-(bD_i t+1)^{1/b} + D_i t + 1]}{[-(bD_i t+1)^{1/b} + D_i t + 1]^2} \quad \text{.....(H.26)}$$

Differentiation the rest of the sum term in the numerator by first factoring out constants:

$$b_{\text{int}}(t) \equiv 1 + (b-1)D_i \frac{2t[-(bD_it+1)^{1/b} + D_it + 1] - t^2[-\frac{\partial}{\partial t}(bD_it+1)^{1/b} + D_i]}{[-(bD_it+1)^{1/b} + D_it + 1]^2} \quad \text{.....(H.22)}$$

To complete the last partial derivative, we will use the chain rule and *u*-substitution. In this case, the chain rule is defined as:

$$\frac{\partial}{\partial t}\left\{(bD_it+1)^{1/b}\right\} = \frac{\partial u^{1/b}}{\partial u}\frac{\partial u}{\partial t} \quad \text{.....(H.23)}$$

Where:

$$u = bD_it + 1 \quad \text{.....(H.24)}$$

$$\frac{\partial}{\partial t}(u^{1/b}) = \frac{u^{-1+1/b}}{b} \quad \text{.....(H.25)}$$

Plugging in Eq. H.23 though H.25 into Eq. H.22 and simplifying:

$$b_{\text{int}}(t) \equiv 1 + (b-1)D_i \frac{2t[-(bD_it+1)^{1/b} + D_it + 1] - t^2\left[D_i - \frac{(bD_it+1)^{-1+1/b}\frac{\partial}{\partial t}(bD_it+1)}{b}\right]}{[-(bD_it+1)^{1/b} + D_it + 1]^2}$$

$$b_{\text{int}}(t) \equiv 1 + (b-1)D_i \frac{2t[-(bD_it+1)^{1/b} + D_it + 1] - t^2\left[D_i - bD_i\frac{(bD_it+1)^{-1+1/b}}{b}\right]}{[-(bD_it+1)^{1/b} + D_it + 1]^2}$$

$$b_{\text{int}}(t) \equiv 1 + (b-1)D_i \frac{2t[-(bD_it+1)^{1/b} + D_it + 1] - t^2[D_i - D_i(bD_it+1)^{-1+1/b}]}{[-(bD_it+1)^{1/b} + D_it + 1]^2}$$

.....(H.26)

Expanding Eq. H.26 with common denominator to continue simplifying

$$b_{\text{int}}(t) \equiv 1 + \frac{2t(b-1)D_i[-(bD_it+1)^{1/b} + D_it + 1]}{[-(bD_it+1)^{1/b} + D_it + 1]^2} - \frac{t^2(b-1)D_i[D_i - D_i(bD_it+1)^{-1+1/b}]}{[-(bD_it+1)^{1/b} + D_it + 1]^2}$$

$$b_{\text{int}}(t) \equiv -\frac{(b-1)D_it^2[D_i - D_i(bD_it+1)^{-1+1/b}]}{[-(bD_it+1)^{1/b} + D_it + 1]^2} + \frac{2(b-1)D_it}{[-(bD_it+1)^{1/b} + D_it + 1]} + 1 \quad \text{.....(H.27)}$$

Eq. H.27 is the loss-ratio derivative of the rate-integral for the hyperbolic section of the modified hyperbolic decline curve. The modified hyperbolic decline curve, consists of two sections of decline; the hyperbolic section and the terminal exponential decline. For simplicity we will derive all equations for Arp's exponential decline and then put it in the correct variables for the modified hyperbolic equation. Arp's exponential decline is defined as:

$$q(t) = q_i \exp[-D_it]$$

……(H.28)

Plugging in Eq. H.28 into Eq. H.1 to solve for the rate-integral:

$$q_{\text{int}}(t) = \frac{\int_0^t q_i \exp[-D_it]\, dt}{t} \quad \text{.....(H.29)}$$

Completing the integral:

$$q_{\text{int}}(t) = \frac{q_i - q_i e^{(-D_it)}}{D_it} \quad \text{.....(H.30)}$$

Eq. H.30 is the time-rate integral equation for Arps' exponential decline.

To solve for the reciprocal loss-ratio of Eq. H.30 we need to take the derivative of it with respect to time:

$$\frac{dq_{\text{int}}(t)}{dt} = \frac{\delta}{\delta t}\frac{q_i - q_i e^{(-D_i t)}}{D_i t}$$

……(H.31)

Completing the partial derivative in Eq. H.31 by first factoring out the constants:

$$\frac{dq_{\text{int}}(t)}{dt} = \frac{1}{D_i}\frac{\delta}{\delta t}\frac{q_i - q_i e^{(-D_i t)}}{t}$$

……(H.32)

Recalling the quotient rule:

$$\frac{\partial}{\partial t}\left(\frac{u}{v}\right) = \frac{v\frac{\partial u}{\partial t} - u\frac{\partial v}{\partial t}}{v^2} \quad \text{……(H.11)}$$

Where:

$$u = q_i - q_i e^{-(D_i t)}$$

……...(H.33)

$$v = t \quad \text{……...(H.34)}$$

Plugging in Eq. H.11, H.33, and H.34 into Eq. H.32:

$$\frac{dq_{\text{int}}(t)}{dt} = \frac{1}{D_i}\frac{t\frac{\delta}{\delta t}\left[q_i - q_i e^{(-D_i t)}\right] - \left[q_i - q_i e^{(-D_i t)}\right]\frac{\delta}{\delta t}(t)}{t^2} \quad \text{.....(H.35)}$$

Simplifying Eq. H.35:

$$\frac{dq_{\text{int}}(t)}{dt} = \frac{1}{D_i}\frac{-t\frac{\delta}{\delta t}[q_i e^{(-D_i t)}] - \left[q_i - q_i e^{(-D_i t)}\right]}{t^2}$$

$$\frac{dq_{\text{int}}(t)}{dt} = \frac{-q_i + q_i e^{(-D_i t)} + q_i D_i e^{(-D_i t)} t}{D_i t^2}$$

$$\frac{dq_{\text{int}}(t)}{dt} = \frac{-q_i + q_i e^{(-D_i t)} + q_i D_i e^{(-D_i t)} t}{D_i t^2}$$

$$\frac{dq_{\text{int}}(t)}{dt} = \frac{q_i e^{(-D_i t)}[1 + D_i t - e^{(D_i t)}]}{D_i t^2} \quad \text{.....(H.36)}$$

Plugging in Eq. H.36 into Eq.8 to solve for loss ratio:

$$\frac{1}{D} \equiv -\frac{\frac{q_i - q_i e^{(-D_i t)}}{D_i t}}{\frac{q_i e^{(-D_i t)}[1 + D_i t - e^{(D_i t)}]}{D_i t^2}} \quad \text{.....(H.37)}$$

Simplifying Eq: H.37:

$$\frac{1}{D} \equiv -\frac{q_i - q_i e^{(-D_i t)}}{D_i t}\frac{D_i t^2}{q_i e^{(-D_i t)}[1 + D_i t - e^{(D_i t)}]}$$

$$\frac{1}{D} \equiv -\frac{t[q_i - q_i t e^{(-D_i t)}]}{q_i e^{(-D_i t)}[1 + D_i t - e^{(D_i t)}]}$$

$$\frac{1}{D} \equiv t + \frac{D_i t^2}{e^{(D_i t)} - D_i t - 1} \quad \text{.....(H.38)}$$

Eq. H.38 is the loss ratio for the time-rate integral form of Arp's exponential decline. For graphical purposes we are more interested in the reciprocal of Eq. H.38:

$$D_{\text{int}}(t) \equiv \left[t + \frac{D_i t^2}{e^{D_i t} - D_i t - 1} \right]^{-1} \quad \text{.....(H.39)}$$

Plugging in Eq. H.38 into Eq. H.9 to solve for derivative of the loss-ratio derivative of Arps' exponential decline:

$$b_{\text{int}}(t) \equiv \frac{d}{dt}\left[\frac{1}{D}\right] \equiv \frac{d}{dt}\left[t + \frac{D_i t^2}{e^{D_i t} - D_i t - 1} \right] \quad \text{.....(H.40)}$$

Differentiating Eq. H.40 term by term:

$$b_{\text{int}}(t) \equiv \frac{\delta}{\delta t}(t) + D_i \frac{\delta}{\delta t}\left[\frac{t^2}{e^{D_i t} - D_i t - 1} \right]$$

$$b_{\text{int}}(t) \equiv 1 + D_i \frac{\delta}{\delta t}\left[\frac{t^2}{e^{D_i t} - D_i t - 1} \right]$$

.....(H.41)

Recalling the quotient rule:

$$\frac{\partial}{\partial t}\left(\frac{u}{v}\right) = \frac{v\frac{\partial u}{\partial t} - u\frac{\partial v}{\partial t}}{v^2} \quad \text{.....(H.11)}$$

Where:

$$u = t^2$$

…….(H.42)

$$v = e^{D_i t} - D_i t - 1$$

……...(H.43)

Plugging in Eq. H.11, H.42, and H.43 into Eq. H.41:

$$b_{\text{int}}(t) \equiv 1 + D_i \frac{(e^{D_i t} - D_i t - 1)\frac{\partial}{\partial t}(t^2) - t^2 \frac{\partial}{\partial t}(e^{D_i t} - D_i t - 1)}{(e^{D_i t} - D_i t - 1)^2}$$

$$b_{\text{int}}(t) \equiv 1 + D_i \frac{2t(e^{D_i t} - D_i t - 1) - t^2 \frac{\partial}{\partial t}(e^{D_i t} - D_i t - 1)}{(e^{D_i t} - D_i t - 1)^2} \quad \text{…….(H.44)}$$

Differentiating the sum term in the numerator by term

$$b_{\text{int}}(t) \equiv 1 + D_i \frac{2t(e^{D_i t} - D_i t - 1) - t^2 \left[\frac{\partial}{\partial t}(e^{D_i t}) - D_i \frac{\partial}{\partial t}(t) - \frac{\partial}{\partial t}(1)\right]}{(e^{D_i t} - D_i t - 1)^2}$$

$$b_{\text{int}}(t) \equiv 1 + D_i \frac{2t(e^{D_i t} - D_i t - 1) - t^2 \left[e^{D_i t} \frac{\partial}{\partial t}(D_i t) - D_i\right]}{(e^{D_i t} - D_i t - 1)^2}$$

$$b_{\text{int}}(t) \equiv 1 + D_i \frac{2t(e^{D_i t} - D_i t - 1) - t^2 (D_i e^{D_i t} - D_i)}{(e^{D_i t} - D_i t - 1)^2} \quad \text{……...(H.45)}$$

Simplifying Eq. H.45

$$b_{\text{int}}(t) \equiv 1 + \frac{2D_i t}{(e^{D_i t} - D_i t - 1)^2} - \frac{D_i t^2 (D_i e^{D_i t} - D_i)}{(e^{D_i t} - D_i t - 1)^2}$$

…….(H.46)

Eq. H.46 is the loss-ratio derivative of the rate-integral for Arps exponential decline curve. Upon further investigation it can be seen in Eq. H.46 when t is large the loss-ratio derivative converges to 1.0. The modified hyperbolic equation uses Eq. H.30, H.39 and H.46, but with slightly modified variables, since it is not the initial decline parameters that are dictating the exponential tail decline characteristics. Therefore, for the exponential segment of the modified hyperbolic, the rate-integral equation is defined as:

$$q_{\text{int}}(t) = \frac{q_i^* - q_i^* e^{-D_{\min}(t-t^*)}}{D_{\min}(t-t^*)} \quad \text{.....(H.46)}$$

The time at which the exponential portion of the decline occurs (t^*) still occurs at the same time as the time-rate equation. This time to exponential decline is defined as:

$$t^* = \frac{\frac{D_i}{D_{\lim}} - 1}{bD_i} \quad \text{.....(H.47)}$$

The rate integral at which the exponential segment of the modified hyperbolic decline curve begins (q_i^*) is defined as:

$$q_i^* = \frac{q_i - q_i e^{(-D_i t^*)}}{D_i t^*} \quad \text{.....(H.48)}$$

The reciprocal loss-ratio for the exponential portion of the modified hyperbolic is defined as:

$$D_{\text{int}}(t) \equiv \left[(t-t^*) + \frac{D_{\min}(t-t^*)^2}{e^{D_{\min}(t-t^*)} - D_{\min}(t-t^*) - 1} \right]^{-1} \quad \text{.....(H.49)}$$

The derivative of the loss-ratio for the exponential portion of the modified hyperbolic is defined as:

$$b_{\text{int}}(t) \equiv 1 + \frac{2D_{\min}(t-t^*)}{[e^{D_{\min}(t-t^*)} - D_{\min}(t-t^*) - 1]^2} - \frac{D_{\min}(t-t^*)^2(D_{\min}e^{D_{\min}(t-t^*)} - D_{\min})}{(e^{D_{\min}(t-t^*)} - D_{\min}(t-t^*) - 1)^2} \quad \text{.....(H.50)}$$

Therefore, in conclusion, the modified hyperbolic time-rate integral decline curve and its respective diagnostic relations are defined as:

$$q_{\text{int}}(t) = \begin{Bmatrix} \frac{q_i}{D_i(1-b)t}\left[1-(1+bD_it)^{1-1/b}\right] & (t < t^*) \\ \frac{q_i^* - q_i^* e^{-D_{\min}(t-t^*)}}{D_{\min}(t-t^*)} & (t > t^*) \end{Bmatrix}$$

.....(H.51)

$$D_{\text{int}}(t) = \begin{Bmatrix} \left[t + \frac{(b-1)D_it^2}{-(bD_it+1)^{1/b} + D_it + 1}\right]^{-1} & (t < t^*) \\ \left[(t-t^*) + \frac{D_{\min}(t-t^*)^2}{e^{D_{\min}(t-t^*)} - D_{\min}(t-t^*) - 1}\right]^{-1} & (t > t^*) \end{Bmatrix} \quad \text{.....(H.51)}$$

$$b_{\text{int}}(t) = \begin{Bmatrix} 1 + \frac{2(b-1)D_it}{[-(bD_it+1)^{1/b} + D_it + 1]} - \frac{(b-1)D_it^2[D_i - D_i(bD_it+1)^{-1+1/b}]}{[-(bD_it+1)^{1/b} + D_it + 1]^2} & (t < t^*) \\ 1 + \frac{2D_{\min}(t-t^*)}{[e^{D_{\min}(t-t^*)} - D_{\min}(t-t^*) - 1]^2} - \frac{D_{\min}(t-t^*)^2(D_{\min}e^{D_{\min}(t-t^*)} - D_{\min})}{(e^{D_{\min}(t-t^*)} - D_{\min}(t-t^*) - 1)^2} & (t > t^*) \end{Bmatrix} \quad \text{.....(H.52)}$$

Where:

$$t^* = \frac{\frac{D_i}{D_{\lim}} - 1}{bD_i} \quad \text{.....(H.47)}$$

$$q_i^* = \frac{q_i - q_i e^{(-D_i t^*)}}{D_i t^*} \quad \text{.....(H.48)}$$

APPENDIX I

MECHANISTIC MODEL GOVERNING EQUATIONS

The fit-for-purpose mechanistic model used in this research is an enhanced version of the Texas A&M FTSim mechanistic model. The original FTSim that was used as the foundation for the validation mechanistic model is an isothermal, single-phase flow simulator used to model fluid flow through porous media. It is based off the TOUGH+ simulator developed at the Lawrence Berkeley National Laboratory (Moridis 2014). This base mechanistic model was then expanded to be able to describe non-isothermal multiphase-multicomponent flow through porous media. This modified version of FTSim is able to model the following processes and phenomena in porous and fractured media:

1. The partitioning of the mass components among the possible phases (i.e., Organic, Aqueous and Gaseous phases).
2. The flow of gases and liquids in the geologic system.
3. The corresponding heat flow and transport in the geologic system.
4. Heat exchanges due to:
    a. Conduction.
    b. Advection and convection.
    c. Latent heat due to phase changes.
    d. Dissolution of different mass components in each phase.

For additional information please refer to the TOUGH+ user's manual [Moridis *et al*. 2012].

I.1 The Mass and Energy Balance Equation

Pruess *et al*. (1999) presented the following equation to describe the mass and heat balance for every subdomain (i.e., gridblock) into which the entire simulation domain has been subdivided into by using the integral finite difference method:

$$\frac{d}{dt}\int_{V_n} M^{\kappa} dV = \int_{\Gamma_n} \mathbf{F}^{\boldsymbol{\kappa}} \cdot \mathbf{n}\, d\tilde{A} + \int_{V_n} q^{\kappa} dV, \qquad \kappa \equiv o, w, g \quad \text{.....(I.1)}$$

Where:

V, V_n	= volume, volume of subdomain n, [L^3]
M^{κ}	= mass accumulation term of component κ, [kg m^{-3}]
A, Γ_n	= surface area, surface area of subdomain n, [L^3]
$\mathbf{F}^{\kappa}$	= Darcy flux vector of component κ, [kg m^{-2} s^{-1}]
$\mathbf{n}$	= inward unit normal vector [dimensionless]
q^{κ}	= source/sink term of component κ, [kg m^{-3} s^{-1}]
t	= time, [T]

The three components incorporated in the mechanistic model were oil (o), water (w), and gas (g).

I.2 Mass Accumulation Terms

The mass accumulation term in Eq. I.1 can be represented using the following equation:

$$M^{\kappa} = \sum_{\beta \equiv O,A,G} \phi S_{\beta} \rho_{\beta} X_{\beta}^{\kappa}, \qquad \kappa \equiv o, w, g \quad \text{.....(I.2)}$$

Where:

ϕ	= porosity, [dimensionless]

ρ_β = density of phase β, [kg m^{-3}]

S_β = saturation of phase β, [dimensionless]

X_β^κ = mass fraction of component κ in phase β, [kg/kg]

In the mechanistic model used for this research the possible phases (β) are Organic (O), Aqueous (W) and Gaseous (G). The possible components are oil (o), water (w), and gas (g).

I.3 Heat Accumulation Terms

The heat accumulation term includes both the contribution from the rock matrix and all the present phases, and is defined as:

$$M^\theta = (1-\phi)\rho_R C_R T + \sum_{\beta \equiv O,A,G} \phi S_\beta \rho_\beta U_\beta \quad \text{.....(I.3)}$$

Where:

ρ_R = rock density, [kg m^{-3}]

C_R = heat capacity of the dry rock, [J kg^{-1} K^{-1}]

ϕ = porosity, [dimensionless]

ρ_β = density of phase β, [kg m^{-3}]

S_β = saturation of phase β, [dimensionless]

U_β = specific internal energy of phase β, [J kg^{-1}]

The specific internal energy of the gaseous phase (U_G) is a strong function of the composition and is related to the specific enthalpy of the gas phase (H_G), which is defined as:

$$U_G = \sum_{\kappa \equiv o,w,g} X_G^\kappa u_G^\kappa + U_{dep} \left(= H_G - \frac{p}{\rho_G} \right) \quad \text{.....(I.4)}$$

Where:

u_G^{κ} = specific internal energy of component κ in the gaseous phase, [J kg^{-1}]

U_{dep} = specific internal energy departure of the gas mixture, [J kg^{-1}]

X_G^{κ} = mass fraction of component κ in the gaseous phase, [kg/kg]

p = pressure, [Pa]

ρ_G = density of the gaseous phase, [kg m^{-3}]

The internal energy of the aqueous phase accounts for the effects of gas and oil in solution, and it is estimated using the following equation:

$$U_A = X_A^w u_A^w + X_A^o (u_A^o + U_{sol}^o) + X_A^g (u_A^g + U_{sol}^g) \quad \text{.....(I.5)}$$

Where:

X_A^w = mass fraction of the water component in the aqueous phase, [kg/kg]

X_A^o = mass fraction of the oil component in the aqueous phase, [kg/kg]

X_A^g = mass fraction of the gas component in the aqueous phase, [kg/kg]

u_A^w = specific internal energy of the water component in the aqueous phase, [J kg^{-1}]

u_A^o = specific internal energy of the oil component in the aqueous phase, [J kg^{-1}]

u_A^g = specific internal energy of the gas component in the aqueous phase, [J kg^{-1}]

U_{sol}^o = specific internal energy of the dissolution of oil in the aqueous phase, [J kg^{-1}]

U_{sol}^g = specific internal energy of the dissolution of gas in the aqueous phase, [J kg^{-1}]

The specific internal energy for each component in the aqueous phase is determined from:

$$u_A^\kappa = h_A^\kappa - \frac{P}{\rho_\kappa} = \int_{T_0}^{T} C_\kappa dT - \frac{P}{\rho_\kappa}, \qquad \kappa \equiv o, w, g$$

……..(I.6)

Where:

$h_A{}^\kappa$ = specific enthalpy of component κ in the aqueous phase, [J kg^{-1}]

T_0 = reference temperature, [K]

T = temperature, [K]

C_κ = temperature-dependent heat capacity of component κ, [J kg^{-1} K^{-1}]

The internal energy of the organic phase accounts for the effects of gas and water in solution, and it is estimated using the following equation:

$$U_O = X_O^o u_O^o + X_O^w (u_O^w + U_{sol}^w) + X_O^g (u_O^g + U_{sol}^g) \text{ …….....(I.7)}$$

Where:

$X_O{}^o$ = mass fraction of the oil component in the organic phase, [kg/kg]

$X_O{}^w$ = mass fraction of the water component in the organic phase, [kg/kg]

$X_O{}^g$ = mass fraction of the gas component in the organic phase, [kg/kg]

$u_O{}^o$ = specific internal energy of the oil component in the organic phase, [J kg^{-1}]

$u_O{}^w$ = specific internal energy of the water component in the organic phase, [J kg^{-1}]

$u_O{}^g$ = specific internal energy of the gas component in the organic phase, [J kg^{-1}]

$U_{sol}{}^w$ = specific internal energy of the dissolution of water in the organic phase, [J kg^{-1}]

$U_{sol}{}^g$ = specific internal energy of the dissolution of gas in the organic phase, [J kg^{-1}]

The specific internal energy for each component in the aqueous phase is determined from:

$$u_O^\kappa = h_O^\kappa - \frac{p}{\rho_\kappa} = \int_{T_0}^{T} C_\kappa dT - \frac{p}{\rho_\kappa}, \qquad \kappa \equiv o, w, g \quad \text{.....(I.8)}$$

Where:

h_O^κ = specific enthalpy of component κ in the organic phase, [J kg^{-1}]

T_0 = reference temperature, [K]

T = temperature, [K]

C_κ = temperature-dependent heat capacity of component κ, [J kg^{-1} kg^{-1}]

p = pressure, [Pa]

ρ_κ = density of component κ, [kg m^{-3}]

I.4 Mass Flux Terms

The mass flux for each component κ includes contribution from all mobile phases, which can be expressed as:

$$\mathbf{F}^\kappa = \sum_{\beta \equiv O,A,G} \mathbf{F}_\beta^\kappa, \qquad \kappa \equiv o, w, g \quad \text{.....(I.9)}$$

Where

$\mathbf{F}_\beta^\kappa$ = flux of component κ in phase β, [kg m^{-2} s^{-1}]

For the water component, $\mathbf{F}_A^w = X_A^w \mathbf{F}_A$, and the aqueous phase flux $\mathbf{F}_\mathrm{A}$ is described by Darcy's law as follows:

$$\mathbf{F}_A = -k\frac{k_{rA}\rho_A}{\mu_A}(\nabla p_A - \rho_A \mathbf{g})$$

……(I.10)

Where:

k = rock intrinsic permeability, [m^2]

k_{rA} = relative permeability of the aqueous phase, [dimensionless]

μ_A = viscosity of the aqueous phase, [Pa s]

p_A = pressure of the aqueous phase, [Pa]

$\mathbf{g}$ = gravitational acceleration vector, [m s^{-2}]

For the oil component, $\mathbf{F}_O^o = X_O^o \mathbf{F}_O$, and the organic phase flux $\mathbf{F}_O$ can also be described by Darcy's law as follows:

$$\mathbf{F}_O = -k\frac{k_{rO}\rho_O}{\mu_O}(\nabla p_O - \rho_O \mathbf{g}) \quad \text{.....(I.11)}$$

Where:

k = rock intrinsic permeability, [m^2]

k_{rO} = relative permeability of the organic phase, [dimensionless]

μ_O = viscosity of the organic phase, [Pa s]

p_O = pressure of the organic phase, [Pa]

$\mathbf{g}$ = gravitational acceleration vector, [m s^{-2}]

The phase pressures in Eq. I.10 and I.11 are given by:

$$p_A = p_G + p_{cGW} \quad \text{.....(I.12)}$$

$$p_O = p_G + p_{cGO} \quad \text{(I.13)}$$

$$p_G = p_G^g + p_G^w + p_G^o \quad \text{(I.14)}$$

Where:

p_A = pressure of the aqueous phase, [Pa]

p_O = pressure of the organic phase, [Pa]

p_G = pressure of the gaseous phase, [Pa]

$p_G{}^g$ = vapor partial pressure of the gas component in the gaseous phase, [Pa]

$p_G{}^o$ = vapor partial pressure of the oil component in the gaseous phase, [Pa]

$p_G{}^w$ = vapor partial pressure of the water component in the gaseous phase, [Pa]

p_{cGW} = gas-water capillary pressure, [Pa]

p_{cGO} = gas-oil capillary pressure, [Pa]

The three-phase mechanistic model capillary pressures were determined using the Parker *et al*. (1987) three-phase extension of the Van Genuchten (1980) two-phase capillary pressure model given by:

$$p_{cOW} = \frac{g}{\alpha_{OW}}\left[\left(\frac{S_A - S_{irA}}{1 - S_{irA}}\right)^{1-1/n}\right]^{1/n} \quad \text{(I.15)}$$

$$p_{cGW} = \frac{g}{\alpha_{GW}}\left[\left(\frac{1 - S_G - S_{irA}}{1 - S_{irA}}\right)^{1-1/n} - 1\right]^{1/n} \quad \text{(I.16)}$$

$$p_{cGO} = p_{cGW} + p_{cOW} \quad \text{(I.17)}$$

Where:

S_A = aqueous phase saturation, [dimensionless]

S_{irA} = irreducible aqueous phase saturation, [dimensionless]

α_{OW} = oil-water capillary pressure parameter, [dimensionless]

α_{GW} = gas-water capillary pressure parameter, [dimensionless]

n = capillary pressure parameter, [dimensionless]

g = gravitational acceleration constant, [m s^{-2}]

In the three-phase mechanistic model it was assumed that the aqueous phase was the wetting phase.

The partial pressure of the gas component in the gaseous phase was determined using Henry's Law, which is defined as:

$$p_G^g = H^g X_A^g \quad \text{.....(I.18)}$$

Where:

X_A^g = mass fraction of the gas component in the aqueous phase, [kg/kg]

H^g = Henry's Constant, [Pa]

The Henrys constant is a pressure and temperature dependent factor, that can be denoted as:

$$H^g = H^g(p_G, T) \quad \text{.....(I.19)}$$

The mass flux of the gaseous phase incorporates advection and diffusion contributions, and is defined as:

$$\mathbf{F}_G^\kappa = -k_0\left(1+\frac{b}{P_G}\right)\frac{k_{rG}\rho_G}{\mu_G} X_G^\kappa(\nabla p_g - \rho_g \mathbf{g}) + \mathbf{J}_G^\kappa \quad \text{.....(I.20)}$$

Where:

k_0 = absolute permeability at large gas pressures (= k), [m^2]

b = Klinkenberg (1941) b-factor accounting for gas slippage effects, [m^2]

k_{rG} = relative permeability of the gaseous phase, [dimensionless]

μ_G = viscosity of the gaseous phase, [Pa s]

p_G = pressure of the gaseous phase, [Pa]

$\mathbf{g}$ = gravitational acceleration vector, [m s^{-2}]

$\mathbf{J}_G^{\kappa}$ = diffusive mass flux of component κ in the gaseous phase, [kg m^{-2} s^{-1}]

Diffusive mass flux was not considered in the mechanistic model because it is negatable in most oil and gas systems.

I.5 Heat Flux Terms

The heat flux term used in the mechanistic model accounts for convection and advection heat transfer and is given by:

$$\mathbf{F}^{\theta} = -\lambda_{\Theta}\nabla T + \sum_{\beta \equiv O,A,G} h_{\beta}\mathbf{F}_{\beta} \quad \text{.....(I.21)}$$

Where:

λ_{Θ} = an approximate thermal conductivity of the rock-fluid system, [W m^{-1} K^{-1}]

h_{β} = specific enthalpy of phase β, [J kg^{-1}]

$\mathbf{F}_{\beta}$ = total flux of phase β, [kg m^{-2} s^{-1}]

T = temperature, [K]

The specific enthalpy of the gas phase is computed using the following equation.

$$H_G = \sum_{\kappa=o,w,g} X_G^{\kappa} h_G^{\kappa} + H_{dep} \quad \text{.....(I.22)}$$

Where:

X_G^{κ} = mass fraction of component κ in the gaseous phase, [kg/kg]

h_{β}^{κ} = specific enthalpy of component κ in phase β, [J kg^{-1}]

H_{dep} = specific enthalpy departure of the gas mixture, [J kg^{-1}]

The specific enthalpy of the aqueous phase is estimated from:

$$H_A = X_A^w h_A^w + X_A^o (h_A^o + H_{sol}^o) + X_A^g (h_A^g + H_{sol}^g) \quad \text{.....(I.23)}$$

Where:

X_A^w = mass fraction of the water component in the aqueous phase, [kg/kg]

X_A^o = mass fraction of the oil component in the aqueous phase, [kg/kg]

X_A^g = mass fraction of the gas component in the aqueous phase, [kg/kg]

h_A^w = specific enthalpy of the water component in the aqueous phase, [J kg^{-1}]

h_A^o = specific enthalpy of the oil component in the aqueous phase, [J kg^{-1}]

h_A^g = specific enthalpy of the gas component in the aqueous phase, [J kg^{-1}]

H_{sol}^o = specific enthalpy of the dissolution of oil in water, [J kg^{-1}]

H_{sol}^g = specific enthalpy of the dissolution of gas in water, [J kg^{-1}]

The specific enthalpy of the organic phase is estimated from:

$$H_O = X_O^o h_O^o + X_O^w (h_O^w + H_{sol}^w) + X_O^g (h_O^g + H_{sol}^g) \quad \text{.....(I.24)}$$

Where:

X_O^o = mass fraction of the oil component in the organic phase, [kg/kg]

X_O^w = mass fraction of the water component in the organic phase, [kg/kg]

X_O^g = mass fraction of the gas component in the organic phase, [kg/kg]

h_O^o = specific enthalpy of the oil component in the organic phase, [J kg^{-1}]

h_O^w = specific enthalpy of the water component in the organic phase, [J kg^{-1}]

h_O^g = specific enthalpy of the gas component in the organic phase, [J kg^{-1}]

U_{sol}^w = specific enthalpy of the dissolution of water in the organic phase, [J kg^{-1}]

U_{sol}^g = specific enthalpy of the dissolution of gas in the organic phase, [J kg^{-1}]

I.6 Source and Sink Terms

All of the validation cases performed for this research incorporated sinks with a specified production pressure. If a specified mass production rate is provided for the sink, the withdrawal of mass component k can be described by:

$$\hat{q}^{\kappa} = \sum_{\beta \equiv O,A,G} X_{\beta}^{\kappa} q_{\beta}, \qquad \kappa \equiv o,w,g \quad \text{.....(I.25)}$$

Where:

X_β^κ = mass fraction of component κ in phase β, [kg/kg]

q_β = production rate of phase β, [kg m^{-3}]

For source terms (i.e., injection wells) with a specified injection rate Eq. I.25 includes a mass component term, which is defined as:

$$\hat{q}^{\kappa} = \sum_{\beta \equiv O,A,G} X_{\beta}^{\kappa} q_{\beta}^{\kappa}, \qquad \kappa \equiv o,w,g \quad \text{.....(I.26)}$$

Where:

X_β^κ = mass fraction of component κ in phase β, [kg/kg]

q_β^κ = injection rate of component κ in phase β, [kg m^{-3}]

The heat exchange associated with the addition or withdraw of mass from the system at any given source or sink is given by

$$Q^\theta = \sum_{\kappa \equiv o,w,g} \hat{q}^\kappa h^\kappa \quad \text{.....(I.27)}$$

Where:

h^κ = specific enthalpy of component κ, [J kg^{-1}]

q_β^κ = production rate of phase component κ, [kg m^{-3}]

APPENDIX J

MECHANISTIC MODEL THERMOPHYSICAL PROPERTIES

The purpose of this appendix is to outline the different equations used estimate the thermophysical properties of the oil, water, and gas phases within the mechanistic model.

J.1. Oil Thermophysical Properties

The oil phase within the mechanistic model was considered as a single pseudo-component. Therefore, live-oil (*i.e.*, oil with dissolved gas) correlations were used to estimate the thermophysical properties of the oil phase.

Bubble Point Pressure

The oil bubble-point pressure was calculated using the Vazquez and Beggs (1980) correlation, which is defined as:

$$p_b = \left[\frac{R_s}{C_1 \gamma_g \exp\left(\frac{C_3 \gamma_{API}}{T_R + 459.67} \right)} \right]^{1/C_2} \quad \text{.....(J.1)}$$

Where:

p_b = oil bubble point pressure, [psi]

R_s = solution gas-oil ratio, [scf/STB]

γ_g = dissolved gas specific gravity, [air = 1.0]

γ_{API} = oil API gravity, [ºAPI]

T_r = reservoir temperature, [ºF]

C_1, C_2, C_3 = constants given in Table J.1, [dimensionless]

Solution Gas-Oil Ratio

The solution gas-oil ratio was also calculated using the Vazquez and Beggs (1980) correlation. Rearranging Eq. J.1 for solution gas-oil ratio it can be determined:

$$R_s = C_1 \gamma_g p^{C_2} \exp\left(\frac{C_3 \gamma_{API}}{T_r + 459.67}\right) \quad \text{.....(J.2)}$$

Where:

R_s = solution gas-oil ratio, [scf/STB]

p = pressure, [psi]

γ_g = dissolved gas specific gravity, [air = 1.0]

γ_{API} = oil API gravity, [ºAPI]

T_r = reservoir temperature, [ºF]

C_1, C_2, C_3 = constants given in Table J.1, [dimensionless]

Oil Formation Volume Factor

The oil formation volume factor was also calculated using the Vazquez and Beggs (1980) correlation. For saturated oils, the oil formation volume factor can be estimated using:

$$B_{o,sat} = 1 + A_1 R_s + A_2 (T_r - 60)\frac{\gamma_{API}}{\gamma_g} + A_3 R_s (T_r - 60)\frac{\gamma_{API}}{\gamma_g} \quad \text{.....(J.3)}$$

Where:

$B_{o,sat}$ = saturated oil formation volume factor, [RB/STB]

R_s = solution gas-oil ratio, [scf/STB]

γ_g = dissolved gas specific gravity, [air = 1.0]

γ_{API} = oil API gravity, [ºAPI]

T_r = reservoir temperature, [ºF]

A_1, A_2, A_3 = constants given in Table J.1, [dimensionless]

The oil formation volume factor for undersaturated oils can be estimated using:

$$B_{o,unsat} = B_{ob} \exp[c_{o,unsat}(p_b - p)] \quad \text{.....(J.4)}$$

Where:

$B_{o,unsat}$ = unsaturated oil formation volume factor, [RB/STB]

B_{ob} = oil formation volume factor at the bubble point pressure, [RB/STB]

c_o = oil compressibility, [psi^{-1}]

p_b = oil bubble point pressure, [psi]

p = pressure, [psi]

Oil Compressibility

The oil compressibility was also calculated using the Vazquez and Beggs (1980) correlation. By investigating Eq. J.3 and J.4 it can be seen that only undersaturated oil compressibility is required, which is defined as:

$$c_{o,unsat} = \frac{-1433 + 5R_{spb} + 17.2T_r - 1180\gamma_g + 12.61\gamma_{API}}{10^5 p} \quad \text{.....(J.5)}$$

Where:

$c_{o,unsat}$ = unsaturated oil formation volume factor, [RB/STB]

R_{spb} = solution gas-oil ratio at the bubble point pressure, [scf/STB]

γ_g = dissolved gas specific gravity, [air = 1.0]

γ_{API} = oil API gravity, [API]

T_r = reservoir temperature, [ºF]

p = pressure, [psi]

Vasquez and Beggs (1980) developed their correlation from over 600 laboratory PVT analyses from a wide range of oil fields from all over the world. The correlation is suitable for a wide range of reservoir pressure and temperatures, as well as oil types. The correlation groups oil properties into two groups; one for oils with an API gravity greater than 30º API, and one for oils with an API gravity less than 30º API. The constants used in Eq. J.1 – J.3 for these two groups are summarized in Table J.1.

Table J.1 — Coefficient values for the Vasquez and Beggs (1980) bubble point pressure, solution gas-oil ratio, and oil formation volume factor correlations.

Coefficient	$\gamma_{API} \leq 30º$ API	$\gamma_{API} > 30º$ API
A_1	0.0362	0.0178
A_2	1.0937	1.1870
A_3	25.7240	23.9310
C_1	4.677E-4	4.670E-4
C_2	1.751E-5	1.100E-5
C_3	- 1.811E-8	1.377E-9

Oil Density

The live oil density is calculated using the following relation:

$$\rho_o = \frac{62.42796\gamma_{o,sc} + 0.0136\gamma_{g,sc}R_s}{B_o} \quad \text{.....(J.6)}$$

Where:

ρ_o = live oil density, [lb ft^{-3}]

$\gamma_{o,sc}$ = oil specific gravity at standard conditions, [water = 1.0]

$\gamma_{g,sc}$ = gas specific gravity at standard conditions, [air = 1.0]

R_s = solution gas-oil ratio, [scf/STB]

B_o = oil formation volume factor, [RB/STB]

Oil Viscosity

The oil compressibility for the oil-phase was calculated using the Dindoruk and Christman (2004) correlation. To calculate the live-oil viscosity, the dead oil viscosity must first be calculated, which can be done by using the following equation:

$$\mu_{oD} = \frac{a_3 T_r^{a4} [\log(API)]^A}{a_5 p_{pb}^{a6} + a_7 R_{spb}^{a8}} \quad \text{.....(J.7)}$$

$$A = a_1 \log(T_r) + a_2 \quad \text{.....(J.8)}$$

Where:

μ_{oD} = dead oil viscosity, [cP]

API = oil API gravity, [ºAPI]

T_r = reservoir temperature, [ºF]

p_{pb} = oil bubble point pressure, [psi]

R_{spb} = solution gas-oil ratio at the bubble point pressure, [scf/STB]

a_n = dead oil viscosity constants determined from Table J.2

Table J.2 — Coefficients for the Dindorunk and Christman (2004) dead oil viscosity correlation.

Coefficient (μ_{oD} Correlation)	Value
a_1	14.505357625
a_2	- 44.868655416
a_3	9.36579E+9
a_4	- 4.194017808
a_5	- 3.1461171E-9
a_6	1.517652716
a_7	0.010433654
a_8	-0.000776880

The oil viscosity for saturated live oils can be calculated using the following equations:

$$\mu_{opb} = A(\mu_{oD})^B \quad \text{.....(J.9)}$$

$$A = \frac{a_1}{\exp(a_2 R_s)} + \frac{a_3 R_s^{a4}}{\exp(a_5 R_s)} \quad \text{.....(J.10)}$$

$$B = \frac{a_6}{\exp(a_7 R_s)} + \frac{a_8 R_s^{a9}}{\exp(a_{10} R_s)} \quad \text{.....(J.11)}$$

Where:

μ_{oD} = dead oil viscosity, [cP]

R_s = solution gas-oil ratio, [scf/STB]

a_n = saturated oil viscosity constants determined from Table J.3

Table J.3 — Coefficients for the Dindorunk and Christman (2004) saturated oil viscosity correlation.

Coefficient (μ_{opb} Correlation)	Value
a_1	1.000000E+0
a_2	4.740729E+4
a_3	- 1.023451E-2
a_4	6.600358E-1
a_5	1.075080E-3
a_6	- 2.191172E-5
a_7	4.233179E-1
a_8	- 2.273945E-4

The oil viscosity for undersaturated live oils can be calculated using the following equations:

$$\mu_o = \mu_{obp} + a_6(p - p_{pb})10^A \quad \text{.....(J.12)}$$

$$A = a_1 + a_2 \log(\mu_{obp}) + a_3 \log(R_s) + a_4 \mu_{bop} \log(R_s) + a_5(p - p_{bp}) \quad \text{.....(J.13)}$$

Where:

μ_o = undersaturated oil viscosity, [cP]

p_{pb} = oil bubble point pressure, [psi]

p = pressure, [psi]

μ_{obp} = saturated oil viscosity, [cP]

μ_{bop} = oil viscosity at the bubble point, [cP]

R_s = solution gas-oil ratio, [scf/STB]

a_n = undersaturated oil viscosity constants determined from Table J.4

Table J.4 — Coefficients for the Dindorunk and Christman (2004) undersaturated oil viscosity correlation.

Coefficient (μ_o Correlation)	Value
a_1	0.776644115
a_2	0.987658646
a_3	- 0.190564677
a_4	0.009147711
a_5	- 0.000019111
a_6	0.000063340

Oil Specific Heat

The isobaric oil specific heat was calculated using the Edwards et al. (1983) correlation, which is defined as:

$$c_p = A_1 + A_2 T_r + A_3 T_r^2 \quad \text{.....(J.13)}$$

$$A_3 = -1.17126 + (0.023772 + 0.02722 + 0.024907\gamma_o)K + \frac{1.14982 + 0.046535K}{\gamma_o} \quad \text{.....(J.14)}$$

$$A_2 = 10^{-4}(1.0 + 0.82463K)\left(1.12172 - \frac{0.27634}{\gamma_o}\right) \quad \text{.....(J.15)}$$

$$A_1 = 10^{-8}(1.0 + 0.82463K)\left(2.9027 - \frac{0.70958}{\gamma_o}\right) \quad \text{.....(J.16)}$$

Where:

c_p = live oil isobaric heat capacity, [Btu lb^{-1} ^{o}F^{-1}]

K = Watson characterization factor, [dimensionless]

γ_o = oil specific gravity (water = 1.0), [dimensionless]

T_r = reservoir temperature [Fahrenheit]

Oil Thermal Conductivity

The oil thermal conductivity was determined using the Edwards et al. (1983) correlation, which is defined as:

$$\lambda_o = 137.0\rho_o[1.0 - 0.00054(T_r - 273.0)] \quad \text{.....(J.17)}$$

Where:

λ_o = oil thermal conductivity, [W m^{-1} K^{-1}]

T_r = reservoir temperature, [K]

ρ_o = oil density, [kg m^{-3}]

Oil Solubility

The mutual oil solubility was determined using the Tsonopoulus (1999) correlation, which is defined as:

$$Y_A^o = \exp(-3.9069 - 1.51897\text{CN}) \quad \text{.....(J.18)}$$

$$Y_O^w = \exp\left(\frac{-79.6677 - 6.6547\text{CN}}{9.5470 + \text{CN}}\right) \quad \text{.....(J.19)}$$

Where:

$Y_A{}^o$ = mole faction of the oil in the aqueous phase, [dimensionless]

$Y_O{}^w$ = mole faction of water in the organic phase, [dimensionless]

CN = carbon number, [dimensionless]

Heat of Solution

The heat of solution for oil was determined using the Tsonopoulus (1999) correlation, which is defined as:

$$h^{o}_{A,sol} = \exp[A_1 + B_1 / T_r + C_1 \ln(T_r)] \quad \text{.....(J.20)}$$

$$h^{w}_{O,sol} = \exp[A + B / T_r] \quad \text{.....(J.21)}$$

Where:

$h_A{}^o$ = heat of solution for the dissolution of oil in the aqueous phase, [dimensionless]

$Y_O{}^w$ = heat of solution for the dissolution of water in the organic phase, [dimensionless]

T_r = reservoir temperature, [K]

A, B, C = heat of solution constants determined from Table J.5

Table J.5 — Coefficients for the Tsonopoulus (1999) heat of solution correlation.

Alkane	A_1	B_1	C_1	A_2	B_2
Pentane	- 333.59719	14537.472	47.97436	6.951930	- 4381.365
Hexane	- 374.90804	16327.128	53.89582	6.698073	- 4291.186
Heptane	- 396.93979	17232.298	56.95927	6.76126	- 4290.700
Octane	- 415.7563	17975.386	59.55451	6.839365	- 4290.165

J.2. Gas Thermophysical Properties

The gas component was assumed to be made up of entirely Methane (CH_4) for this research. The mechanistic model also accounted for vaporous water in the gaseous phase, but since that is related to the water component please refer to Section J.3 for more information. The gas component was

assumed to be a real gas (rather than ideal) for the mechanistic model, therefore all PVT properties were modeled in relation to the real gas law, which is defined as:

$$p_g V = ZnRT \quad \text{.....(J.22)}$$

Where:

p_g = gas pressure, [Pa]

V = volume of the gas, [m^3]

n = number of moles, [dimensionless]

Z = gas z-factor, [dimensionless]

R = 8.31441, gas constant, [J K^{-1} mol^{-1}]

T = temperature, [K]

Please note that Eq. J.22 can have different units, but then a different gas constant value must be used.

Gas Z-factor

The gas *z*-factor was determined from the Peng Robinson (1978) cubic equation of state, which is defined as:

$$p = \frac{RT}{V_m - b} - \frac{a\alpha}{V_m^2 + 2bV_m - b^2} \quad \text{.....(J.23)}$$

$$a \approx 0.45724 \frac{R^2 T_c^2}{p_c} \quad \text{.....(J.24)}$$

$$b \approx 0.07780 \frac{RT_c}{p_c} \quad \text{.....(J.25)}$$

$$\alpha = [1 + \kappa(1 - T_r^{1/2})]^2 \quad \text{.....(J.26)}$$

$$\kappa \approx 0.37464 + 1.54266\omega - 0.26922\omega^2 \quad \text{.....(J.27)}$$

$$T_r = \frac{T}{T_c} \quad \text{.....(J.28)}$$

Where:

p = pressure, [Pa]

p_c = gas critical pressure, [Pa]

V_m = molar volume of the gas, [m^3 mol^{-1}]

R = 8.31441, gas constant, [J K^{-1} mol^{-1}]

T_c = gas critical temperature, [K]

T_r = reduced temperature, [dimensionless]

ω = acentric facto,r [dimensionless]

Eq. J.23 can be written in polynomial form, which is as follows:

$$Z^3 - (1 - B)Z^2 + (A - 2B - 3B^2)Z - (AB - B^2 - B^3) = 0 \quad \text{.....(J.29)}$$

$$A = \frac{\alpha a p}{R^2 T^2} \quad \text{.....(J.30)}$$

$$B = \frac{bp}{RT} \quad \text{.....(J.31)}$$

$$a \approx 0.45724 \frac{R^2 T_c^2}{p_c} \quad \text{.....(J.24)}$$

$$b \approx 0.07780 \frac{RT_c}{p_c} \quad \text{.....(J.25)}$$

$$\alpha = [1 + \kappa(1 - T_r^{1/2})]^2 \quad \text{.....(J.26)}$$

$$\kappa \approx 0.37464 + 1.54266\omega - 0.26922\omega^2 \quad \text{.....(J.27)}$$

$$T_r = \frac{T}{T_c} \quad \text{.....(J.28)}$$

Where:

Z = gas compressibility factor, [dimensionless]

p = pressure, [Pa]

p_c = gas critical pressure, [Pa]

V_m = molar volume of the gas, [m^3 mol^{-1}]

R = 8.31441, gas constant, [J K^{-1} mol^{-1}]

T_c = gas critical temperature, [K]

T_r = reduced temperature, [dimensionless]

ω = acentric factor, [dimensionless]

Gas Z-factor

By rearranging Eq. J.22, gas density can be determined by using the following equation

$$\rho_g = \frac{pMW_g}{ZRT} \quad \text{.....(J.32)}$$

Where:

ρ_g = gas density, [kg m^{-3}]

p = pressure, [Pa]

MW_g = gas molecular weight, [g mol^{-1}]

Z = gas Z-factor, [dimensionless]

R = 8.31441, gas constant, [J K^{-1} mol^{-1}]

T = temperature, [K]

Gas Viscosity

Gas viscosity was determined using the Chung *et al*. (1988) relation, which is as follows:

$$\mu_g = \frac{3.6644\eta^* \sqrt{MW_g T_c}}{v_c} \quad \text{.....(J.33)}$$

$$\eta^* = \frac{\sqrt{T^*}}{\Omega_v}\left(\frac{F_c}{G_2} + E_6 y\right) + \eta^{**} \quad \text{.....(J.34)}$$

$$\eta^{**} = E_7 y^2 G_2 \exp\left[E_8 + \frac{E_9}{T^*} + \frac{E_{10}}{(T^*)^2}\right] \quad \text{.....(J.35)}$$

$$G_2 = \frac{E_1 \frac{1-\exp(-E_4 y)}{y} + E_1 G_1 \exp(E_5 y) + E_3 G_1}{E_1 E_4 + E_2 + E_3} \quad \text{.....(J.36)}$$

$$E_i = a_i + b_i \omega \quad \text{.....(J.37)}$$

$$G_1 = \frac{1.0 - 0.5y}{(1-y)^3} \quad \text{.....(J.38)}$$

$$y = \frac{\rho v_c}{6.0} \quad \text{.....(J.39)}$$

$$F_c = 1.0 - 0.2756\omega \quad \text{.....(J.40)}$$

$$\Omega_v = 1.16145(T^*)^{-0.14874} + 0.52487\exp(-0.7732T^*) + 2.16178\exp(-2.43787T^*) \quad \text{(J.41)}$$

$$T^* = 1.2593T_r \quad \text{(J.42)}$$

$$T_r = \frac{T}{T_c} \quad \text{(J.43)}$$

Where:

μ_g = gas viscosity, [μP]

MW_g = gas molecular weight, [g mol^{-1}]

T_c = gas critical temperature, [K]

T_r = reduced temperature, [dimensionless]

v_c = molar critical volume of the gas, [cm^3 mol^{-1}]

a_i, b_i = gas viscosity constants determined from Table J.6

Table J.6 — Coefficients for the Chung *et al*. (1988) gas viscosity correlation.

i	a_i	b_i
1	6.324E+0	5.041E+1
2	1.210E-3	- 1.154E-3
3	2.283E+0	2.542E+2
4	6.623E+0	3.810E+1
5	1.975E+1	7.630E+0
6	- 1.900E+0	- 1.254E+1
7	2.428E+1	3.450E+0
8	7.972E-1	1.117E+0
9	- 2.382E-1	6.770E-2
10	6.863E-2	3.479E-1

Ideal Gas Isobaric Specific Heat

The ideal gas isobaric specific heat was calculated using the Poling *et al*. (2007) correlation, which is defined as:

$$C_p = \frac{R}{MW_g}(4.568 - 8.975 \cdot 10^{-3} T + 3.631 \cdot 10^{-5} T^2 - 3.407 \cdot 10^{-8} T^3 + 1.091 \cdot 10^{-11} T) \quad \text{.....(J.44)}$$

Where:

C_p = ideal gas isobaric specific heat, [J kg^{-1} K^{-1}]

T = temperature, [K]

MW_g = gas molecular weight [g mol^{-1}]

Ideal Gas Isochoric Specific Heat

The ideal gas isochoric specific heat can be calculated using the following relation with the isobaric specific heat capacity:

$$C_v = C_p - R \quad \text{.....(J.45)}$$

Where:

C_v = ideal gas isochloric specific heat, [J kg^{-1} K^{-1}]

C_p = ideal gas isobaric specific heat, [J kg^{-1} K^{-1}]

R = 8.31441, gas constant, [J K^{-1} mol^{-1}]

Real Gas Specific Enthalpy

The real gas specific enthalpy can be determined using the following equation:

$$H_g = H_{ideal} + H_{dep} \quad \text{.....(J.46)}$$

Where:

H_g = ideal gas isochloric specific heat, [J kg^{-1}]

H_{ideal} = ideal gas isobaric specific heat, [J kg^{-1}]

H_{dep} = departure from ideal gas isobaric specific heat, [J kg^{-1}]

The ideal portion of Eq. J.43 can be determined by integrating Eq. J.42.

$$H_{ideal} = \int_{T_{ref}}^{T} C_v dT \quad \text{.....(J.47)}$$

Where:

H_{ideal} = Ideal gas isobaric specific heat [J kg^{-1}]

C_v = Ideal gas isochloric specific heat [J kg^{-1} K^{-1}]

T = Temperature [K]

T_{ref} = Reference temperature [K]

The departure from the ideal specific gas enthalpy can be calculated by using the Poling *et al*. (2007) relation, which is defined as:

$$H_{dep} = \frac{RT_c}{MW_g}\left\{T_r(Z-1) - 2.078(1+\kappa)\sqrt{\alpha}\ln\left[\frac{Z+(1+\sqrt{2})b}{Z-(1-\sqrt{2})b}\right]\right\} \quad \text{.....(J.48)}$$

$$b \approx 0.07780 \frac{RT_c}{p_c} \quad \text{.....(J.25)}$$

$$\alpha = [1 + \kappa(1 - T_r^{1/2})]^2 \quad \text{.....(J.26)}$$

$$\kappa \approx 0.37464 + 1.54266\omega - 0.26922\omega^2 \quad \text{.....(J.27)}$$

$$T_r = \frac{T}{T_c} \quad \text{.....(J.28)}$$

Where:

H_{dep} = departure from ideal gas isobaric specific heat, [J kg^{-1}]

p_c = gas critical pressure, [Pa]

R = 8.31441, gas constant, [J K^{-1} mol^{-1}]

T_c = gas critical temperature, [K]

T = temperature, [K]

MW_g = gas molecular weight, [g mol^{-1}]

ω = acentric factor, [dimensionless]

J.3. Water Thermophysical Properties

The water thermophysical properties for the mechanistic model were calculated using the outlined procedure by the International Association for the Properties of Water and Steam (IAPWS, 2018). IAPWS outlines the thermophysical properties for the ordinary water substance for general and scientific use.

The water vapor component in the gaseous phase was calculated using the following equations for partial pressures:

$$p_G^{CH_4} = p_g - p_G^{H_2O} \quad \text{(J.49)}$$

$$Y_G^{CH_4} = p_G^{CH_4} / p_G \quad \text{(J.50)}$$

$$Y_G^{H_2O} = 1 - Y_G^{CH_4} \quad \text{(J.51)}$$

Where:

$p_G^{CH_4}$ = Partial pressure of methane in the gas phase, [Pa]

p_G = Gaseous phase pressure, [Pa]

$p_G^{H_2O}$ = Partial pressure of water vapor in the gas phase, [Pa]

$Y_G^{CH_4}$ = Mole fraction of methane in the gas phase, [dimensionless]

$Y_G^{H_2O}$ = Mole fraction of water vapor in the gas phase, [dimensionless]